

**Bio-Engineered Earth Retaining Structure (BEERS)**  
**A timber sheet pile-vegetation system for stream bank protection**

Kamath, A.C.

**DOI**

[10.4233/uuid:890a1ddd-1957-4732-988a-eb4204e454ce](https://doi.org/10.4233/uuid:890a1ddd-1957-4732-988a-eb4204e454ce)

**Publication date**

2022

**Document Version**

Final published version

**Citation (APA)**

Kamath, A. C. (2022). *Bio-Engineered Earth Retaining Structure (BEERS): A timber sheet pile-vegetation system for stream bank protection*. [Dissertation (TU Delft), Delft University of Technology].  
<https://doi.org/10.4233/uuid:890a1ddd-1957-4732-988a-eb4204e454ce>

**Important note**

To cite this publication, please use the final published version (if applicable).  
Please check the document version above.

**Copyright**

Other than for strictly personal use, it is not permitted to download, forward or distribute the text or part of it, without the consent of the author(s) and/or copyright holder(s), unless the work is under an open content license such as Creative Commons.

**Takedown policy**

Please contact us and provide details if you believe this document breaches copyrights.  
We will remove access to the work immediately and investigate your claim.

**BIO-ENGINEERED EARTH RETAINING  
STRUCTURE (BEERS)**

A TIMBER SHEET PILE-VEGETATION SYSTEM FOR  
STREAM BANK PROTECTION



# **BIO-ENGINEERED EARTH RETAINING STRUCTURE (BEERS)**

**A TIMBER SHEET PILE-VEGETATION SYSTEM FOR  
STREAM BANK PROTECTION**

## **Dissertation**

for the purpose of obtaining the degree of doctor  
at the Delft University of Technology,  
by the authority of the Rector Magnificus Prof.dr.ir. T.H.J.J. van der Hagen  
chair of the Board of Doctorates,  
to be defended publicly on  
Thursday 23 June 2022 at 12:30 o'clock

by

**Abhijith Chandrakaran KAMATH**

Master of Science in Civil engineering, Texas A&M university, United States  
born in Kerala, India.

This dissertation has been approved by the promotors.

Composition of the doctoral committee:

|                                      |  |
|--------------------------------------|--|
| Rector Magnificus,                   | chairperson                              |
| Prof. dr. ir. J.W .G. Van de Kuilen, | Delft University of Technology, promotor |
| Prof. dr. ir. C. Jommi,              | Delft University of Technology, promotor |

*Independent members:*

|                               |  |
|-------------------------------|--|
| Prof.dr. H.M. Jonkers,        | Delft University of Technology                 |
| Assoc.Prof.dr. D. Sterpi,     | Politecnico di Milano, Italy                   |
| Dr. A. Stokes,                | INRAE, France                                  |
| Dr. P.H. Waarts,              | Provincie Noord-Holland                        |
| Prof. dr. ir. A.V. Metrikine, | Delft University of Technology, reserve member |

*Other member:*

|                 |                                |
|-----------------|--------------------------------|
| Drs. W.F. Gard, | Delft University of Technology |
|-----------------|--------------------------------|

The work described in this publication was supported by the European Commission H2020 Framework Programme through the grant to the budget of the Marie Skłodowska-Curie European Training Networks (ETN) project TERRE, Contract H2020-MSCA-ITN-2015-675762.



*Keywords:* Sheet pile, vegetation, roots, cohesion

*Printed by:* Ipskamp Printing

*Front & Back:* Vegetation roots (front), Decayed wood (Back)

Copyright © 2022 by A.C. Kamath

ISBN 978-94-6421-769-8

An electronic version of this dissertation is available at  
<http://repository.tudelft.nl/>.

All rights reserved. No parts of this publication may be reproduced, stored in a retrieval system, or transmitted, in any form or by any means, electronic, mechanical, photocopying, recording, or otherwise, without the prior written permission of the author.

# CONTENTS

|   |              |
|---|--------------|
| <b>Summary</b>  | <b>ix</b>    |
| <b>Samenvatting</b>   | <b>xi</b>    |
| <b>List of Figures</b>  | <b>xiii</b>  |
| <b>List of Tables</b>   | <b>xix</b>   |
| <b>Preface</b>  | <b>xxi</b>   |
| <b>Acknowledgements</b>   | <b>xxiii</b> |
| <b>1 Introduction</b>   | <b>1</b>     |
| 1.1 Background . . . . .  | 3            |
| 1.2 Problem statement . . . . .   | 5            |
| 1.3 Research objectives . . . . .   | 7            |
| 1.4 Thesis organization . . . . .   | 8            |
| References . . . . .  | 9            |
| <b>2 Shear strength characteristics of rooted soils</b>                                   | <b>11</b>    |
| 2.1 Abstract . . . . .  | 13           |
| 2.2 Introduction . . . . .  | 14           |
| 2.3 Materials . . . . .   | 15           |
| 2.3.1 Selection of vegetation . . . . .   | 15           |
| 2.3.2 Boxes for growing the plants and shear testing . . . . .                            | 16           |
| 2.3.3 Soil properties and conditions of growth . . . . .                                  | 16           |
| 2.4 Methods . . . . .   | 17           |
| 2.4.1 Large scale direct shear apparatus . . . . .  | 17           |
| 2.4.2 Direct shear test . . . . .   | 18           |
| 2.4.3 Root analysis . . . . .   | 20           |
| 2.4.4 Data Analysis . . . . .   | 20           |
| 2.4.5 Rheological models . . . . .  | 21           |
| 2.5 Results . . . . .   | 22           |
| 2.5.1 Vegetation . . . . .  | 22           |
| 2.5.2 Load controlled shear tests . . . . .   | 22           |
| 2.5.3 Displacement-controlled test . . . . .  | 28           |
| 2.6 Discussion . . . . .  | 30           |
| 2.6.1 Considerations on the root system architecture effect on soil reinforcing . . . . . | 30           |
| 2.6.2 Stress-strain behavior . . . . .  | 30           |
| 2.6.3 Effect of roots on the soil volume change during shearing . . . . .                 | 31           |

|          |   |           |
|----------|---|-----------|
| 2.6.4    | Effect of roots on the shear strength of root permeated soil . . . . .                          | 32        |
| 2.6.5    | Visco-elastic behaviour of root permeated soil. . . . .   | 34        |
| 2.6.6    | Usefulness for bio-engineered earth retaining system . . . . .                                  | 34        |
| 2.7      | Conclusions. . . . .  | 35        |
| 2.8      | Appendix A: Stress vs displacement & Vertical displacement vs Horizontal displacement . . . . . | 36        |
| 2.9      | Appendix B: Root area at different orientations . . . . .                                       | 42        |
|          | References . . . . .  | 44        |
| <b>3</b> | <b>Root mechanical strength characterization</b>  | <b>49</b> |
| 3.1      | Abstract . . . . .  | 51        |
| 3.2      | Introduction . . . . .  | 52        |
| 3.3      | Materials & Methods . . . . .   | 53        |
| 3.3.1    | Testing overview . . . . .  | 53        |
| 3.3.2    | Growing condition . . . . .   | 53        |
| 3.3.3    | Root sampling . . . . .   | 54        |
| 3.3.4    | Tensile testing . . . . .   | 54        |
| 3.3.5    | Rheological models . . . . .  | 55        |
| 3.4      | Results . . . . .   | 57        |
| 3.4.1    | Root tensile strength within species . . . . .  | 57        |
| 3.4.2    | Viscous behaviour of roots . . . . .  | 59        |
| 3.5      | Discussion . . . . .  | 63        |
| 3.5.1    | Tensile strength and young's modulus variation . . . . .  | 69        |
| 3.5.2    | Effect of drying of roots . . . . .   | 69        |
| 3.5.3    | Viscous behaviour of roots . . . . .  | 70        |
| 3.5.4    | Implications for practical applications . . . . .   | 70        |
| 3.6      | Conclusions. . . . .  | 71        |
| 3.7      | Appendix A: Strain time experimental curves fitted with Burger and power law model. . . . .     | 71        |
|          | References . . . . .  | 75        |
| <b>4</b> | <b>Physical modelling of timber sheet pile-vegetation system</b>                                | <b>79</b> |
| 4.1      | Abstract . . . . .  | 81        |
| 4.2      | Introduction . . . . .  | 82        |
| 4.3      | Materials and Methods . . . . .   | 83        |
| 4.3.1    | <i>Humulus Lupulus</i> L. 3D model root . . . . .   | 83        |
| 4.3.2    | Physical modelling. . . . .   | 84        |
| 4.3.3    | Instrumentation . . . . .   | 87        |
| 4.3.4    | Testing method and protocol . . . . .   | 88        |
| 4.4      | Results . . . . .   | 89        |
| 4.4.1    | Bare soil . . . . .   | 89        |
| 4.4.2    | Root pattern 1 . . . . .  | 92        |
| 4.4.3    | Root pattern 2 . . . . .  | 93        |
| 4.4.4    | Summary of tests . . . . .  | 94        |

---

|          |  |            |
|----------|--|------------|
| 4.5      | Finite element modelling . . . . .   | 94         |
| 4.5.1    | Model . . . . .  | 94         |
| 4.5.2    | Results . . . . .  | 96         |
| 4.6      | Parametric Analysis . . . . .  | 99         |
| 4.6.1    | Effect of cohesion increase due to presence of roots . . . . .                               | 103        |
| 4.6.2    | Effect of root area pattern . . . . .  | 104        |
| 4.6.3    | Implications for on-going research & Practical implementation . . .                          | 105        |
| 4.7      | Conclusions. . . . .   | 105        |
| 4.8      | Appendix A: PIV images . . . . .   | 106        |
|          | References . . . . .   | 109        |
| <b>5</b> | <b>Approach to the design of timber sheet pile-vegetation system</b>                         | <b>113</b> |
| 5.1      | Abstract . . . . .   | 115        |
| 5.2      | Introduction . . . . .   | 116        |
| 5.3      | Methods . . . . .  | 117        |
| 5.3.1    | System approach (SA): Vegetation and timber sheet pile<br>combination as a system. . . . .   | 117        |
| 5.3.2    | Discrete approach (DA): Vegetation and timber sheet pile as dis-<br>crete elements . . . . . | 119        |
| 5.3.3    | Assumptions . . . . .  | 121        |
| 5.4      | Results . . . . .  | 125        |
| 5.4.1    | System approach. . . . .   | 125        |
| 5.4.2    | Discrete approach . . . . .  | 127        |
| 5.5      | Discussion & Conclusions. . . . .  | 129        |
|          | References . . . . .   | 131        |
| <b>6</b> | <b>Conclusions and Outlook</b>   | <b>133</b> |
| 6.1      | Observations and conclusions . . . . .   | 134        |
| 6.2      | Limitations . . . . .  | 137        |
| 6.3      | Future recommendations. . . . .  | 138        |
|          | <b>Curriculum Vitæ</b>   | <b>139</b> |
|          | <b>List of Publications</b>  | <b>141</b> |



# SUMMARY

The Netherlands has an extensive network of rivers and canals systems serving purposes like irrigation, transportation and water removal. The banks along the canals are either protected by earth retaining structures such as sheet pile walls or left unprotected. A bulk of the engineered sheet piles used to protect the canal banks in the Netherlands are made of timber. Tropical hardwoods such as Azobé (*Lophira alata*) are used to make these timber sheet piles durable, owing to its high biological resistance to decay. Pine from North-west Europe is also used, but need to be treated chemically for sufficient durability.

Even though roots of vegetation are known to increase the shear strength of soil, the positive effects of vegetation are not quantified in depth. Vegetation roots in a root-soil composite primarily act in tension when subjected to load, thus acting similar to steel in reinforced concrete. This thesis summarizes the efforts to study a bio-engineered earth retaining structure made of non-durable locally available wood species and vegetation to protect the canal banks as an alternative to the currently used bank protection structures. Such a retaining structure would not only reduce the need for durable hardwoods, but are also more environmentally friendly than the 'hard' retaining structures currently in use.

Two vegetation types, *Humulus lupulus* L. and *Salix fragilis* L. were chosen for investigation based on their potential to reinforce canal banks, nativity, root characteristics and growth conditions such as presence of high ground water table. An extensive laboratory campaign was planned and conducted to characterize the strength of roots, root-soil composite and to study the behaviour of the timber sheet pile-vegetation combination as a system. The experimental results were further extended to develop approaches in the design of timber sheet pile-vegetation system.

To study the root-soil composite behaviour in shear, a large scale direct shear apparatus was built. The apparatus was built in the view of conducting tests in dual loading modes, displacement controlled and load controlled shear. In order to simulate the canal bank conditions as closely as possible, the samples were tested in saturated conditions at low confining pressure. Bare soil, rooted samples of *Humulus lupulus* L. and *Salix fragilis* L. were tested in both displacement controlled and load controlled conditions. The roots were excavated after the test and analysis of root orientation, diameter and root biomass was conducted. Rooted samples showed a higher friction angle when compared to bare soil. Contractive behaviour was shown by rooted samples and the peak stress ratio vs displacement trend of rooted samples were seen to diverge from the trend for bare soil. Burger model was seen to be able to capture the time dependent behaviour under loading mode, when simulated over the experimental results.

A tensile testing program was devised to test roots in tension in a displacement controlled and load controlled tests. Roots of *Humulus lupulus* L. and *Salix fragilis* L. were tested in both wet and dry conditions in displacement controlled tests. Load controlled

tensile testing was conducted on samples of *Humulus lupulus* L. of two diameters. Power law was observed to estimate volume-effect and fit all the tensile strength-diameter variations. Comparison of tensile strength in dry and wet conditions revealed that significant difference in tensile strength was observed for *Salix fragilis* L. while no significant difference in tensile strength was observed for *Humulus lupulus* L. Further, time to failure of roots were studied using a power law model.

A physical modelling approach was attempted to study the behaviour of the timber sheet pile-vegetation system. A root system similar to *Humulus lupulus* L. was 3D printed using PLA material to be used in physical model. A comparison of unreinforced bank and bank reinforced with root analogues revealed that the presence of roots increase the volume of soil that needs to be mobilized for failure to occur. It was also observed that when root analogues were placed in the most efficient spatial pattern, among the conducted tests, are able to sustain twice the drawdown pressure. Subsequently, finite element modelling was conducted by including the effect of roots as an increased cohesion parameter. The results from modelling were seen to be able to capture the failure. Parametric analysis revealed that the influence of spatial distribution of the roots on forces acting on the sheet pile is higher, after a threshold value of additional cohesion is reached. That implies any additional cohesion after the threshold value might not provide any additional benefits to the stability. The results thus indicate that vegetation with more spatially distributed roots will be more suitable to be used in timber sheet pile-vegetation retaining system.

Finally, two different perspectives in design approach of a timber sheet pile-vegetation system are investigated. The system approach is based on the concept that the mechanical reinforcement of the soil with growth of vegetation could result in a reduction of horizontal pressure against the sheet pile, bending moments and shear stresses acting on the sheet pile over time. This results in decreasing the duration of load effect in the timber and counteracting the effects of slow biological degradation of wood in air-water-soil conditions. Timber sheet pile components that are below the water level are less prone to decay. However, those components that are at the air water-soil interface are more susceptible to decay. In the discrete approach the vegetation is perceived as supporting the top parts of the stream bank (< 2meters) after timber decay has occurred. The effect of vegetation is analyzed as both increase in internal friction angle and increase in cohesion, on stream banks of retaining height of 2m and 3m. An increase in service life of the timber sheet pile-vegetation system is achieved in a system approach compared to when only timber sheet pile is present. In the discrete approach, it was observed that modification to the landscape by changing the slope angle of the bank might be necessary when the influence of vegetation is incorporated as an increase in friction angle of soil.

In laboratory scale, as in this study, timber sheet pile-vegetation earth retaining systems show promises to be used for stream bank protection. Future studies need to focus on field scale system level studies and quantification of reinforcement of vegetation in presence of multiple species of vegetation.

# SAMENVATTING

Nederland heeft een uitgebreid netwerk van rivieren en kanalen voor o.m. irrigatie, transport en waterafvoer. De oevers langs kanalen worden ofwel beschermd door grondkerende constructies zoals damwanden, beschoeiingen of onbeschermd gelaten. Een groot deel van de kunstmatige damwanden die worden gebruikt om de oevers in Nederland te beschermen is gemaakt van hout. Om houten damwanden te maken wordt o.m. tropisch hardhout zoals Azobé (*Lophira alata*) gebruikt vanwege de hoge natuurlijke duurzaamheid. Grenen afkomstig uit Europa wordt ook toegepast, en wordt verduurzaamd om voldoende weerstand tegen biologische degradatie te hebben.

Een nieuwe grondkerende constructie is ontwikkeld, gemaakt van lokaal beschikbaar naaldhout en vegetatie. Hiermee kunnen kanaaloevers worden uitgerust, als alternatief voor de momenteel gebruikte oeverbeschermingsconstructies. Een dergelijke constructie vermindert het materiaalgebruik, maar is ook milieuvriendelijker dan 'harde' oeverconstructies die nu in gebruik zijn.

Hoewel bekend is dat wortels van vegetatie de afschuifsterkte van de grond verhogen, is het positieve effect van vegetatie in de grond nog onvoldoende bekend en gekwantificeerd. Vegetatiewortels in een wortel-grondcomposiet worden voornamelijk op trek belast, en gedragen zich dus vergelijkbaar met staal in gewapend beton. Twee typen vegetatie, nl. *Humulus lupulus* L. en *Salix fragilis* L. zijn gekozen voor het onderzoek op basis van hun potentieel om oevers te versterken: de lokale beschikbaarheid, de wortelkenmerken en de groeiomstandigheden, waar onder bv. de weerstand tegen een hoge grondwaterspiegel.

Een uitgebreide reeks van laboratoriumproeven is uitgevoerd om de sterkte van de wortels, de wortel-grondcomposiet, alsmede het gedrag van de combinatie van vegetatie en houten damwand als systeem te kunnen bestuderen en karakteriseren. De resultaten van het experiment zijn verder geanalyseerd om benaderingen te ontwikkelen voor het ontwerp van het geïntegreerde houten damwand-vegetatiesysteem. Om het gedrag van wortel-grondcomposiet bij afschuiving te bestuderen, is een grootschalige opstelling gebouwd voor het uitvoeren van tests op afschuiving, zowel verplaatsingsgestuurd als belastingsgestuurd. Om de omstandigheden van de kanaaloever zo goed mogelijk te simuleren zijn alle monsters getest in verzadigde omstandigheden en bij een lage zijdelingse druk. Zuivere grond en bewortelde grondmet *Humulus lupulus* L. en *Salix fragilis* L. zijn zowel verplaatsingsgestuurd als krachtsgestuurd getest. Na iedere test zijn de wortels uitgegraven is de oriëntatie, de diameter en de biomassa geanalyseerd. De monsters met wortels vertoonden een hogere wrijvingshoek in vergelijking met zuivere grond. Contractief gedrag van grondmonsters met wortels gedragen zich anders dan zuivere grondmonsters. Het Het Burgers model is geschikt om het tijdsafhankelijk gedrag zoals gemeten in de proeven te beschrijven.

Wortels van *Humulus lupulus* L. en *Salix fragilis* L. zijn getest in zowel natte als droge omstandigheden waarbij voor *Humulus lupulus* L. twee diameters ter beschikking ston-

den. Naast een volume-effect, werd een significant verschil in treksterkte tussen nat en droog waargenomen voor *Salix fragilis* L. maar niet voor *Humulus lupulus* L.

Met behulp van een fysiek model is het gedrag van het houten damwand -vegetatie systeem nader onderzocht. Een wortelsysteem vergelijkbaar met dat van *Humulus lupulus* L. is hiertoe 3D-geprint met PLA-materiaal. Een vergelijking van een onversterkte oever en een oever versterkt met wortelanalogiën heeft aangetoond dat de aanwezigheid van wortels het volume van de grond dat moet worden gemobiliseerd vergroot. Bij de meest efficiënte ruimtelijke verdeling van de wortels, bleek de grond in staat een 2x zo hoge druk te weerstaan. Vervolgens is een eindige-elementenmodel gemaakt waarin het effect van wortels als een verhoogde cohesieparameter is opgenomen. Het model is in staat het bezwijken van de grond goed te voorspellen. Uit een parametrische analyse volgt dat de invloed van de ruimtelijke verdeling van de wortels op de krachten op de damwand groter is nadat een drempelwaarde van extra cohesie is bereikt. Dat impliceert dat eventuele extra cohesie na deze drempelwaarde mogelijk geen extra voordelen voor de stabiliteit oplevert. De resultaten geven aan dat vegetatie met meer ruimtelijk verdeelde wortels geschikter zal zijn om te worden gebruikt in houten damwand-vegetatiekeringen.

Ten slotte zijn twee mogelijke ontwerpbenaderingen van een houten damwand -vegetatiesysteem onderzocht. De systeembenadering is gebaseerd op het concept dat de mechanische versterking van de grond met groei van vegetatie zou kunnen resulteren in een vermindering van de horizontale gronddruk tegen de damwand. Hierdoor verminderen de buig- en schuifspanningen die over de levensduur op de damwand inwerken, waardoor het langeduuereffect van de belasting wordt verminderd. Daarmee kan een gedeelte van de biologische degradatie worden gecompenseerd. Het gedeelte van de houten damwand dat zich onder de waterlijn bevindt, is over het algemeen minder vatbaar voor biologische aantasting. In de discrete benadering wordt de vegetatie waargenomen als ondersteunend aan de bovenste delen van de oever (< 2 meter) nadat houtdegradatie is opgetreden. Het effect van vegetatie wordt geanalyseerd als zowel een toename van de interne wrijvingshoek alsmede een toename van de cohesie, op beekoever met een steunhoogte van 2 m en 3 m. Door de gekozen systeembenadering wordt een verlenging van de levensduur van het houten damwand-vegetatiesysteem bereikt, in vergelijking met uitsluitend een houten damwand aanwezig is. Bij de discrete benadering werd waargenomen dat een verandering van de hellingshoek van de oever noodzakelijk kan zijn wanneer de invloed van vegetatie wordt meegenomen als een toename van de wrijvingshoek van de grond.

Op laboratoriumschaal is aangetoond dat een combinatie van een houten damwand met vegetatie een realistisch alternatief kan zijn voor bestaande oeverconstructies. Bij een pilot-study in het veld, moet nader aandacht worden besteed aan het type van de vegetatie en de daarmee samenhangende versterking van de grond.

# LIST OF FIGURES

|      |  |    |
|------|--|----|
| 1.1  | a) failure of banks due to insufficient protection. b) unprotected bank. c) canal banks with natural protection, willows growing along canals. d) long unprotected streams in the rural areas of the Netherlands. . . . .  | 4  |
| 1.2  | Example of current situation in the Netherlands. Canal banks are protected by wooden structures, left unprotected or natural vegetation growing along the banks providing partial protection. . . . .  | 4  |
| 1.3  | Decay of timber sheet pile. The decay is more prone in the air-soil-water interface and the sheet pile below the water level shows high resistant to decay. . . . .  | 6  |
| 1.4  | From unprotected stream bank to stream bank protected by timber sheet pile and vegetation. . . . .   | 7  |
| 2.1  | a) HL and SF grown in Botanical garden TU Delft b) Shear testing setup c) Fine root collection d) Coarse root excavation . . . . .   | 17 |
| 2.2  | Particle size distribution of representative soil sample from the volume of soil used obtained by wet sieving . . . . .  | 18 |
| 2.3  | Large direct shear testing setup. a) Displacement controlled tests b) Load controlled tests. . . . .   | 19 |
| 2.4  | Estimation of vertical displacement at center (C) of the top plate using vertical displacements of three vertical displacements recorded at (x1, y1, z1), (x2, y2, z2), (x3, y3, z3) which is (0, -15.2, 0), (-11.8,12.8,0), (11.8,12.8,0) respectively. . . . . | 21 |
| 2.5  | Vertical root orientation of D_HL_50_1 and D_SF_50_1. (Terminology: Displacement controlled (D), <i>Humulus lupulus</i> L. (HL), <i>Salix fragilis</i> L. (SF), Normal load (50 kg), 1-repetition number) . . . . .  | 23 |
| 2.6  | Bare soil stress-controlled tests at two different normal stress levels: a) 4.4 kPa, and b) 6.4 kPa. . . . .   | 23 |
| 2.7  | HL stress-controlled tests at two different normal stress levels: a) 4.4 kPa, and b) 6.4 kPa. . . . .  | 25 |
| 2.8  | SF stress-controlled tests at two different normal stress levels: a) 4.4 kPa, and b) 6.4 kPa. . . . .  | 25 |
| 2.9  | Horizontal strain measured over time at a normal stress of 6.4kPa and fitted Burger model for load controlled direct shear tests performed on: a) bare soil, b) soil with roots of HL, and c) soil with roots of SF . . . . .                                    | 26 |
| 2.10 | Variation of Burger model parameters over the holding stress applied in each loading step for bare soil, soil with roots of HL, soil with roots of SF. . . . .   | 27 |
| 2.11 | Peak stress vs effective normal stress envelope for bare soil, HL, SF of samples tested in large scale direct shear apparatus . . . . .  | 29 |

|   |    |
|---|----|
| 2.12 Peak stress ratio vs the ratio between the vertical and horizontal displacement ( $dy/dx$ ) of bare soil, HL, SF in all tested specimens. . . . .  | 29 |
| 2.13 Schematic illustration of effect of confining pressure on the contribution of root permeated soils. (Adapted from [54]) . . . . .  | 33 |
| 2.14 Corrected stress-displacement plot of bare soil. The first section on the title depicts the control (D for displacement controlled, L for load controlled), the second section depicts the soil type (S-bare soil, HL- <i>Humulus lupulus</i> L., SF- <i>Salix fragilis</i> L.), Third section depicts the normal load applied (50 for 50kg, 100 for 100kg, 200 for 200 kg), fourth section depicts the repetition number. . . . .   | 36 |
| 2.15 Vertical displacement vs Horizontal displacement of bare soil. The first section on the title depicts the control (D for displacement controlled, L for load controlled), the second section depicts the soil type (S-bare soil, HL- <i>Humulus lupulus</i> L., SF- <i>Salix fragilis</i> L.), Third section depicts the normal load applied (50 for 50kg, 100 for 100kg, 200 for 200 kg), fourth section depicts the repetition number. . . . .                             | 37 |
| 2.16 Corrected stress-displacement plot of HL. Corrected stress-displacement plot of bare soil. The first section on the title depicts the control (D for displacement controlled, L for load controlled), the second section depicts the soil type (S-bare soil, HL- <i>Humulus lupulus</i> L., SF- <i>Salix fragilis</i> L.), Third section depicts the normal load applied (50 for 50kg, 100 for 100kg, 200 for 200 kg), fourth section depicts the repetition number. . . . . | 38 |
| 2.17 Vertical displacement vs Horizontal displacement of HL. The first section on the title depicts the control (D for displacement controlled, L for load controlled), the second section depicts the soil type (S-bare soil, HL- <i>Humulus lupulus</i> L., SF- <i>Salix fragilis</i> L.), Third section depicts the normal load applied (50 for 50kg, 100 for 100kg, 200 for 200 kg), fourth section depicts the repetition number. . . . .                                    | 39 |
| 2.18 Corrected stress-displacement plot of SF. Corrected stress-displacement plot of bare soil. The first section on the title depicts the control (D for displacement controlled, L for load controlled), the second section depicts the soil type (S-bare soil, HL- <i>Humulus lupulus</i> L., SF- <i>Salix fragilis</i> L.), Third section depicts the normal load applied (50 for 50kg, 100 for 100kg, 200 for 200 kg), fourth section depicts the repetition number. . . . . | 40 |
| 2.19 Vertical displacement vs Horizontal displacement of SF. The first section on the title depicts the control (D for displacement controlled, L for load controlled), the second section depicts the soil type (S-bare soil, HL- <i>Humulus lupulus</i> L., SF- <i>Salix fragilis</i> L.), Third section depicts the normal load applied (50 for 50kg, 100 for 100kg, 200 for 200 kg), fourth section depicts the repetition number. . . . .                                    | 41 |
| 2.20 Root distribution of HL at different orientations. The first section on the title depicts the control (D for displacement controlled, L for load controlled), the second section depicts the vegetation type (HL for <i>Humulus lupulus</i> L.), Third section depicts the normal load applied (100 for 100kg, 50 for 50kg, 200 for 200 kg), fourth section depicts the repetition number. . . . .   | 42 |

|      |   |    |
|------|---|----|
| 2.21 | Root distribution of SF at different orientations. The first section on the title depicts the control (D for displacement controlled, L for load controlled), the second section depicts the vegetation type ( SF for <i>Salix fragilis</i> L.), Third section depicts the normal load applied ( 100 for 100kg, 50 for 50kg, 200 for 200 kg), fourth section depicts the repetition number. . . . . | 43 |
| 3.1  | Testing setup: (a) root attached to the clamps and extensometer, and (b) wet tissue used to maintain the moisture content stable in the root during the load-control tests. . . . .   | 56 |
| 3.2  | Illustration of the loading steps of the load-controlled test. . . . .  | 57 |
| 3.3  | Representative load-displacement curve of dry and wet root samples, HLD-HLW . . . . .   | 58 |
| 3.4  | Variation of tensile strength and Young's modulus of HLW with diameter and tensile stress respectively. . . . .   | 59 |
| 3.5  | Variation of tensile strength and Young's modulus of SFW with diameter and tensile stress respectively. . . . .   | 60 |
| 3.6  | Variation of tensile strength and Young's modulus of HLD with diameter and tensile stress respectively. . . . .   | 60 |
| 3.7  | Variation of tensile strength and Young's modulus of SFD with diameter and tensile stress respectively. . . . .   | 60 |
| 3.8  | Box plots showing the variation in tensile strength and Young's modulus. The dots represent outliers, the Boxes represent the 25%-75% percentile variation. . . . .   | 61 |
| 3.9  | Load-displacement (left end side) and $\log(t/t_1)$ versus $\log(s/s_1)$ (right end side) in load-controlled tests on roots with a diameter of 2.16mm. a) and b) for root number 1, c) and d) for root number 2, e) and f) for root number 3. . . . .   | 64 |
| 3.10 | Load-displacement (left end side) and $\log(t/t_1)$ versus $\log(s/s_1)$ (right end side) in load-controlled tests on roots with a diameter of 3.6mm. a) and b) for root number 1, c) and d) for root number 2, e) and f) for root number 3. . . . .  | 65 |
| 3.11 | Load-displacement (left end side) and $\log(t/t_1)$ versus $\log(s/s_1)$ (right end side) in load-controlled tests on roots with a diameter of 3.6mm. a and b for root number 4, c and d for root number 5, e and f for root number 6. . . . .  | 66 |
| 3.12 | N value vs stress level. . . . .  | 67 |
| 3.13 | Prediction of time to failure. . . . .  | 68 |
| 3.14 | Burger and power law model fitted to experimental strain-time curves of root of diameter 2.16 mm.a) and b) for root 1, b) and c) for root 2, e) and f) for root 3. . . . .  | 72 |
| 3.15 | Burger and power law model fitted to experimental strain-time curves of root of diameter 3.6 mm. a) for root 1, b and c) for root 2, d) for root 3,e) and f) for root 4. . . . .  | 73 |
| 3.16 | Burger and power law model fitted to experimental strain-time curves of root of diameter 3.6 mm. a), b), c) for root 5, d) for root 5. One extra root test loaded for 300000 s is shown. . . . .  | 74 |
| 4.1  | Three different zones of roots in a <i>Humulus lupulus</i> L. plant [26] . . . . .  | 84 |

|      |  |     |
|------|--|-----|
| 4.2  | Root architecture of <i>Humulus lupulus</i> L. modelled in AutoCAD. The DWG file can be obtained from the repository 10.5281/zenodo.4555335 . . . . .  | 85  |
| 4.3  | Area of roots of the model root with depth. The area of roots is the sum of the cross-section area of all roots crossing a horizontal plain at a given depth                                   | 86  |
| 4.4  | Dimensions of the physical model container and positioning of the sheet pile. . . . .  | 87  |
| 4.5  | Sensors used in the physical model and dimensions of the embankment. .   | 88  |
| 4.6  | Plan view of the stream embankment. Location of tap root within the embankment according to the root placement geometry 1 (Root pattern 1) (a) and geometry 2 (b) (Root pattern 2) . . . . .   | 89  |
| 4.7  | Testing method used in the physical model . . . . .  | 90  |
| 4.8  | Horizontal displacement of sheet pile with drawdown depth. . . . .   | 91  |
| 4.9  | Vertical displacement measured at a distance of 150 mm from the timber sheet pile in the stream embankment. . . . .  | 91  |
| 4.10 | Horizontal displacement of soil particles in the stream embankment in bare soil test, obtained from PIV) . . . . .   | 92  |
| 4.11 | Horizontal displacement of soil particles in the stream embankment in the root pattern-1 test, obtained from PIV. . . . .  | 93  |
| 4.12 | Node fixities and model mesh . . . . .   | 95  |
| 4.13 | Location of rooted area in root pattern 1 in the model . . . . .   | 96  |
| 4.14 | Comparison of experimentally measured and predicted a) horizontal displacement of the sheet pile, and b) vertical displacement in the embankment with bare soil. . . . .                       | 97  |
| 4.15 | Comparison of experimentally measured and predicted a) horizontal displacement of the sheet pile, and b) vertical displacement in the embankment in the test with the root pattern-1 . . . . . | 97  |
| 4.16 | Horizontal displacement contour from the simulation of the bare soil test.   | 98  |
| 4.17 | Horizontal displacement contour from the simulation of the root pattern-1 test. . . . .  | 99  |
| 4.18 | Top view of the root area patterns (RAP) evaluated in this study. . . . .  | 101 |
| 4.19 | Top view of the root area patterns (RAP) evaluated in this study. . . . .  | 102 |
| 4.20 | Normalised sheet pile displacement and bending moment with variation of cohesion for different root area pattern (RAP) . . . . .   | 104 |
| 4.21 | Failure wedge formation in bare soil a) 5cm drawdown b) 10 cm drawdown c) 12 cm drawdown d) 14 cm drawdown. . . . .  | 106 |
| 4.22 | Failure wedge formation in root pattern-1 a) 5cm drawdown b) 10 cm drawdown c) 15 cm drawdown d) 17 cm drawdown. . . . .   | 107 |
| 4.23 | Failure wedge formation in root pattern-2 a) 5cm drawdown b) 10 cm drawdown c) 15 cm drawdown d) 25 cm drawdown. . . . .   | 108 |
| 5.1  | Approaches for design of timber sheet pile-vegetation system. . . . .  | 117 |
| 5.2  | Dimensional characteristics of the timber sheet pile-vegetation system investigated in SA. . . . .   | 119 |

---

|     |  |     |
|-----|--|-----|
| 5.3 | Twin-wood sheet pile, combination of tropical hardwood and softwood resulting in improved service life. (Taken from FORECO hout producten. <a href="https://www.foreco.nl/nl/producten/twinwood">https://www.foreco.nl/nl/producten/twinwood</a> ) . . . . . | 120 |
| 5.4 | Illustration of a 2 m and 3 m retaining head without the presence of vegetation (2m: Case 1 and 3m: Case 2, respectively) in DA. . . . .   | 123 |
| 5.5 | Illustration of 2m Case 3 and 3m Case 3 in DA . . . . .  | 123 |
| 5.6 | Illustration of 2m Case 6 and 3m Case 6 in DA . . . . .  | 124 |
| 5.7 | Illustration of 2m Case 8 and 3m Case 8 in DA . . . . .  | 124 |
| 5.8 | Damage accumulation a) in bending b) in shear . . . . .  | 126 |



# LIST OF TABLES

|     |  |     |
|-----|--|-----|
| 2.1 | Vegetation biological properties: above ground and below ground biomass (Rounded off to nearest gram). Shoot diameter of SF, number of shoots of HL. Specimens are named as follows, the first letter specifies the type of test (D-displacement controlled L-Load controlled), followed by species (HL- <i>Humulus lupulus</i> L., SF- <i>Salix fragilis</i> L.), followed by normal load applied in kg, (50,100,200), followed by repetition number. Eg. D_HL_50_1 represents displacement-controlled test on <i>Humulus lupulus</i> L. at 50kg normal load, first repetition. . . . . | 24  |
| 3.1 | Overview of the methods and moisture conditions of the tensile strength testing. . . . .   | 53  |
| 3.2 | Summary of the root sampling and soil moisture adopted for each root . .   | 54  |
| 3.3 | Tensile strength of the different testing conditions and species (HLW, HLD, SFW, SFD): used equations, fitting parameters, coefficient of determination ( $R^2$ ), p-value, . . . . .  | 59  |
| 3.4 | Young's modulus of the different testing conditions and species (HLW, HLD, SFW, SFD): used equations, fitting parameters, coefficient of determination ( $R^2$ ), p-value, . . . . .   | 59  |
| 3.7 | Burger model parameters 3.6 mm root . . . . .  | 62  |
| 3.5 | Burger model parameters 2.16 mm root . . . . .   | 62  |
| 3.6 | Power law model parameters 2.16 mm root . . . . .  | 62  |
| 3.8 | Power law model parameters 3.6 mm root . . . . .   | 63  |
| 4.1 | Mechanical properties of PLA and <i>Humulus lupulus</i> L. . . . .   | 84  |
| 4.2 | Input properties of soil and sheet pile used in the PLAXIS 3D modelling . .  | 96  |
| 4.3 | Cohesion distribution used in the parametric analyses . . . . .  | 100 |
| 4.4 | Soil properties for the soil model . . . . .   | 100 |
| 4.5 | Timber sheet pile properties . . . . .   | 100 |
| 5.1 | Summary of all the cases analysed in the system approach . . . . .   | 119 |
| 5.2 | Summary of all cases analysed in the discrete approach. TSP-timber sheet pile . . . . .  | 122 |
| 5.3 | Input parameters to PLAXIS 3D. . . . .   | 125 |
| 5.4 | Maximum bending moment and shear force acting on the timber sheet pile obtained from PLAXIS 3D . . . . .   | 125 |
| 5.5 | Soil and sheet pile properties used for safety analysis . . . . .  | 127 |
| 5.6 | Safety factors obtained for various cases analysed according to the DA. . .  | 127 |
| 5.6 | Safety factors obtained for various cases analysed according to the DA. . .  | 128 |



# PREFACE

During conducting research reported in this dissertation a conscious and sincere effort was taken to "discover new oceans by leaving the shores" or in simple words risks associated with conducting experiments aimed at innovation was not avoided and new perspectives were explored.

The crux in preparing this dissertation lay in the preparing all the testing setups from scratch.

I hope you have a good time reading the dissertation.

*Abhijith Chandrakaran Kamath  
Delft, July 2021*



# ACKNOWLEDGEMENTS

I would like to thank each and everyone who supported me during the past few years. First of all I would like to thank my supervisors Wolfgang and Jan-Willem for giving me this opportunity to work on such a interesting and challenging project. I really appreciate both of you for being patient with my style of working and the amount of time you have spent to train me in improving my communication and technical skills. Finally, I want to thank you also for the support in my daily life (from having a roof over my head to listening to all the other things that I have complained about). Cristina, firstly I would like to thank you for all the discussions, meeting and advises you have given. You were always there to advice me at the right time, when I was lost. To most of our meeting I used to come overwhelmed with problems and you made sure I leave your office happy.

I could not have completed this thesis without my friends at Delft. Delft quintet (Jishnu, Manu, Aj, AM), for everything from letting me stay with you on the first days to cooking together to the long discussions, getting me on right track whenever I was lost. You guys were always there for me in one way or another. Viswajeeth, bhayya, thanks for being there, talking to me in the past years. Chris, George, Geo, Narasimhan, Aswin, made my life less stressful with the "Koodiyalo" question every now and then. I would like to thank the whole KSA team for all the celebrations we had together. I enjoyed all the discussion in the gym I had with RV, Aravind, Adeep which made my evenings for many months. Theres, I am grateful to you for all the fun we had together. Preetha, thanks for dropping by few times during the corona period.

This thesis would not have been possible without the excellent support from the laboratory colleagues. John and Louis, thanks for all the help, dutch lessons and making days in lab fun. Ruben, thanks for making all the boxes for testing. Cees, Fred, Ron, Giorgios, Paul, I really appreciate stepping up for me when I come with problems. Marco, I could not have completed this thesis without your patience and help in conducting the tests towards the end. Reuben Joseph, I really want to thank you for all the support in testing and sharing of frustrations during the corona period and beyond.

A majority of my PhD life was spent in the botanical garden of TU delft, I would like to thank Bob Ursem for giving me the opportunity to work in the garden. I would like to thank all the Botanical garden staff, Dan for helping me throughout, Hans and Ernst for giving me advices, Sabine for all the chats, and everyone in the garden for the advice and support.

I would like to thank all my colleagues and then ESR's from the TERRE group. All the meeting were fruitful technically and fun to attend. Sofia, I do not know how to thank you for all your efforts in reading, commenting on my thesis, long discussions about everything under the sun, helping me become a better human being, I will cherish all the memories.

Govind I really appreciate your help with the cover page and all the lunch breaks. Manu, every time I called you with problems in my thesis or other issues you have solved

it for me, I cannot thank you enough for all that effort. Michele, I would like to thank you for your patience answering all my administrative questions. Xiuli, Rui, Linda you guys made my life in office fun. Rui, thanks for helping me train in gym, Xiuli, thanks for being my best buddy and confidante, listening to my daily frustrations, feeding me and helping me with my work. Peter, thanks for being supportive with everything in the lab and for being patient with the mess we had in the lab. Geert, the hundreds of calculations we did for the manual, really kicked off my PhD work on timber sheet pile design, thanks for the opportunity.

My family, Appa, Amma, Anjukka, Dudumma, Annu , Paru, has been my backbone in my life. I apologize for being far away from you all and not calling you everyday. All those calls, voice messages from dudumma used to make me smile even during hard times. Last one year had been a real challenge for me with uncertainties and challenges in my work, personal and social life, I do not think I could have overcome those difficulties without the unconditional support of my parents and my home girl who listened to me whenever I needed.

# 1

## INTRODUCTION

*"To have one basis for life and another for science is apriori a lie."*  
Karl Marx



## 1.1. BACKGROUND

Ensuring sustainable development is the need of the hour. Increase in carbon emissions and subsequent climate change poses the greatest challenge in sustainable development goals. The construction industry is a major contributor to the carbon emissions in the world. European commission aims at reducing the carbon emissions in construction industry by 90% by 2050. European commission training network TERRE aimed to train new generations of engineers and scientists in carbon efficient design of civil infrastructure. This PhD thesis is part of the objective 3 “Develop/implement novel structural materials for concrete/steel-free geostructures” of the training network TERRE. Thus, the overarching goal of this thesis is to study the use of natural materials and its implementation in geotechnical construction purposes. Canals, among other features, are one of the prominent landmark features of the Netherlands. This thesis evaluates the prospects of nature-based construction, specifically a combination of timber sheet pile-vegetation systems, to protect the banks of the canals.

Protecting land and nutrient rich soil from being washed away by water has always been of concern to humans. The Netherlands has thousands of kilometers of canals, river and streams. The bank of these water ways is either unprotected or protected by hard banks made of materials like concrete, steel, rock, timber etc. Construction works in unprotected banks are necessary to prevent the loss of soil by bank failure and loss of bank biodiversity. Maintenance work goes on all around the year to protect the ‘hard’ engineered banks. Millions of Euro’s are spent on such activities by local authorities, national and regional governments. Currently, these activities rely on conventional construction materials and techniques, which contribute to carbon emissions and result in non-natural embankments. Non-natural embankments affect the establishment of natural flora and fauna and brings changes in natural landscape of the area.

From over the 7000km of protected stream banks in the Netherlands, about 3500km is made of timber sheet piles. The timber sheet piles are made of either impregnated softwood or durable tropical hardwood. Of the other materials (stone, concrete, steel etc) used for protecting the stream banks timber is the most carbon friendly material. Hardwood timber is less susceptible to decay and hence favorable to be used in extreme decay probable conditions like the stream banks with air-water-soil interface. However, the Netherlands has minimum exploitable hardwood timber to be used for sheet piles. Currently, the timber is imported from other continents like Africa and South America. This results in incurring direct transportation costs and making the material less carbon friendly to be used in the Netherlands. This calls for the use of locally available material which reduces the impact of transportation related carbon emission on the material. However, the locally available timber, softwood or less durable hardwood, is prone to decay and hence less durable than durable hardwoods. These locally available timber is subjected to surface treatment to make it resistant to bacterial attacks and exposure to atmosphere when used.

Apart from the banks protected by conventional protection techniques, there exist a larger part of regions where banks are left unprotected, see (Fig.1.1). Such banks are susceptible to bank failure. Sometimes, natural vegetation grows along these canals giving partial protection to the soil, see (Fig.1.2).

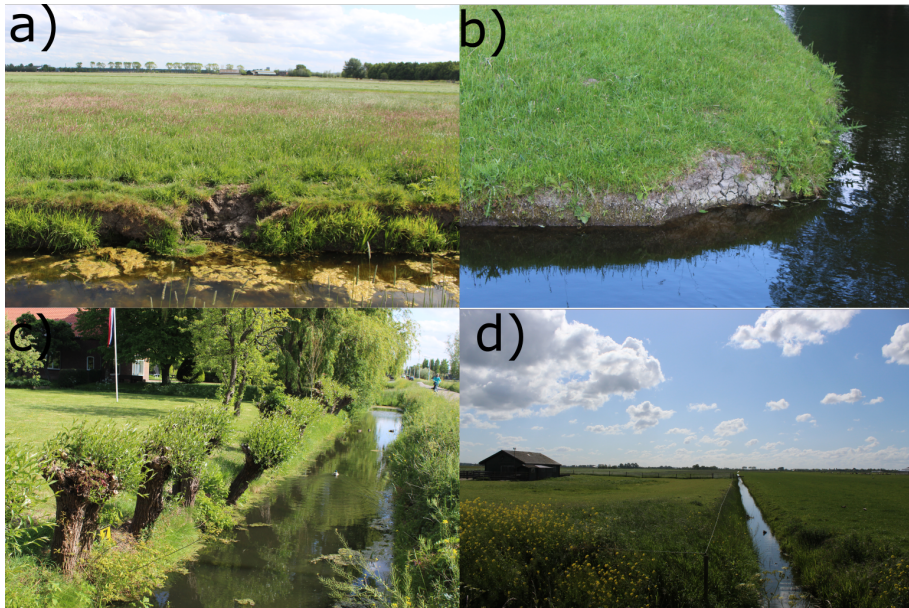


Figure 1.1: a) failure of banks due to insufficient protection. b) unprotected bank. c) canal banks with natural protection, willows growing along canals. d) long unprotected streams in the rural areas of the Netherlands.



Figure 1.2: Example of current situation in the Netherlands. Canal banks are protected by wooden structures, left unprotected or natural vegetation growing along the banks providing partial protection.

## 1.2. PROBLEM STATEMENT

Vegetation has always been an integral part in sustaining human life. It takes a variety of roles ranging from providing food and shelter to regulating earth's energy balance. Humans have a long history of managing vegetation to serve a variety of purposes, for example wood from trees have been used for construction purposes while with the onset of agriculture certain crops were grown in ever larger scales to produce food. It is intuitive to believe that agriculture and soil erosion would have been a concurrent process and evidences of use of vegetation to prevent erosion even at the beginning of BC period supports this assumption [1]. A study of the evolution of bioengineering techniques by [1] shows evidence of use of woody species to stabilize river banks dated back from 16<sup>th</sup> century. Prominent examples include that of King Frederick William I of Prussia who ordered to plant Willow (*Salix*) on river banks and that of Dugied in France, who suggested to plant exotic species like Chinese Varnish tree (*Toxicodum\_verricifluum* (Stokes) F. Barkley) and White Mulberry (*Morus\_alba* L.) to form dense barriers along streams [1, 2].

In the last five decades research has focused on understanding various mechanisms by which vegetation reinforces soil. In general presence of vegetation improves the soil shear strength through hydrological [3, 4] and mechanical [5, 6] reinforcement effects. The mechanical reinforcement is generally seen in a cohesion-anchorage spectrum, where the presence of fine roots result in a soil-root matrix with increased cohesion, while coarse roots allow for anchorage of potential unstable layers to stable soil layers. Evapotranspiration results in a decrease in soil moisture content and thereby exerting "suction" reinforcement on the soil. Vegetation is also seen to alter the hydraulic properties of the soil due to the presence of roots [7]. Other reinforcement effects of vegetation include buttressing and arching, which are generally considered static due to their slow nature and gradual increment [8].

As mentioned, above, durable tropical hardwood timber sheet pile is employed in many rural and urban regions to protect stream banks. Sometimes, tropical hardwoods used to make sheet pile to protect stream banks may not be locally available, and have to be imported. Hence, locally available wood which has low resistant to decay compared to tropical hardwoods might have to be used. Among other factors, in addition to biological decay, the service life of wood is determined by magnitude and duration of the load acting on it. A timber sheet pile-vegetation composite stream bank protection structure is proposed in this study as an alternative to currently employed conventional methods. The use of natural materials in construction gives the added benefits of flexibility and resilience in the design.

The role of vegetation in a timber sheet pile-vegetation system can be perceived in two ways. Firstly, the mechanical reinforcement of the soil with growth of vegetation could result in a reduction of horizontal pressure against the sheet pile, bending moments and shear stresses acting on the sheet pile over time, thereby decreasing the duration of load effect in the timber and counteracting the effects of slow biological degradation of wood in air-water-soil conditions. Secondly, the vegetation can be perceived as supporting the top parts of the bank (< 2meters) after timber decay has occurred. The timber sheet pile is less resistant to decay in these top layers of soil where there is a soil-water-air interface See (Fig.1.3).

Bio engineered earth retaining system (BEERS) are the complex systems which require design methods combining knowledge from the disciplines of bio-engineering, structural engineering and geotechnical engineering. According to current design methodology of BEERS involves the combination of an inert element and a live element. Wood, stone rip-raps, bamboo, willow bundles or geocells are the commonly used inert elements. The live elements used are plants (grasses, shrubs) or trees. The combination of inert and live elements supports the slope for a certain period until the vegetation is established to such a level that it is and able to retain the soil on its own. A transient load transfer from the inert material to the soil with vegetation reinforcement is a key factor in the design. Therefore, BEERS design is done in a time dependent framework, with number of iterations to check for interim stability and component strength. Bio-engineered soil-inert structure interactions and variations in earth pressure are additional aspects in the design of BEERS compared to bio-engineering slopes. Vegetated crib walls [9] is an examples of BEERS.

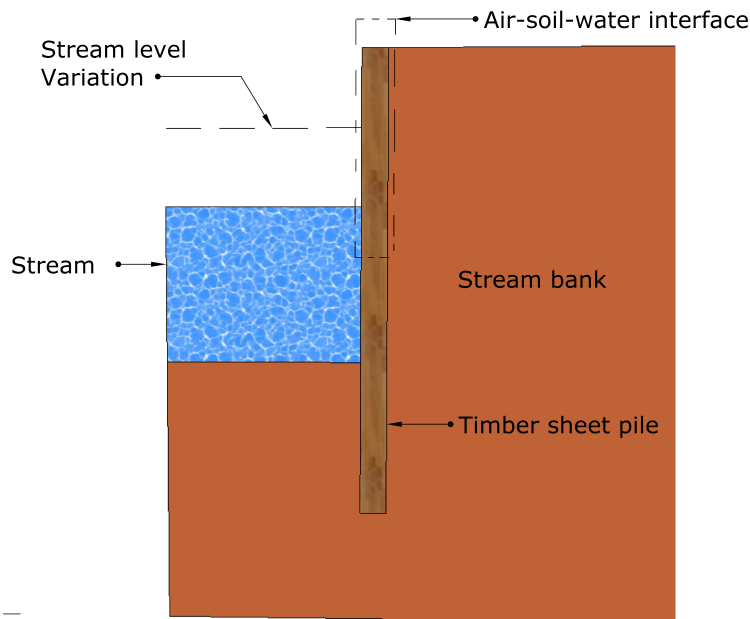


Figure 1.3: Decay of timber sheet pile. The decay is more prone in the air-soil-water interface and the sheet pile below the water level shows high resistant to decay.

This thesis aims to advance the current knowledge of BEERS in an element scale, composite scale and system scale in a time framework. BEERS consist of vegetation roots, soil and wood in the element scale. This thesis focuses on investigating tensile strength of roots in element scale. On the composite scale the root-soil composite is studied and on the system scale timber sheet pile-vegetation system is investigated. An extensive experimental program was planned and executed to characterize the behavior of roots, root soil composite and root-soil-wood system behavior. Root soil composite

was tested in shear using a newly developed Dual controlled large-scale shear testing equipment (DCLS) in the Biobased structures and Material laboratory at TU Delft. The effect of roots on peak stress, vertical deformation and time dependent behavior was investigated. Further, the mechanical behavior of roots in tension was investigated in different loading conditions and moisture content. A physical model was developed to characterize the soil-root-wooden sheet pile system, in which roots were 3D printed. Finally, two approaches to include the effect of vegetation in timber sheet pile-vegetation system is discussed.

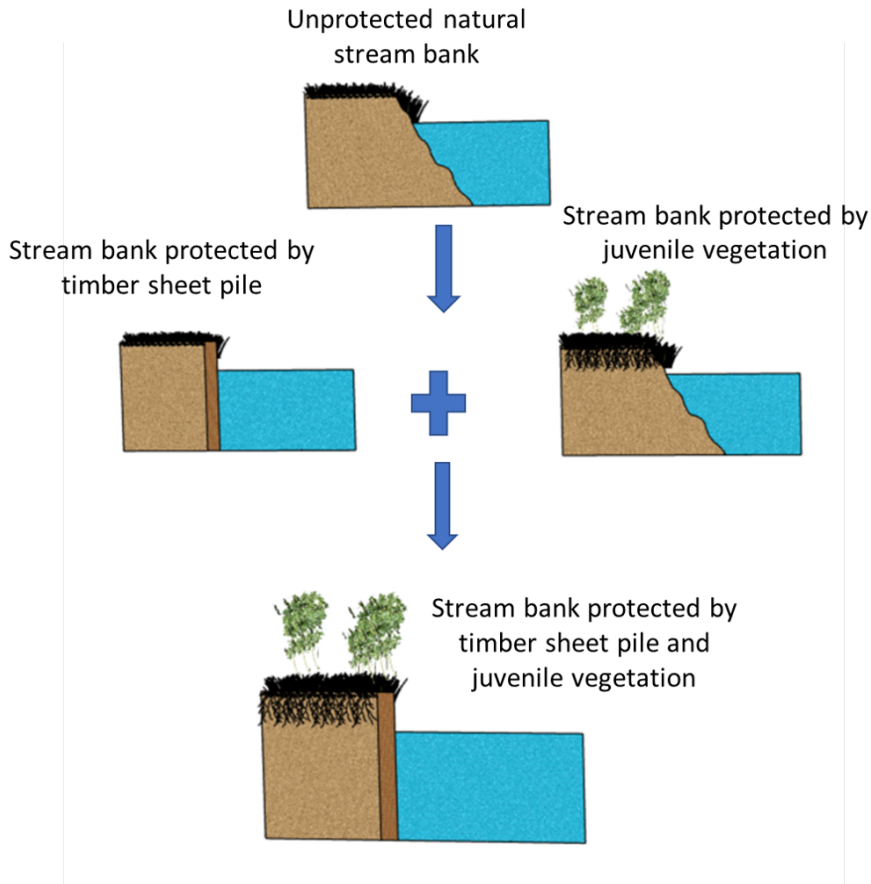


Figure 1.4: From unprotected stream bank to stream bank protected by timber sheet pile and vegetation.

### 1.3. RESEARCH OBJECTIVES

The key objectives of this thesis are as follows:

- Determine the effect of roots on shear strength characteristics, vertical deformation and time dependent behavior of root permeated soils. Determine the effect of root spatial pattern on shear strength of soil-root mixture;

- Characterize the tension strength of roots of the selected vegetation. Understand the time dependent behavior of tension strength of roots and tension strength in different moisture conditions;
- Asses the behavior of a timber sheet pile-vegetated earth retaining system using a physical model;
- Asses a service life approach for a combined effect of load and decay for the design of timber sheet pile-vegetation retaining system;

#### 1.4. THESIS ORGANIZATION

The thesis is organized into four independent chapters apart from this chapter and conclusions with the intention of publishing the four chapters into research papers.

Chapter 2 shows the development of a test setup for determining shear strength of root permeated soil and discusses the results from shear tests on root-soil composites. It identifies the influence of roots on the dilatancy of the soil and shear strength characteristics. Further it identifies preferable properties of roots for soil reinforcement.

Chapter 3 reports the results of tensile test on roots. The chapter studies the effects of moisture content and loading mechanism on the tensile strength of roots. How the roots behave under sustained load is studied in this chapter.

Chapter 4 studies the BEERS on system scale. The effects of root reinforcement on the failure pattern and the displacement of the sheet pile is reported.

Chapter 5 reports results of the modelling of soil-root-wooden sheet pile system. The increase in service life due to the presence of roots and its variation is reported.

Chapter 6 concludes the results as a whole and identifies the recommendation for future studies.

## REFERENCES

- [1] A. Evette, S. Labonne, F. Rey, F. Liebault, O. Jancke, and J. Girel, *History of bioengineering techniques for erosion control in rivers in western europe*, Environmental management **43**, 972 (2009).
- [2] P-H. Dugied, *Projet de boisement des Basses-Alpes: présenté à SE le Ministre Secrétaire d'état de l'Intérieur* (De l'Imprimerie royale, 1819).
- [3] D. Boldrin, A. Leung, and A. Bengough, *Hydrologic reinforcement induced by contrasting woody species during summer and winter*, Plant and Soil **427**, 369 (2018).
- [4] N. Pollen-Bankhead and A. Simon, *Hydrologic and hydraulic effects of riparian root networks on streambank stability: Is mechanical root-reinforcement the whole story?* Geomorphology **116**, 353 (2010).
- [5] G. J. Meijer, D. Muir Wood, J. A. Knappett, G. A. Bengough, and T. Liang, *Analysis of coupled axial and lateral deformation of roots in soil*, International Journal for Numerical and Analytical Methods in Geomechanics **43**, 684 (2019).
- [6] S. Mickovski, R. Sonnenberg, F. Bransby, M. Davies, K. Lauder, A. Bengough, and P. Hallett, *Shear reinforcement of soil by vegetation*, Proceedings of the 14th European Conference on Soil Mechanics and Geotechnical Engineering, Madrid **3**, 24 (2007).
- [7] A. S. R. A. Dias, *The effect of vegetation on slope stability of shallow pyroclastic soil covers*, Ph.D. thesis, Université Montpellier; Università degli studi di Napoli Federico II ... (2019).
- [8] A. Stokes, C. Atger, A. G. Bengough, T. Fourcaud, and R. C. Sidle, *Desirable plant root traits for protecting natural and engineered slopes against landslides*, Plant and soil **324**, 1 (2009).
- [9] M. S. Acharya, *Analytical approach to design vegetative crib walls*, Geotechnical and Geological Engineering **36**, 483 (2018).



# 2

## SHEAR STRENGTH CHARACTERISTICS OF ROOTED SOILS

*"Study hard what interests you the most in the most undisciplined, irreverent and original manner possible."*

Richard P. Feynman



## 2.1. ABSTRACT

History, experience and scientific literature provides sufficient evidence of the potential benefits of the use of vegetation to stabilize the banks of streams and rivers. However, quantifying root reinforcement and its influence on soil behavior is challenging and needs a comprehensive approach. This study is conducted in context of an overarching objective of using rooted vegetation in combination with wooden sheet piles to form a bio-engineered earth retaining structure to protect canal and stream banks in the Netherlands. Thereby the service life design of stream banks can be optimized, either by reducing the sizes of the structural components or by a prolonged design life.

Displacement controlled and load controlled direct shear tests were conducted on bare and rooted soil samples using a newly developed adaptable direct shear testing apparatus. Rooted soil samples contained *Humulus lupulus* L. or *Salix fragilis* L. Saturated samples were tested under low confining stresses for a realistic simulation of stream bank conditions as typical for the Netherlands. The effect of roots on time dependent behavior of soils is investigated using simulation of a Burger model on to the experimentally observed strain-time behavior. Contractive behavior was shown by rooted samples when compared to bare soil samples. Rooted samples tested in displacement-controlled mode under saturated conditions and low confining stresses, presented a higher friction angle and showed that the root pull-out behavior was dominant. This increase in frictional component is attributed to the additional confining stress provided by the roots. The effect of roots is more evident when the soil expands vertically. Rooted samples show a higher peak stress ratio and diverge from the peak stress ratio-vertical displacement trend of bare soil.

## 2.2. INTRODUCTION

Various types of vegetation grow naturally along stream banks. The vegetation reinforces the top layer of the soil through its roots and protects the stream banks from erosion. Evidences can be found in history that vegetation was deliberately introduced to prevent soil erosion and bank failure in regions where the vegetation did not exist along the bank and where it did not provide sufficient protection [1]. Most of such projects were based on the qualitative knowledge that roots of plants reinforce the soil. In the last few decades, there has been attempts to quantify the mechanical reinforcement provided by the roots to the soil. Experimental studies mainly focused on conducting shear tests using conventional direct shear apparatus of varying sizes [2–8] or using newly developed large-scale direct shear apparatus [9] to understand the root-soil interactions. Very few triaxial tests on rooted soil are reported in the literature [10, 11]. Direct shear tests on laboratory scale are relatively easy to conduct and numerous tests could be conducted compared to large scale direct shear tests. However, root systems in such small size samples are likely to be not representative of field conditions. For instance, roots will have limited anchoring depth available when they are not allowed to grow naturally. In triaxial tests, the confining stresses applied are often much higher than the confining stresses experienced by roots in the field (0-15 kPa).

In majority of the reported shear tests the plants were grown from seedlings or from cuttings directly into the samples or artificial materials were used as root analogues. Use of root analogues and conventional test apparatus have the advantage of ease of testing and repeatability. The vegetated soil which can be tested in small scale apparatus is limited to plants with polyrhizoid type of root structure, such as grasses. Manual installation of root analogues is less likely to provide a comparable root-soil interaction as with naturally growing roots. The moisture content of the soil can influence the root failure mode, root tensile failure or root pullout from the soil. Relatively small variation in moisture could govern the global pull-out behavior of bundle of roots [12].

Conventionally, the results of direct shear tests showed that the Mohr-Coulomb envelop of root-permeated soils presented a higher intercept but similar slope of bare soils [9, 13]. Therefore, root-permeated soil is represented with the same angle of internal friction of bare soil and with an additional cohesion provided by the roots [9]. The previous observation opens the door for the development of analytical models intending to estimate the additional cohesion due to roots ( $C_R$ ). The efficacy of the analytical models was determined by comparing the predicted  $C_R$  value to the  $C_R$  value obtained from experimental results. The first analytical model developed to predict the shear strength of rooted soils assumed that all roots break in tension and are oriented perpendicular to the shear surface [14]. Such model resulted in over prediction of the shear strength compared to that obtained from experimental direct shear tests. Further improvements in analytical modelling of root permeated soils involved using correction factors taking into account the overestimation and gradual failure of roots [15, 16] etc.

Additionally, soils show volume change behavior, which depends on density of packing and the confining stress during shearing. Excluding volume change behavior, dilatancy, into account would result in amplification of the effect of roots [9]. A continuum modelling framework for polyrhizoid type of plants like grasses, taking into account dilatancy was provided by [17]. Testing conditions of root-permeated soils are critical for

understanding the shear behavior and root reinforcement mechanism. Slope instability is more likely when the soil moisture content or ground water table is high, which usually occurs due to heavy rainfalls or raise in water table. On stream banks, the roots are expected to reinforce the first couple of meters of soil where the highest root density is concentrated in the first meter of soil. Hence, unlike other soil reinforcement techniques, root-reinforced soils need to be tested at low confining pressures for realistic representation of the loading conditions in a slope. Testing at high moisture conditions provides an insight into the reinforcement when the effect of roots is most desired.

The root architecture plays an important role for the resistance against shear. Root systems with more oblique and vertical roots presented higher shear strength than root systems with dominantly horizontal roots, for five different plant species [7]. In contrast, [5] found that *J. curcas* with dominant vertical and oblique roots had less resistance to shear than *R. communis*. The orientation of the roots determines the type of load (tension, compression, bending) acting on the roots when the soil is sheared [18]. The root fibers that cross shear bands get distorted and elongate increasing the tensile stresses on the root that are transferred to the soil through an increase in the normal stress along the shear band [14, 19]. In bio-engineered earth retaining structures as in [20] or in natural slopes reinforced by vegetation, the roots will be subjected to a constant stress for long periods of time. A plethora of studies on time-dependent behavior of soil have been reported in the literature [21–24]. However, to the best knowledge of the authors, there is no experimental data available on time dependent behavior of rooted soils. This could possibly be due to the complexity of the testing involved, which would require applying a constant load on large samples for a considerable amount of time.

The objective of this study is to investigate the shear behavior of root-permeated soils, aiming at answering the following research questions:

- (i) How can the effect the root orientations on shear strength be explained?
- (ii) How does the root -soil composite behave under long term constant load?
- (iii) How does the failure envelope of rooted soils differ from that of bare soil in field confining stress levels?
- (iv) Do the selected species have the potential to be used as a live element in bioengineered earth retaining sheet pile walls to protect stream banks?.

Direct shear tests were conducted on root-permeated soils of *Humulus lupulus* L. (HL) and *Salix fragilis* L. (SF). The vertical displacement behavior was recorded and used in the evaluation of shear strength of rooted samples. In addition to displacement-controlled tests, load controlled tests with step loading was adopted to characterize viscous behavior of root-permeated soils. A Burger model was used to compare the behavior of bare and rooted samples under constant loading conditions. Spatial root distribution and dimensions were measured post testing.

## 2.3. MATERIALS

### 2.3.1. SELECTION OF VEGETATION

The purpose, growth condition and benefits to the society play a key and central role in selection of vegetation in stream bank soil bio-engineering projects. The selected vegetation should ideally be able to grow roots deep and dense into the permanent wa-

ter source. In bio engineering projects involving an inert material like wood, the growth rate of roots is crucial for successful implementation of the project. Taking into account the previous criteria, *Salix fragilis* L. (SF), commonly known as crack willows, and *Humulus lupulus* L. (HL), commonly known as hops, were chosen in this study. SF are pioneer species which can grow deep, extensive roots in permanently wet conditions and hence provide both shallow and deep reinforcement [25]. Added benefits such as being a source of pollen and honey for bees [26] and providing habitats and food for organisms make willow an excellent candidate for river bank stabilization projects. The second selected species HL is native perennial, as the Netherlands falls within the range of wild hop growth, latitudes 35°N to 55°N [27]. Even though the above ground portion of HL is annual, it can climb to heights of above 6 meters growing more than 25 cm a day under ideal conditions. The root system of HL can have permanent root stock upto a depth of 3.6 meters or more [28] which is ideal for plantation in stream banks, which are generally 1 to 6 m of total height from founding depth. The root system of HL is perennial and can survive low winter temperatures. HL are also widely used to flavor and give aroma to beer during brewing. Thus, the use of hops for stream bank stabilization could also serve other societal needs.

### 2.3.2. BOXES FOR GROWING THE PLANTS AND SHEAR TESTING

Boxes of inner dimensions 500mm\*500mm with a depth of 400mm were built using formwork grade plywood to contain the soil samples where the plants would be grown. The large size was selected based on suggestions by [29] in order to avoid pot bound roots caused by a limited growing medium. The boxes were split into two halves at a depth of 200mm (Fig.2.1a) with the intent of being used to perform direct shear tests. In order to avoid the build-up of friction at the contact of the boxes, the surfaces between the boxes were coated with Teflon (Polytetrafluoroethylene) with thickness of 1mm. Holes were drilled at the bottom for free drainage of water. The boxes were clamped during any transport to avoid any additional disturbance to the specimens.

### 2.3.3. SOIL PROPERTIES AND CONDITIONS OF GROWTH

The particle size distribution of the soil used in this study is shown in (Fig.2.2). The soil is classified according to USCS classification system as silty sand (SM) with 18% fines. The soil was mixed thoroughly to ensure homogeneity, large boulders and other residuals were removed. The soil was further divided into smaller sections and to air dry during one week. Each box was filled at a dry bulk density of 1.35 g/cc. The boxes were filled in three layers with scratching between the layers with a spatula to ensure good connection between the layers. Direct shear tests conducted in the laboratory gave a peak friction angle of 38°. SF cuttings were placed in water for two weeks, before transplanting into shear boxes. Commercially available, eight weeks old HL plants were placed in the shear boxes after removal of the growing medium in which they were grown. The plants were placed in an open area at the Botanical garden of TU Delft and watered at an average of once in 3 days in summer.

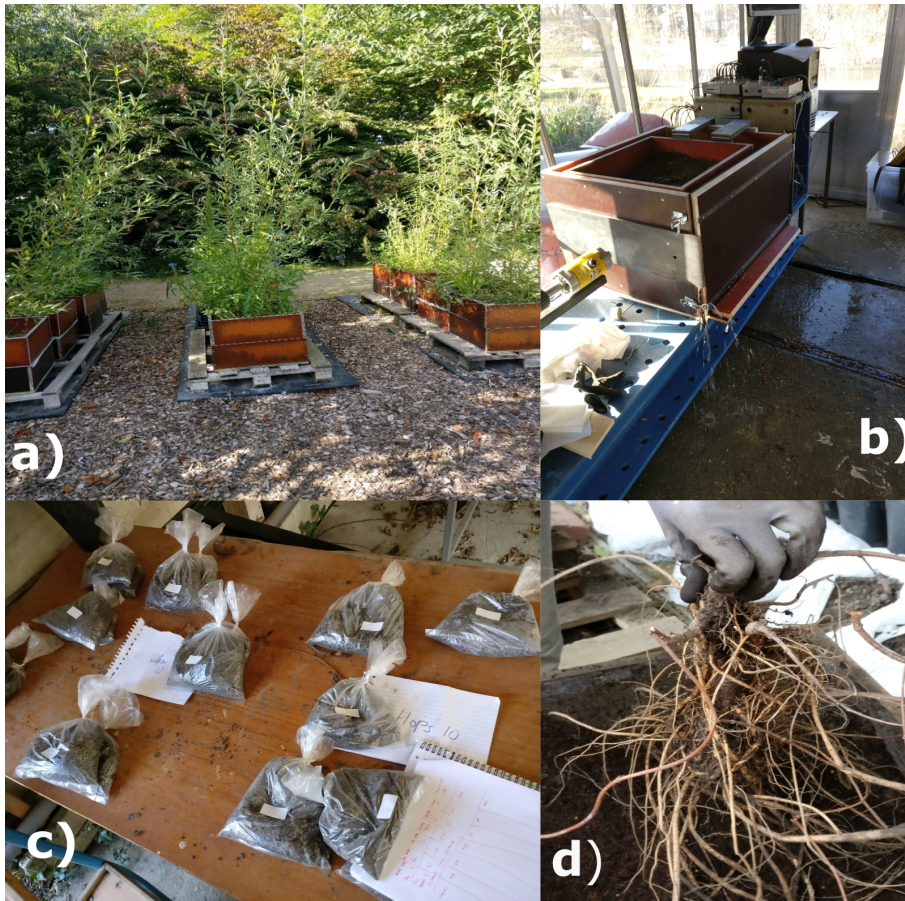


Figure 2.1: a) HL and SF grown in Botanical garden TU Delft b) Shear testing setup c) Fine root collection d) Coarse root excavation

## 2.4. METHODS

### 2.4.1. LARGE SCALE DIRECT SHEAR APPARATUS

A large-scale direct shear apparatus was built in the Bio-based structures and materials laboratory of Delft University of Technology to test root-permeated soils. The apparatus can work on dual loading modes, displacement-controlled mode and load-controlled mode. In displacement-controlled mode, the sample is sheared at a constant displacement rate and in load-controlled mode, the sample is sheared by incremental application of load to the sample. Slight modifications are required each time that loading conditions are changed. The main components of the apparatus are the carrier box, normal load platen, base plate, main frame and data logging system, see (Fig.2.3 a)). The shear box rests inside a carrier box of size 700 mm\* 700 mm. The carrier box rests on circular linear bearing. A flexible membrane, is located above the soil for the uniform

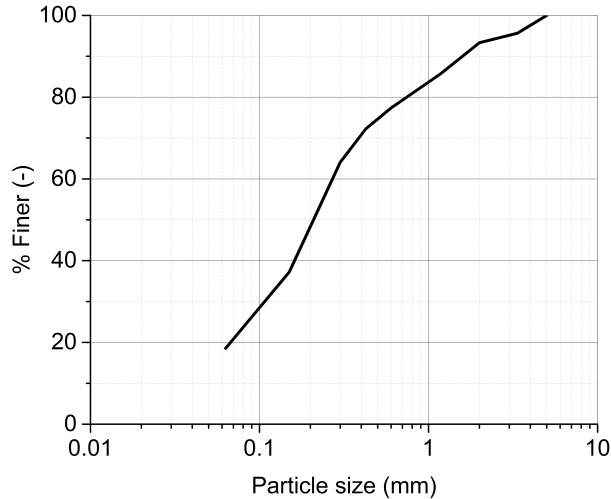


Figure 2.2: Particle size distribution of representative soil sample from the volume of soil used obtained by wet sieving

application of normal load throughout the sample (LDPE). This is done to avoid non-uniform application of the normal load due to the root stump presence or non-level top soil surface. A rigid loading platen is placed on top of the flexible membrane and the normal load is applied using dead weights on to the rigid platen. The constant shear displacement rate is applied using a jack. The maximum shear load of 75 kN can be applied at slowest displacement rate of 0.2 mm/min. In load-controlled tests, the system is adapted to apply a constant load using a pulley system and the load is applied using dead weights (Fig.2.3 b)).

A number of sensors are used in the large-scale direct shear apparatus to measure displacements, load and soil suction. Due to the large size of the box, two load cells (S-type beam, Sensitivity 2.0mv/V, Maximum: 25kN) are used to measure the shear force on the soil. Vertical displacements are measured using three vertical transducers (FMDK30, Sensitivity 0.001mm, Maximum: 150 mm). Horizontal shear displacement is measured using transducers of range, 200 mm, connected to the carrier box. A tensiometer (Stelzner, 0-600mbar) is placed right above the shear surface and the matric suction monitored in order to guarantee that it is as close to zero as possible to ensure saturation. In load-controlled mode two additional load cells (S type beam, Sensitivity 2.0mv/V, Maximum: 25kN) are used to measure the resultant applied load on to the shear box.

#### 2.4.2. DIRECT SHEAR TEST

All the specimens, including the bare soil, were tested after 12-24 months of growth. Considering a range of weight of the vegetation above ground on real slope, 100kg-250kg, acting in a root plate of 0.5m \*0.5 m would result in a pressure of approximately 4kPa to 10kPa. Three normal stresses at the shear surface, 4.4kPa, 6.4kPa, and 10.4 kPa, are used which are in the range of loading conditions used in studies reported in litera-

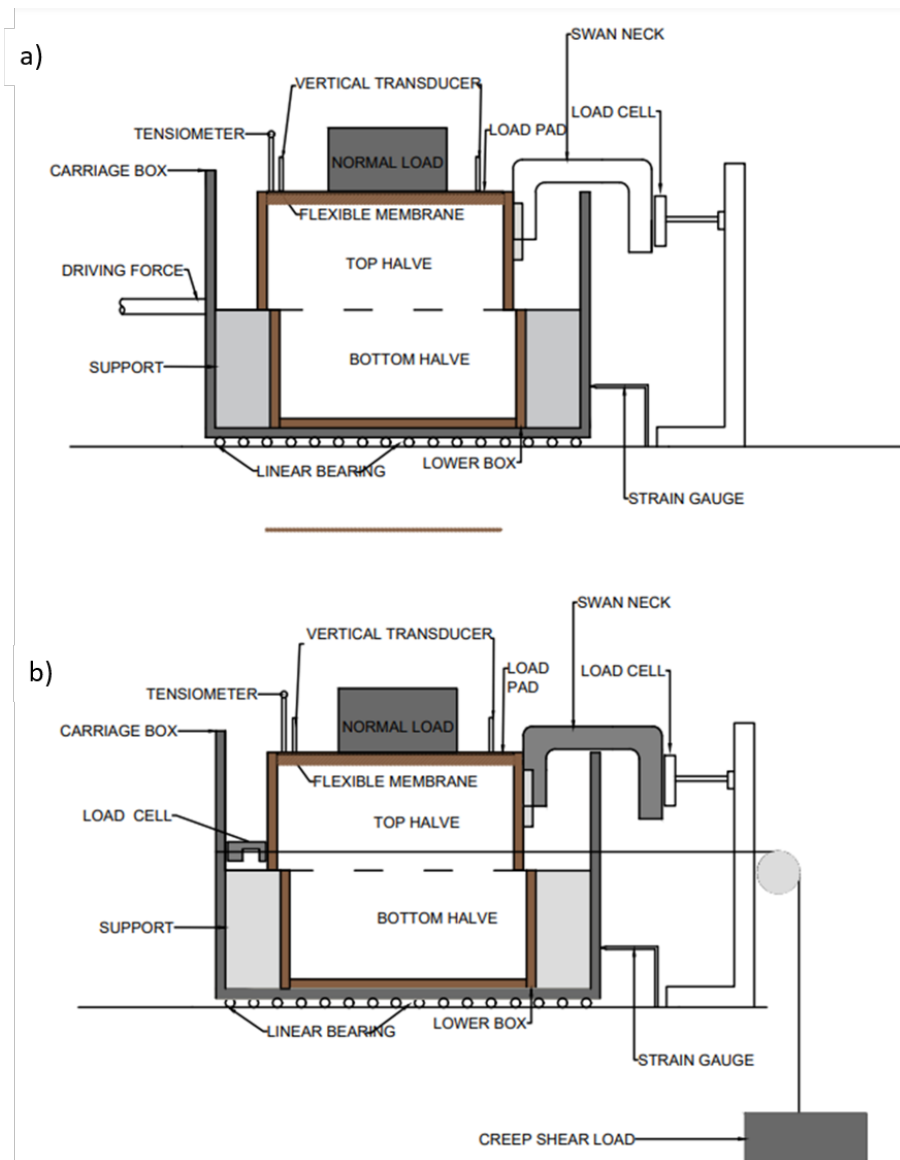


Figure 2.3: Large direct shear testing setup. a) Displacement controlled tests b) Load controlled tests.

ture [5] and that can occur at a bare to highly vegetated slope. After placing the shear box in the carriage box, the carrier box was completely filled with water for 24 hours. Then the confining vertical stress was applied for at least 24 hours and sheared only when the rate of change of vertical displacement was reduced to zero, and suction values were close to zero. To ensure saturation throughout the shearing process, the carrier box was kept filled with water. Negative pore water pressure (suction) was monitored throughout

the shearing process and kept as close to zero as possible. In displacement-controlled mode, a constant displacement rate of 0.2mm/min was used. The displacement rate was chosen based on the minimum possible rate using the apparatus. This shearing rate is in the range that reported in literature by [6, 7, 30] for consolidated drained shear test on rooted samples. In load-controlled mode, loading is applied in incremental steps of 80 N which would approximately represent 1 kPa shear stress in the specimen. After completion of the shear test, the specimens were removed for root analysis.

### 2.4.3. ROOT ANALYSIS

The study of the root system morphology was conducted following the systematic methodology adopted by [5] to analyze the root architectural characteristics. The conventional method of distinguishing coarse roots (Coarse roots = diameter > 2mm, [31]) from fine roots was not followed. Instead, coarse roots were distinguished qualitatively from fine roots based on thickness, length, and stiffness. After each shear test, the wooden boxes were dismantled and soil cores were taken from the top box in four quadrants using a cylindrical mould. The soil from the top half of the box was further removed using running water. After removing the soil from the top half of the box, cores were taken from bottom half of the box (Fig.2.1c) to determine the fine roots in four quadrants. Dry weight of fine roots was taken and fine root density per core of soil was calculated. The fine root density was used to determine the total fine root mass in each half of the box assuming uniform density of fine roots throughout the shear box.

The diameter at the origin and at the shear surface of all coarse roots was measured. The location of roots at the origin and at the shear surface was determined and classified in the four quadrants. The root angle with respect to horizontal was measured at the origin of the root and at the shear plane. Three different types of root orientations were defined based on root angle: horizontal roots (0°-30°), oblique roots (30°-60°) and vertical roots (60°-90°). The failure mode of roots was also determined as 'pulled out' or 'tensile failure' (Fig.2.1d).

### 2.4.4. DATA ANALYSIS

The data processing required the correction of the measured shear force by considering the mechanical friction in the apparatus and soil to plywood interface friction which varied with displacement  $dx$ . A threshold value of 86 N was determined to account for this mechanical friction based on the 'empty' tests and evaluating the readings on the load cell. The frictional force on the supporting plate  $F_{plate}$  when the soil is sheared is evaluated as done by [9] as follows:

$$F_{plate} = R \times \tan \mu \quad (2.1)$$

Where  $R$  is the total vertical force on the plate and  $\mu$  is the interface friction angle between soil and plate. The total vertical force can be calculated as:

$$F_{plate} = \frac{\sigma_{applied}}{(500 \times 500)} \times (dx \times 500) \quad (2.2)$$

Where  $\sigma_{applied}$  is the applied normal load. The interface friction angle is taken as 2/3 of the internal friction angle of the soil determined from the laboratory direct shear tests. The variation of frictional force with shear displacement is given by:

$$F_{plate} = \frac{\sigma_{applied}}{(500 \times 500)} \times (dx) \times \left(\tan\left(\frac{2}{3}\right) \times 38\right) \quad (2.3)$$

and it is used to obtain the corrected value of the shear stress on the soil.

The vertical displacement is measured at three points as shown in (Fig.2.4). The vertical displacement at the center of the shear box is determined using shape function and solving the following system of equations:

$$\begin{bmatrix} 1 \\ x \\ y \\ z \end{bmatrix} = \begin{bmatrix} 1 & 1 & 1 \\ x_1 & x_2 & x_3 \\ y_1 & y_2 & y_3 \\ z_1 & z_2 & z_3 \end{bmatrix} \cdot \begin{bmatrix} L1 \\ L2 \\ L3 \end{bmatrix} \quad (2.4)$$

Where  $(x_1, y_1, z_1)$ ,  $(x_2, y_2, z_2)$ ,  $(x_3, y_3, z_3)$  are the coordinates of the three points of vertical measurements and  $(x, y, z)$  are the coordinates of the center (C). L1, L2, and L3 are the ratios  $a_1/A$ ,  $a_2/A$ , and  $a_3/A$ , respectively, where A is the total area limited by the triangle formed by the displacement transducers. The coordinates of the three points of measurements are  $(-11.8, 12.8, 0)$ ,  $(11.8, 12.8, 0)$  and  $(0, -15.2, 0)$  with respect to center of the top plate.

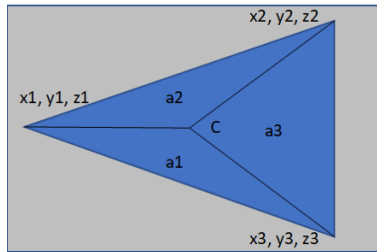


Figure 2.4: Estimation of vertical displacement at center (C) of the top plate using vertical displacements of three vertical displacements recorded at  $(x_1, y_1, z_1)$ ,  $(x_2, y_2, z_2)$ ,  $(x_3, y_3, z_3)$  which is  $(0, -15.2, 0)$ ,  $(-11.8, 12.8, 0)$ ,  $(11.8, 12.8, 0)$  respectively.

#### 2.4.5. RHEOLOGICAL MODELS

**B**urger model is a visco-elastic physical model. The generalized Burger model consists of a Maxwell unit and Kelvin unit combined in series. Sometime multiple Kelvin units are used for accuracy. The Maxwell spring accounts for the instantaneous deformation and the Maxwell dashpot for the linear viscous deformation process. The linear visco-elastic deformation is the resultant of the Kelvin unit. Burger rheological model have been employed to study the time dependent behavior of soils [24, 32, 33] and has been implemented in a number of finite difference software's like Flac 3D. The creep behavior of wood, with the same basic chemical components as roots, and wood fiber-polymer composites have also been seen to fit well with Burger model or a modified version of the generalized Burger model for mechanosorptive effects[34–36], even though it is recognized time extrapolation capacity is limited, depending on the time range used

for the model constants derivation. Hence, Burger model can be considered as having potential to model root-soil composite. General Burger model is given as:

$$\varepsilon(t) = \sigma \left[ \frac{1}{E_m} + \frac{1}{E_k} \left[ 1 - \exp\left(\frac{-E_k}{\eta_k} t\right) \right] + \frac{\sigma}{\eta_m} t \right] \quad (2.5)$$

Where  $\varepsilon(t)$  is the creep strain,  $\sigma$  is the stress,  $t$  is the time,  $E_m$  and  $\eta_m$  are the elastic modulus of spring and viscosity of the spring and dashpot elements in the Maxwell unit respectively.  $E_k$  and  $\eta_k$  are the elastic modulus of the spring and viscosity of the dash pot in the Kelvin's unit respectively. The experimentally observed strain-time curves were fitted using non-linear curve fitting method in Origin pro 8.

## 2.5. RESULTS

### 2.5.1. VEGETATION

The above ground characteristics and below ground biomass (RBM) (above shear plane, below shear plane and total root biomass) of both *Humulus lupulus* L. (HL) and *Salix fragilis* L. (SF) are given in (Table 2.1). HL had multiple shoots which grew to a maximum height of 2.5 meters (maximum height of support provided for the shoots to grow). The shoots of SF grew to an average of 3 meters. The diameter of the shoot measured 50mm above the shear box varied from 23mm to 41 mm. The average RBM of HL and SF were 223g and 188 g respectively. HL presented a dense network of fine roots in the region where shoots were emanating from the root stock, which were only present on the top 30 mm and did not cross the shear surface. Few (3-12) thick and deep roots which crossed the shear surface emerged from the root stock in the vertical direction. These thick roots had branches of smaller diameter, all in the vertical and oblique direction, which further had finer roots. Significant number of horizontal roots (n=4-28) were found, which extended towards the sides of the boxes and the majority extended further towards the shear surface in the vertical direction. These horizontal roots had very few branches which extended in the vertical direction. SF presented few numbers (6-8) of thick roots emanating in the oblique direction from the stem with many branches (>6) and fine roots emanating from them. The branch roots were both present in the horizontal and vertical directions. SF presented, in general, many more long fine roots in both horizontal and vertical directions than HL and the branch roots were thinner (<50% diameter than roots emanating from the stem). The root distribution in different orientations at the shear surface in all specimens of HL are given in (Fig. 2.20) and that of SF is given in (Fig. 2.21). An example root orientation is shown for both species in (Fig. 2.5).

### 2.5.2. LOAD CONTROLLED SHEAR TESTS

The bare soil with a confining stress of 4.4 kPa failed after 24 minutes at applying a shear stress of 3 kPa (Fig. 2.6). Five load steps were applied to the bare soil sample with a confining stress of 6.4 kPa and failure occurred at the sixth load step. The sample failed after 140 minutes of applying the sixth load step of 6.8 kPa. Soil with HL roots failed at 6 and 9 load steps respectively for samples with confining stress of 4.4 kPa and 6.4 kPa respectively. Soil with SF roots failed at 8 and 10 load steps respectively for samples with confining stress of 4.4 kPa and 6.4 kPa.

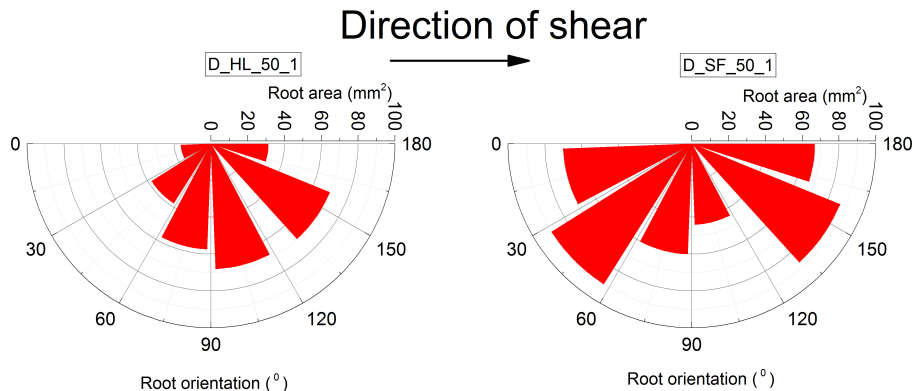


Figure 2.5: Vertical root orientation of D\_HL\_50\_1 and D\_SF\_50\_1. (Terminology: Displacement controlled (D), *Humulus lupulus* L. (HL), *Salix fragilis* L. (SF), Normal load (50 kg), 1-repetition number)

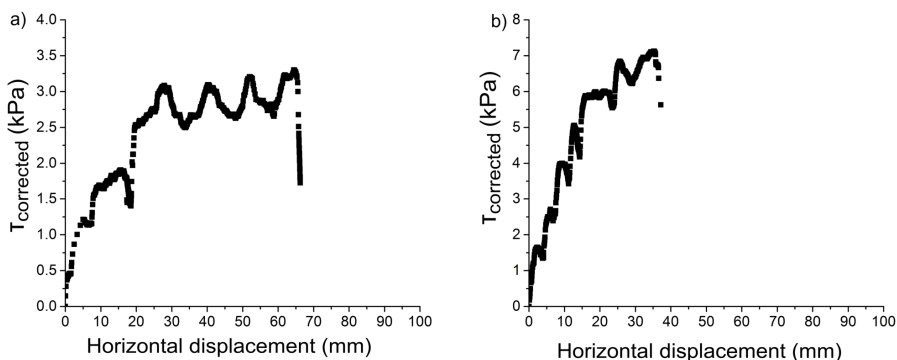


Figure 2.6: Bare soil stress-controlled tests at two different normal stress levels: a) 4.4 kPa, and b) 6.4 kPa.

The Burger model parameters for the normal stress of 6.4kPa are shown in (Fig.2.10) and the fitting of the Burger model onto the experimental strain-time data is shown in (Fig.2.9). The Burger creep model is able to capture the time dependent behavior of both bare soil and root permeated specimens ( $Adj-R^2 > 0.985$ ). Burger model parameters vary with stress level and are not constant, see (Fig.2.10). The combined elastic stiffness of the Maxwell and Kelvin element  $E = E_m + E_k$  is plotted in (Fig.2.10). The bare soil presented a higher elastic stiffness parameter at the lower stress range than both HL and SF specimens. However, at stresses above 75% of the peak stress of soil, SF have slightly higher elastic stiffness. HL specimens showed a less stiff response than bare soil throughout the tested stress range. The validity of the Burger parameters can be seen from the corrected stress-displacement curves given in Fig.(2.6-2.8), where the root strength is mobilized after a certain displacement where damage has occurred. The decrease in the elastic modulus and  $\eta_m$  clearly depicts the damage developing in all specimens and a change to yield phase from elastic phase with shearing. At higher stress level,  $\eta_m$  which represents the viscous

Table 2.1: Vegetation biological properties: above ground and below ground biomass (Rounded off to nearest gram). Shoot diameter of SF, number of shoots of HL. Specimens are named as follows, the first letter specifies the type of test (D-displacement controlled L-Load controlled), followed by species (HL- *Humulus lupulus* L., SF-*Salix fragilis* L.), followed by normal load applied in kg, (50,100,200), followed by repetition number. Eg. D\_HL\_50\_1 represents displacement-controlled test on *Humulus lupulus* L. at 50kg normal load, first repetition.

| Specimen | Shoot Diameter at 50 mm above shear box | Number of shoots | Estimated fine root biomass | RBM above shear plane | RBM below shear plane | Total root biomass |
|----------|---|------------------|-----------------------------|-----------------------|-----------------------|--------------------|
|          | (mm)                                    |                  | (g)                         | (g)                   | (g)                   | (g)                |
| DHL50_1  | -                                       | 8                | 31.1                        | 98                    | 121                   | 220                |
| DHL50_2  | -                                       | 6                | 43.8                        | 126                   | 186                   | 312                |
| DHL100_1 | -                                       | 8                | 39.5                        | 88                    | 102                   | 190                |
| DHL100_2 | -                                       | 5                | 45.2                        | 93                    | 115                   | 208                |
| DHL200_1 | -                                       | 4                | 36.7                        | 85                    | 102                   | 187                |
| LHL50_1  | -                                       | 8                | 62.2                        | 112                   | 86                    | 198                |
| LHL100_1 | -                                       | 8                | 42.1                        | 96                    | 152                   | 248                |
| Min-Max  | -                                       | 4-8              | 31.1-62.2                   | 85-126                | 86-152                | 187-248            |
| Average  | -                                       | -                | 42.9                        | 99.7                  | 123.4                 | 223.2              |
| DSF50_1  | 36                                      | -                | 60.2                        | 68                    | 90                    | 158                |
| DSF50_2  | 41                                      | -                | 59.3                        | 89                    | 179                   | 268                |
| DSF100_1 | 26                                      | -                | 50.8                        | 76                    | 61                    | 137                |
| DSF100_2 | 38                                      | -                | 53.7                        | 108                   | 99                    | 207                |
| DSF200_1 | 38                                      | -                | 76.3                        | 112                   | 131                   | 243                |
| LSF50_1  | 23                                      | -                | 62.2                        | 78                    | 70                    | 148                |
| LSF50_1  | 28                                      | -                | 22*                         | 81                    | 74                    | 155                |
| Min-Max  | 23-41                                   | -                | 50.8-76.3                   | 68-112                | 61-179                | 137-268            |
| Average  | 32                                      | -                | 60.45                       | 88                    | 100.5                 | 188.5              |

damper, long-term behavior is on an average higher for the rooted specimens than that of the bare soil

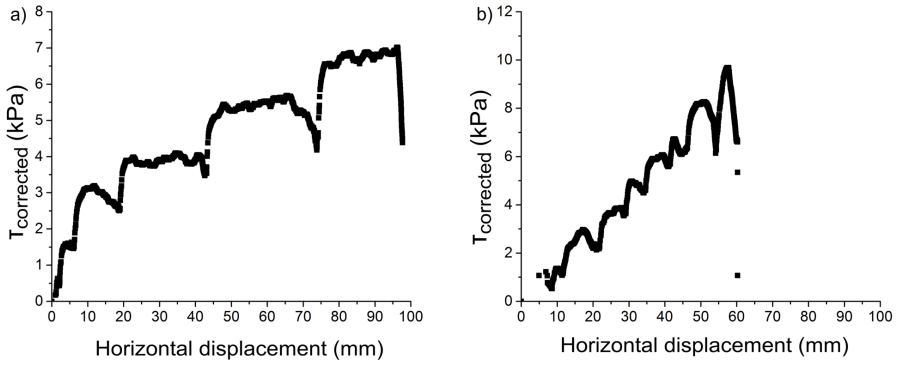


Figure 2.7: HL stress-controlled tests at two different normal stress levels: a) 4.4 kPa, and b) 6.4 kPa.

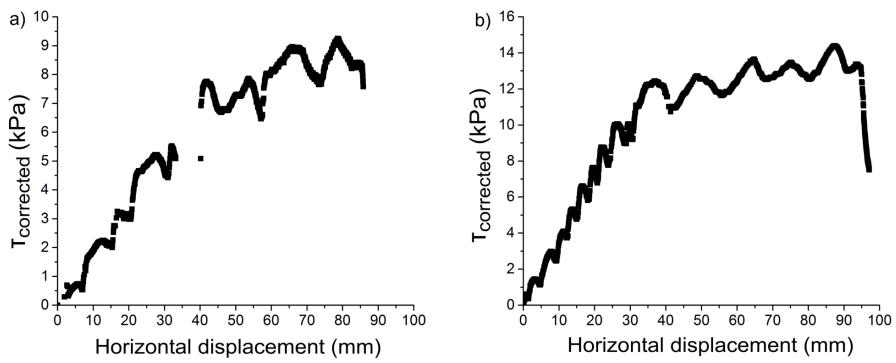


Figure 2.8: SF stress-controlled tests at two different normal stress levels: a) 4.4 kPa, and b) 6.4 kPa.

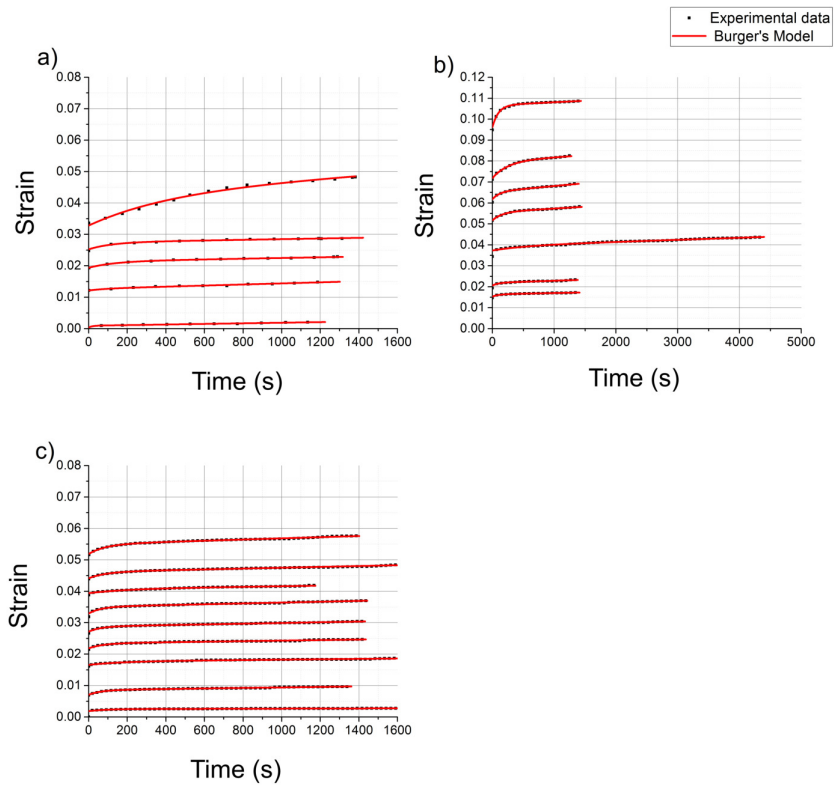


Figure 2.9: Horizontal strain measured over time at a normal stress of 6.4kPa and fitted Burger model for load controlled direct shear tests performed on: a) bare soil, b) soil with roots of HL, and c) soil with roots of SE.

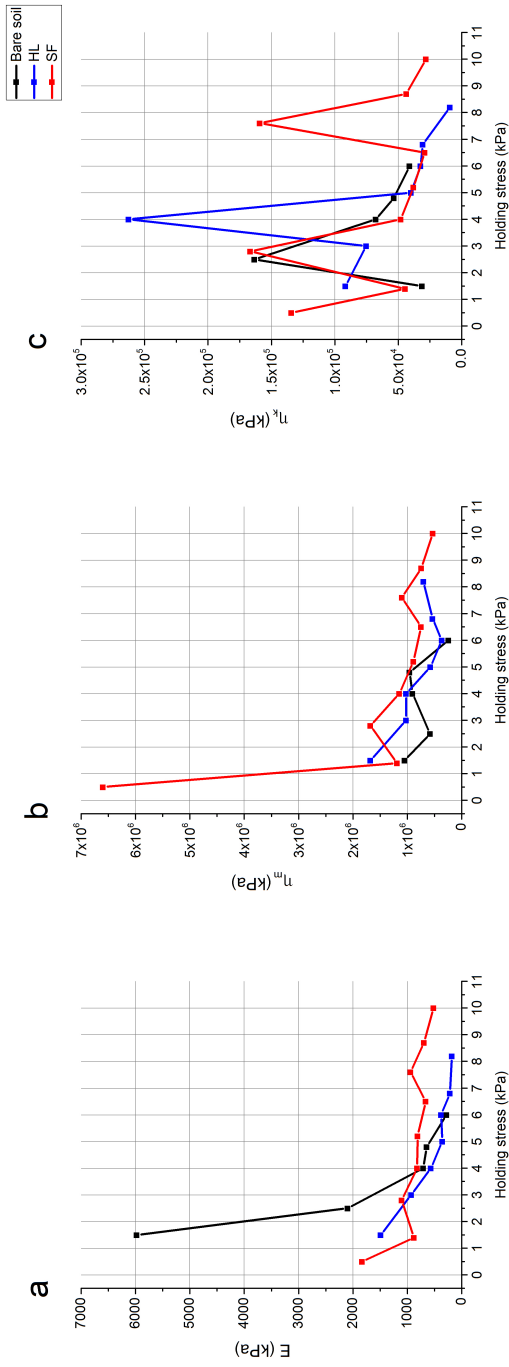


Figure 2.10: Variation of Burger model parameters over the holding stress applied in each loading step for bare soil, soil with roots of HL, soil with roots of SF.

### 2.5.3. DISPLACEMENT-CONTROLLED TEST

The corrected shear force-displacement of bare soil is shown in (Fig.2.14) and that of HL are shown in (Fig.2.16) and that of SF is shown in (Fig.2.18). While all specimens of bare soil reached a constant shear stress after a yield point within the tested displacement of 80mm, the rooted soils of with both HL and SF did not show a clear peak followed by subsequent reduction in  $\tau_{corrected}$ . In general, for all the three normal stress applied,  $\tau_{corrected}$  of rooted specimens showed an increasing trend with displacement. Localised peak and a subsequent drop in  $\tau_{corrected}$  were observed in specimens of D\_HL\_100\_2, D\_SF\_50\_1, D\_SF\_100\_1. With further displacements,  $\tau_{corrected}$  continued to increase progressively reaching a higher shear stress than the localised peak for these specimens. The specimens of D\_SF\_200\_1 and D\_HL\_50\_1 showed a peak with subsequent constant  $\tau_{corrected}$ . The variation of vertical displacement with the horizontal displacement of the tested specimens are shown in (Fig.2.17,(Fig.2.19)). Rooted specimens of both HL and SF show an increased compressive behavior compared to bare soil.

A peak frictional angle of  $39^\circ$  is obtained from the failure envelope of bare soil (Fig.2.11). This is about  $1^\circ$  higher than observed from the lab experiments performed on the traditional direct shear testing apparatus. A difference of  $2^\circ$  between the friction angle found in the lab experiment and field was reported [37], which could be due to difference in the size of the soil particles in the specimens tested at both scales and lack of control in size of particles in the field experiments [9]. The failure envelope of planted specimens was drawn using a weighing factor based on the total root area. A frictional angle of  $50.1^\circ$  was obtained for HL and  $54.2^\circ$  for SF when the best-fit curve was drawn with zero y-intercept. Fig.2.12 shows the relation between peak stress ratio ( $\tau_{corrected\ peak}/\sigma_{peak}$ ) and the ratio between the vertical and horizontal displacement ( $dy/dx$ ). At zero ( $dy/dx$ ), the bare soil, HL and SF had a peak stress ratio of 0.78, 1.37 and 1.11 respectively. All the rooted samples showed a contractive behavior (Fig.2.17),(Fig.2.19).

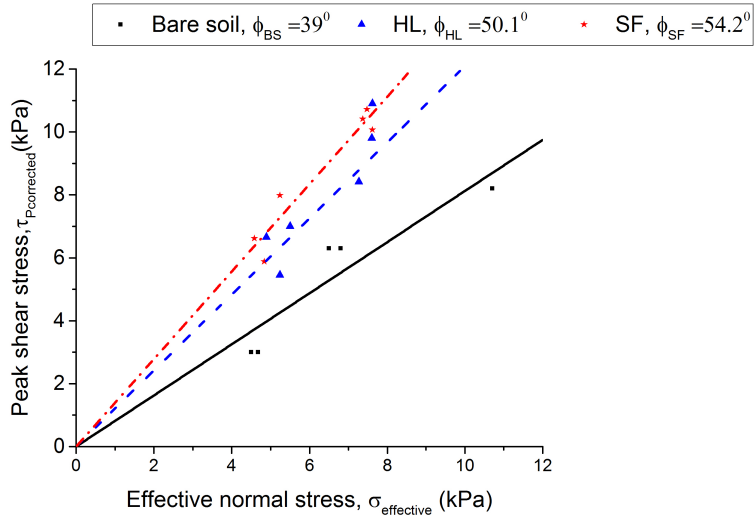


Figure 2.11: Peak stress vs effective normal stress envelope for bare soil, HL, SF of samples tested in large scale direct shear apparatus

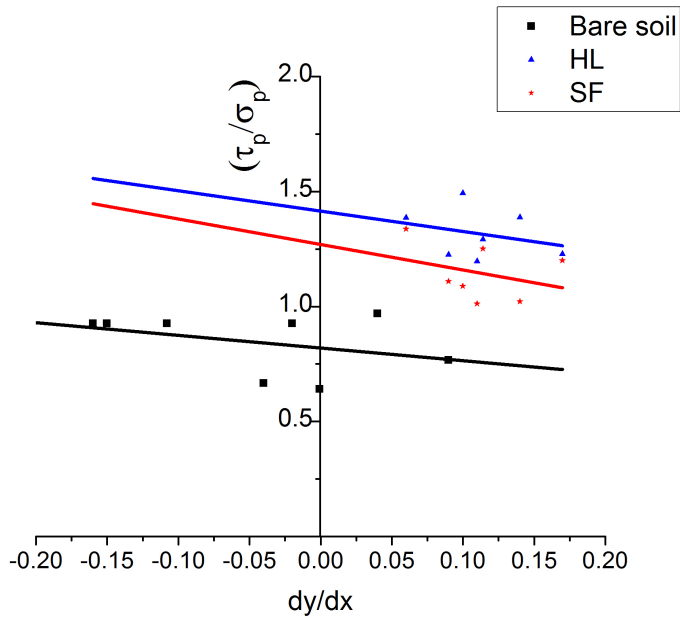


Figure 2.12: Peak stress ratio vs the ratio between the vertical and horizontal displacement ( $dy/dx$ ) of bare soil, HL, SF in all tested specimens.

## 2.6. DISCUSSION

### 2.6.1. CONSIDERATIONS ON THE ROOT SYSTEM ARCHITECTURE EFFECT ON SOIL REINFORCING

**N**o significant difference was found in the peak shear strength mobilized by both HL and SF planted specimens ( $p > 0.05$ ), even though different root architecture was found in both rooted soil specimens. HL was characterized by a large number of thick vertical roots with very few branches, while SF possessed only few vertical roots. On the other hand, SF possessed large number of oblique and horizontal roots with large number of branches, while HL had small amounts of horizontal roots at shear surface and oblique roots had large network of branched fine roots at the bottom of the box. The root area ratio presented high variability within the species and between the species. [5] argued that the soil volume trapped in between the vertical and oblique roots is protected by the structure and does not necessarily contribute to shear resistance. However, within the strain of interest in conventional testing procedures and practical design approaches ( $< 16\%$  strain), this effect might not be significant. Contrarily, [7] suggested that plants with oblique and vertical roots were more suitable for shear strength enhancement. In this study, irrespective of difference in the root architecture and difference in root types (SF is a woody species and HL is a herbaceous species), a significant difference in the shear strength characteristics was not observed. Our observations on fully saturated soils tested at low confining stresses and the above-mentioned studies, point towards the existence of a 'critical' root area ratio, above which the orientation of the roots does not significantly affect the shear strength. The critical root area ratio needs to be combined with the potential failure mechanism (explained in sections below) of roots to deduce the effect of root orientations on the shear strength within the practical deformation range. The concept of 'critical' root area ratio is in line with the studies in fiber reinforced soil, where after a certain fiber density, no significant contribution to the increase in strength of soil is observed [38].

### 2.6.2. STRESS-STRAIN BEHAVIOR

In the displacement-controlled tests, no well-defined strength peak was observed in the majority of the rooted soil specimens. Roots may have not fully mobilized their strength in the measured displacement range. The roots would continue to confer resistance until all the roots are broken or pulled out, which could occur only at very high displacements. The root tortuosity effect could partially explain such observation [39, 40]. Roots stretch as the soil is sheared during which the roots stiffness is very low and the contribution of the root to the rooted soil shear strength is very low as well. Once the root is stretched, the effective stiffness of the root wood is mobilized, the contribution of the root and therefore the shear strength increases. Given the variability in root diameters present in the tests, the roots would have stretched and the root wood stiffness is mobilized at different horizontal displacements during the test. The tortuosity effect would also be overlapped with the progressive pull-out of the roots [41]. During the pull-out of roots, the root tensile stress increases until it reaches the maximum shear stress possible to be mobilized along the root surface. Once this critical shear stress on the root surface is reached the root starts to pull out by gradually detaching itself from the soil (due to

decrease in diameter, poison effect), which leads to a decrease in contribution to the shear strength of the root-permeated soil. However, as pointed out by [5] this might not necessarily be an advantage in the field, the soil could slide away or being washed away from the roots during wet periods with less resistance as it is not confined as in a shear box.

In some specimens, for example SF\_50\_1, SF\_100\_1 a drop in shear resistance was observed followed by an increase in shear strength with further displacements, that reached values above the previous localised peak. In such specimens very few (1-2) broken branches of oblique/horizontal roots were found, which could be a reason for the instant drop in shear strength of soil. The increase in shear strength after the local peak was gradual and could possibly be due to the roots mobilized in bending in the later secondary stages of shear process. [6] suggested that peak type curves would be observed in root systems with plenty of fine roots in the shear surface, which would result in a higher apparent cohesion. In contrast, [5] suggested that root systems with predominantly anchoring roots would give peak type curves. In our observation, the anchoring-type root system does not necessarily provide a peak in the stress-displacement curves. However, relationship between root architecture and type of stress-strain curve can be deduced only when taking into account the number of roots, orientation of roots and testing conditions, for instance, this study and [6] was conducted in saturated conditions.

The testing conditions, saturated or unsaturated, contribute to differences in the failure mechanism of roots and the shear strength of soil, which in turn affects the overall behaviour of root-permeated soil. Hence, major differences can be found between, [6] and the present study, both conducted in saturated conditions, and [5], conducted in unsaturated conditions. [42] found that the roots tend to break with increasingly drier soil, which might result from the full mobilization of the shear strength on the root-soil surface. Additionally, [39] found that dry conditions are responsible for a mobilization of the tensile strength of the root wood at a smaller displacement and reach total final tensile strength. The combined findings of [42] and [39] explain the reason why [5], obtained peak-type curves testing in unsaturated conditions, while the present study observed a gradual increase in shear strength. As observed by other authors, the strength of root permeated soils is mobilized at higher shear displacements compared to bare soil ([43, 44]). The root permeated samples showed a significant increase in shear strength which is accompanied by noticeable decrease in stiffness and an increase of strain as observed in polyamide fiber reinforced soils [45] This shows that root-reinforced soil is able to maintain strength at high deformations and represents a very ductile composite. This character can inhibit its use as a structural element as in timber-vegetation earth retaining system as developed in [46].

### 2.6.3. EFFECT OF ROOTS ON THE SOIL VOLUME CHANGE DURING SHEARING

In the present study, the root permeated soils were observed to inhibit vertical deformation increase of soil sample (Fig.2.17, Fig.2.19). Apart from the increase in confining pressure roots assert when the soil is sheared, the crevices formed by roots during their growth can result in restriction of soil volume increase. The roots acting in tension rather than in shear as in fiber reinforced soils [47–49] increase the confining pressure on the soil, which results in a decreasing tendency to dilate. Such behavior has also been re-

ported in polypropylene fiber reinforced soils [49]. Through their rather crude analysis, it was demonstrated that only a minor suppression of dilatancy ( $2^\circ$ ) was possible when the confining stress was changed from 100kPa to 200 kPa. Similarly, in this study it could be reasoned that only a minor reduction in dilatancy due to the roots acting in tension, would result in a significant increase in confining stress. However, dilatant behavior was observed in root permeated soils by [9], which could be due to relatively lesser number of roots crossing the shear surface and high relative density of the soil which would require very high confining stress to suppress any dilation. Complete suppression of dilatancy for soil with high relative density, would require very high confining stresses in the range of MPa [49].

The contraction behavior observed in this study shows that the particles must be moving towards each other, which implies that the tension on the roots was relatively low and the roots with orientation  $0^\circ$ - $90^\circ$  relative to the horizontal plane in the direction opposite to shear, might even be undergoing bending and/or axial compression. This validates the observation that very few to no roots were broken in tension. Consequently, the maximum potential of the reinforcing effects of roots might not have developed fully. Fig.2.12 suggests that the reinforcement effect of roots would be more significant if the soil had dilated. In that case, larger slip would have occurred, with the consequence of more axial tensile stress in roots that bridge the failure plane. The effect of roots on the peak stress would be minimal when the soil presents a highly contractive behavior. The increase in confining stress incurred by the roots, increases the shear strength. The disparity in observation on preferable root orientations which would aid in increasing the shear strength of soil, could possibly be due to the mechanism in which roots increase the strength of the soil. In saturated conditions, at peak shear strength, the horizontal roots provide less confining stress than oblique roots. If the dominating root failure mechanism is breakage, at peak shear strength, the maximum potential of root reinforcement is achieved. The roots provide a direct additional shear strength component (often called 'root cohesion') where the horizontal roots provide a higher magnitude of this component. Their orientation would become increasingly parallel to the direction of shear with increasing displacement.

#### 2.6.4. EFFECT OF ROOTS ON THE SHEAR STRENGTH OF ROOT PERMEATED SOIL

Mohr-Coloumb model which is generally used to characterize shear strength of soil has a linear envelope for failure criterion. The most widely used techniques to estimate the effect of vegetation on slope stability is to add an empirical "cohesion" ( $C_R$ ) term to the Mohr -Coloumb envelope to account for the effect of roots on the shear strength of soil. The confining pressures used in such studies are usually high (e.g. [50] [10-30 kPa], [51] [>60 kPa]) than expected to be acting on a vegetated slope. The confining pressure has a significant effect on the failure mode of roots [52]. Under high confining pressures, roots tend to break rather than pull out. Slope failure often occurs when there is a high moisture in the soil, again under the conditions which are favorable for root pull out. Under high confining stress and relatively dry soil, the empirical "cohesion" technique stands valid because roots break and the effect of roots could be considered as an increase in cohesion. Nevertheless, these conditions are not only unrealistic for

a vegetated slope, but also do not represent the conditions when the effect of vegetation is most desired (high moisture content). [53] attempted to understand the root reinforcement mechanism through 4D X-ray computed tomography and suggested that the empirical approaches are over simplistic and too uncertain. An alternative but more realistic approach is to assume the effect of roots as a change in stress state of the soil due to the confining stress provided by the roots. Such approaches were proposed by [54] and used in fiber reinforced and peaty soil ([55],[56]). Thus, at lower confining stresses, which exist on a vegetated slope, the effect of roots could be considered as altering the frictional component of the soil see (Fig.2.13).

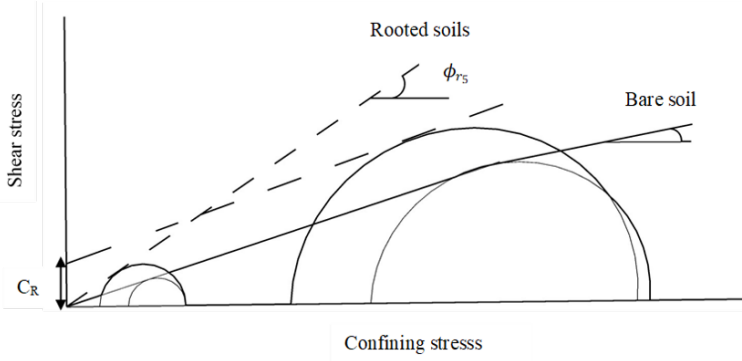


Figure 2.13: Schematic illustration of effect of confining pressure on the contribution of root permeated soils. (Adapted from [54])

The roots of SF and HL were found to increase the frictional component of the failure envelop in this study, Fig 3.12. The following analysis is based on [17], [54] and is deliberately simple to conceptually show how an increase in friction angle could be determined under low confining stresses. In the analysis proposed here, the roots are assumed to be in tension. The externally determined friction angle of bare soil will be

$$\phi_{bs} = \frac{\tau_{bs}}{\sigma_s} \quad (2.6)$$

Where  $\tau_{bs}$  is the shear strength of bare soil. In rooted soils, the normal confining stress increases due to the confinement imposed by the roots resulting in an extra normal stress term  $\sigma_s$

$$\sigma_s = \sigma_{applied} + \sigma_R \quad (2.7)$$

Since the externally applied normal stress  $\sigma_{applied}$  is used to compute the externally determined friction angle

$$\sigma_{applied} = \sigma_s - \sigma_R \quad (2.8)$$

$$\phi_{rs} = \frac{\phi_{bs}}{\sigma_{applied}} \quad (2.9)$$

$$\phi_{rs} = \frac{\tau_{bs}}{\sigma_s - \sigma_R} \quad (2.10)$$

Since at low confining stresses, roots pull out and the normal stress governs the value  $\sigma_R$ , can be written as a factor of the normal stress,  $F$ , which is the friction factor between the roots bundle and the soil. The factor of the normal stress,  $F$ , will depend on the number of properties, such as the stiffness of the root, the area of the root, the angle of orientation of the root, root tortuosity etc.

$$\phi_{rs} = \frac{\sigma_s \times \phi_{bs}}{\sigma_s - F \times \sigma_s} \quad (2.11)$$

$$\phi_{rs} = \frac{\phi_{bs}}{1 - F} \quad (2.12)$$

Thus, for  $0 < F < 1$  the friction angle of the rooted soil will be higher than that of the bare soil, which is in accordance with our findings.

The rooted soil behavior diverges from that of the bare soil in rooted specimens in the dilatancy-peak stress ratio plane. The rooted specimens exhibit higher peak stress ratio than bare soil (Fig 3.13) and hence higher mobilized friction angle is exhibited (Fig 9). The increase in stress ratio would be more evident when the soil dilates. However, such condition could be expected to occur in dense sand, where the roots might not be able to suppress the dilatancy of the soil. Nonetheless, such high-density soils would probably not support deep root growth. The results presented here thus present most likely favourable conditions for root reinforced soils.

### 2.6.5. VISCO-ELASTIC BEHAVIOUR OF ROOT PERMEATED SOIL

The study shows that Burger model has the potential to describe the time dependent behavior of rooted soils (Fig 7). The primary and secondary creep curves are perfectly captured of all the specimens tested. The decrease in the elastic modulus and  $\eta_m$  clearly depicts the damage developing in all specimens and a change to yield phase from elastic phase with shearing. At higher stress level  $\eta_m$ , representing the long-term behavior, is on average higher for the rooted specimens than that for the bare soil. On the other hand, the elastic modulus of bare soil is higher than for rooted specimens. This decrease results from the instantaneous and visco-elastic deformations. The displacement-controlled tests show that rooted specimens undergo higher displacement to mobilize their peak strength than bare soil. Therefore, the results obtained in load-controlled tests can be considered in accordance with the displacement-controlled test observations and the change in Burger parameters with applied stress can explain creep characteristics of rooted specimens. The decrease in  $\eta_m$  for rooted specimens at stresses higher than peak stress of soil shows a possibility of the “mobility” of roots at higher stress levels. Therefore, from the tests conducted in this study, it can be concluded that though the rooted specimens show higher instantaneous deformations, the permanent deformations at stress even higher than bare soil peak stress decrease.

### 2.6.6. USEFULNESS FOR BIO-ENGINEERED EARTH RETAINING SYSTEM

Both HL and SF increased the shear strength of the soil when compared to bare soil and hence can be considered to be useful for use in a bio-engineered earth retaining system.

However, further investigation is required to see the effect of larger displacements required to reach the beneficial effects of rooted soils on the serviceability conditions of the retaining structure. Additionally, the quick growth of HL and SF would be a very useful feature for bio-engineered earth retaining system where the vegetation is expected to contribute to the combined load carrying system of wood and soil, where the wood be allowed to exhibit decay, without compromising the systems' reliability.

## 2.7. CONCLUSIONS

Displacement-controlled and load-controlled tests were conducted on bare soil and soils reinforced by *Humulus lupulus* L. and *Salix fragilis* L. roots on an adaptable direct shear testing setup. The following conclusions were drawn:

- At low confining stress and moisture conditioned roots are observed to be pulled out of soil and increase the frictional component of the shear strength in the Mohr-Columb envelope.
- Load controlled tests show that rooted soils have a lower elastic stiffness than bare soil. From the tests performed, rooted soils are observed to have a higher resistance to long term loading.
- Under the tested conditions, rooted soils resist dilation better than bare soils and the positive effect can be explained as an increase in confining stress.
- In this study, root orientations do not seem to have a huge influence on the shear strength. This is possibly due to existence of a critical root area ratio (cRAR) above which root orientations have no influence when tested in a practical range of strains.
- *Humulus lupulus* L. and *Salix fragilis* L. increase the shearing resistance of the soil, and give the rooted soils some ductility. More research is necessary to ensure that the serviceability requirements may not be violated when vegetation roots are used in bio-engineered earth retaining structures (BEERS).

## 2.8. APPENDIX A: STRESS VS DISPLACEMENT & VERTICAL DISPLACEMENT VS HORIZONTAL DISPLACEMENT

2

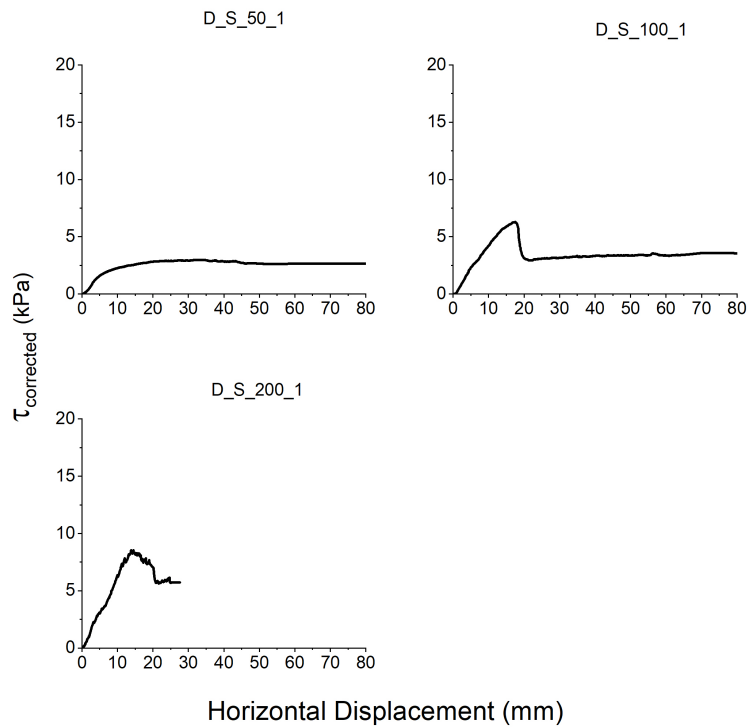


Figure 2.14: Corrected stress-displacement plot of bare soil. The first section on the title depicts the control (D for displacement controlled, L for load controlled), the second section depicts the soil type (S-bare soil, HL-*Humulus lupulus* L., SF-*Salix fragilis* L.), Third section depicts the normal load applied (50 for 50kg, 100 for 100kg, 200 for 200 kg), fourth section depicts the repetition number.

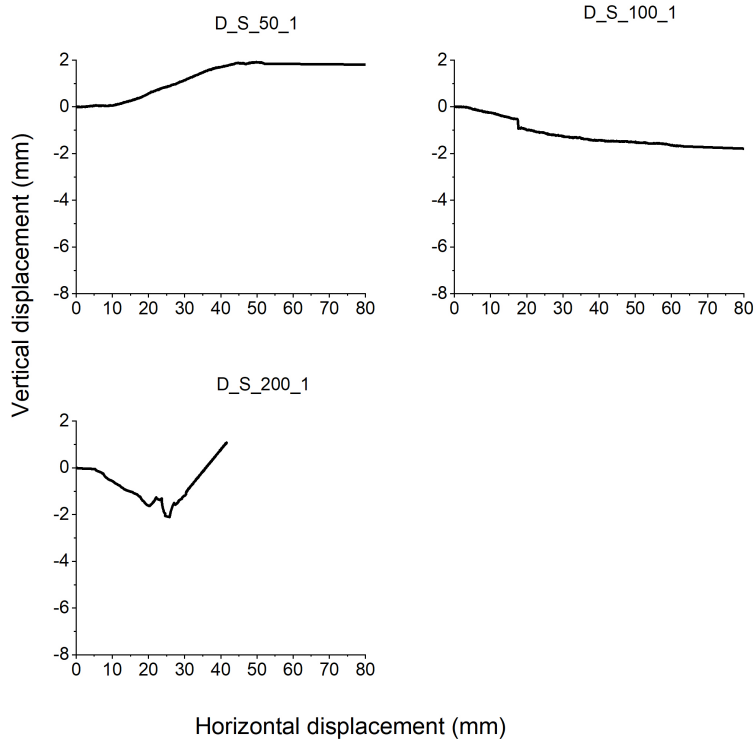


Figure 2.15: Vertical displacement vs Horizontal displacement of bare soil. The first section on the title depicts the control (D for displacement controlled, L for load controlled), the second section depicts the soil type (S- bare soil, HL-*Humulus lupulus* L., SF-*Salix fragilis* L.), Third section depicts the normal load applied (50 for 50kg, 100 for 100kg, 200 for 200 kg), fourth section depicts the repetition number.

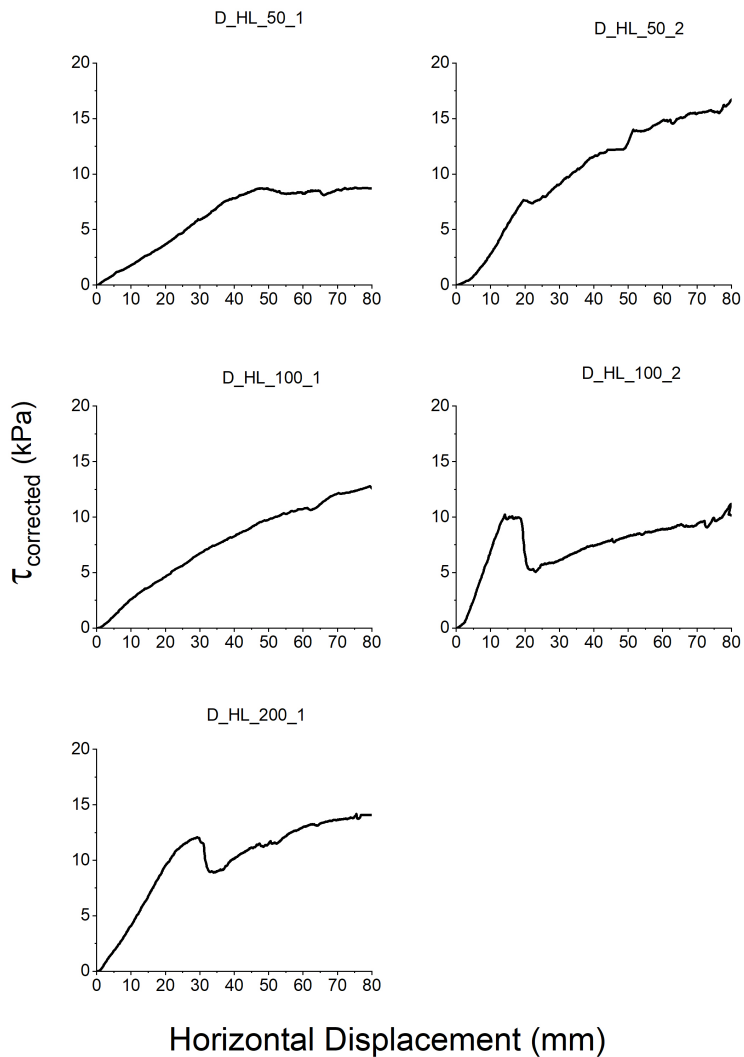


Figure 2.16: Corrected stress-displacement plot of HL. Corrected stress-displacement plot of bare soil. The first section on the title depicts the control (D for displacement controlled, L for load controlled), the second section depicts the soil type (S-bare soil, HL-*Humulus lupulus* L., SF-*Salix fragilis* L.), Third section depicts the normal load applied (50 for 50kg, 100 for 100kg, 200 for 200 kg), fourth section depicts the repetition number.

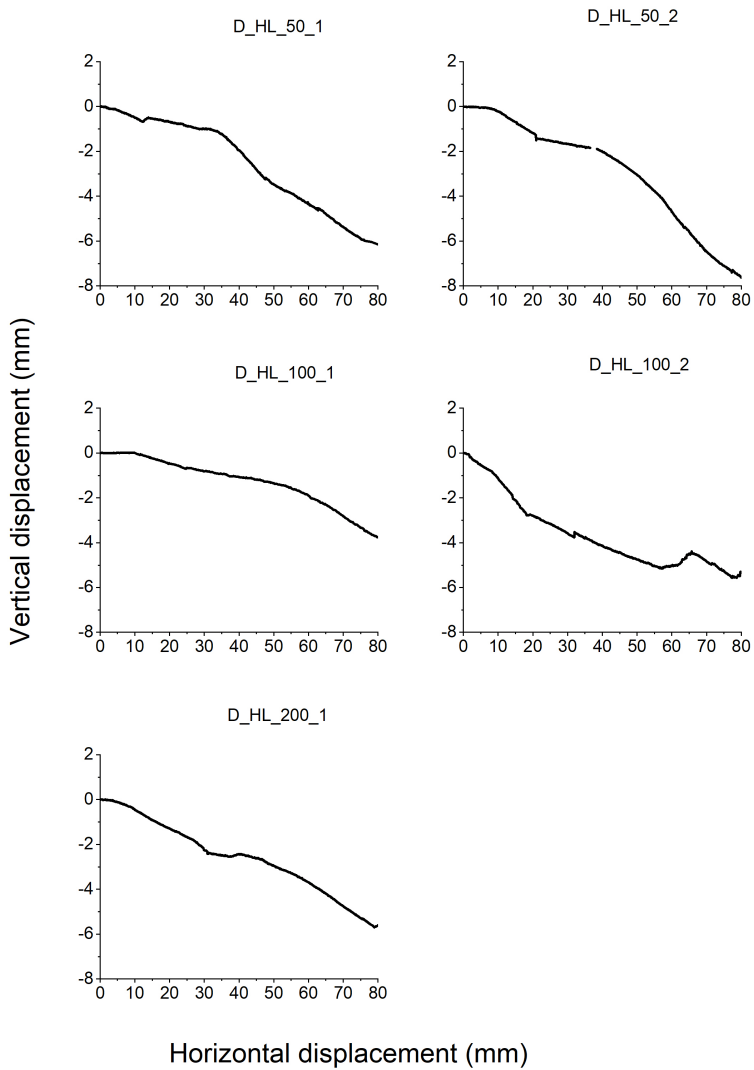


Figure 2.17: Vertical displacement vs Horizontal displacement of HL. The first section on the title depicts the control (D for displacement controlled, L for load controlled), the second section depicts the soil type (S-bare soil, HL-*Humulus lupulus* L., SF-*Salix fragilis* L.), Third section depicts the normal load applied (50 for 50kg, 100 for 100kg, 200 for 200 kg), fourth section depicts the repetition number.

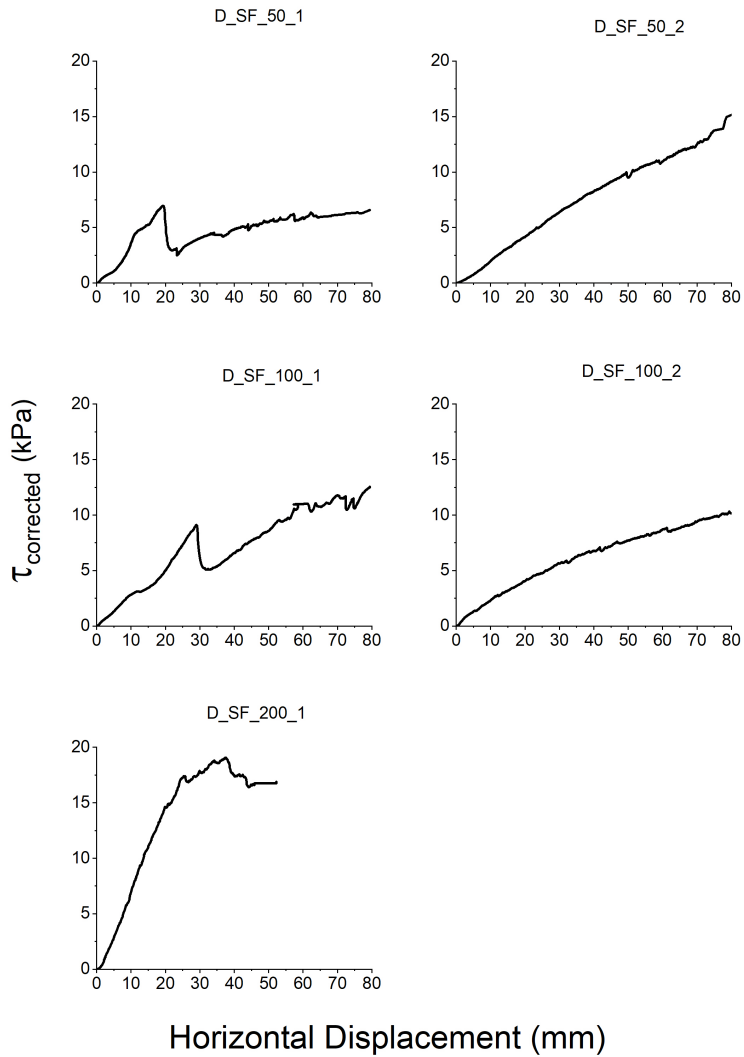


Figure 2.18: Corrected stress-displacement plot of SF. Corrected stress-displacement plot of bare soil. The first section on the title depicts the control (D for displacement controlled, L for load controlled), the second section depicts the soil type (S-bare soil, HL-*Humulus lupulus* L., SF-*Salix fragilis* L.), Third section depicts the normal load applied (50 for 50kg, 100 for 100kg, 200 for 200 kg), fourth section depicts the repetition number.

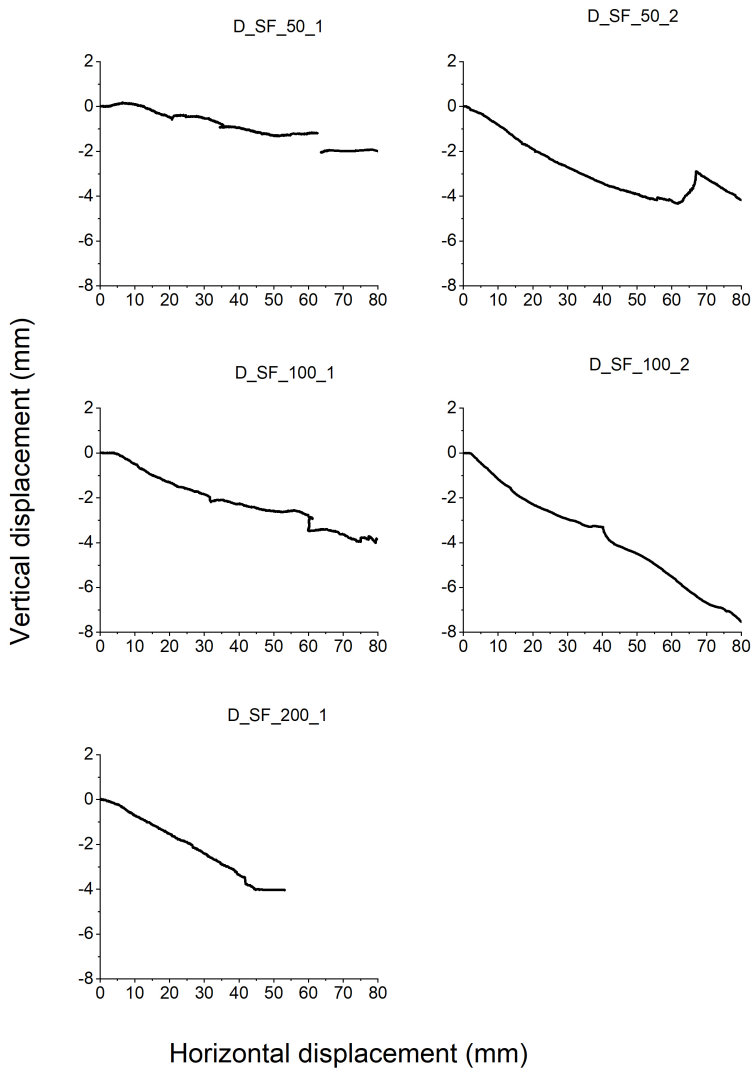


Figure 2.19: Vertical displacement vs Horizontal displacement of SF The first section on the title depicts the control (D for displacement controlled, L for load controlled), the second section depicts the soil type (S-bare soil, HL-*Humulus lupulus* L., SF-*Salix fragilis* L.), Third section depicts the normal load applied (50 for 50kg, 100 for 100kg, 200 for 200 kg), fourth section depicts the repetition number.

## 2.9. APPENDIX B: ROOT AREA AT DIFFERENT ORIENTATIONS

2

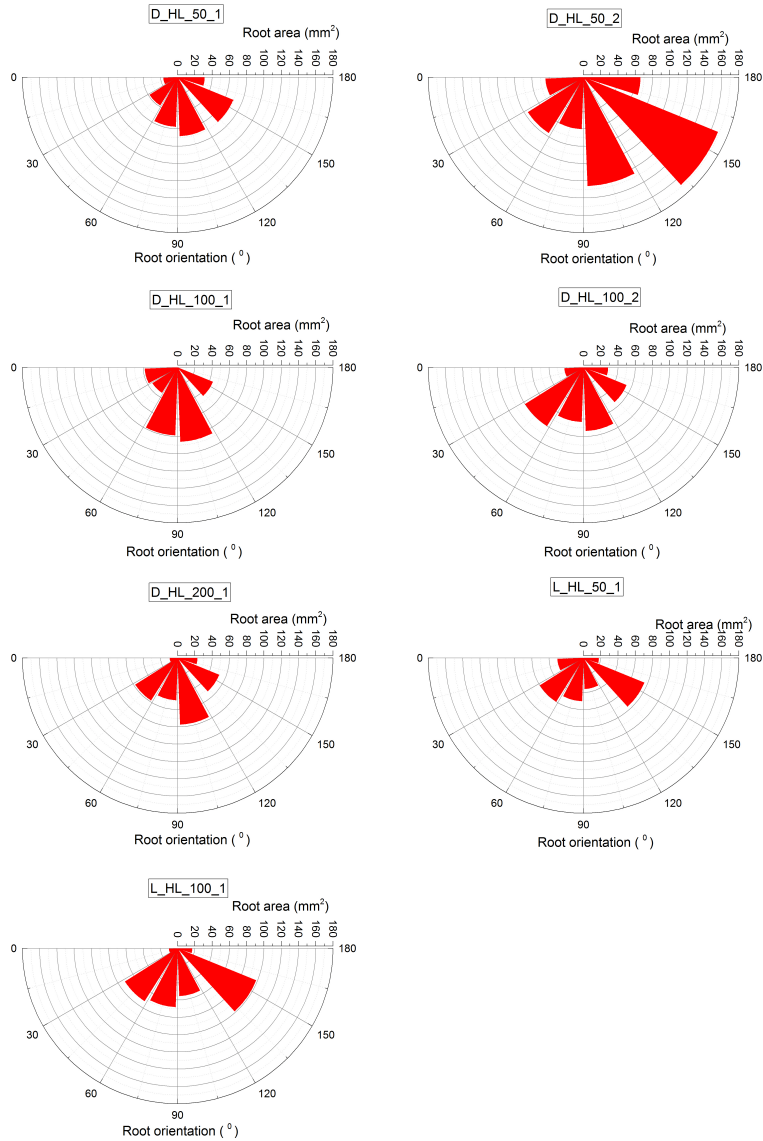


Figure 2.20: Root distribution of HL at different orientations. The first section on the title depicts the control (D for displacement controlled, L for load controlled), the second section depicts the vegetation type (HL for *Humulus lupulus* L.), Third section depicts the normal load applied (100 for 100kg, 50 for 50kg, 200 for 200 kg), fourth section depicts the repetition number.

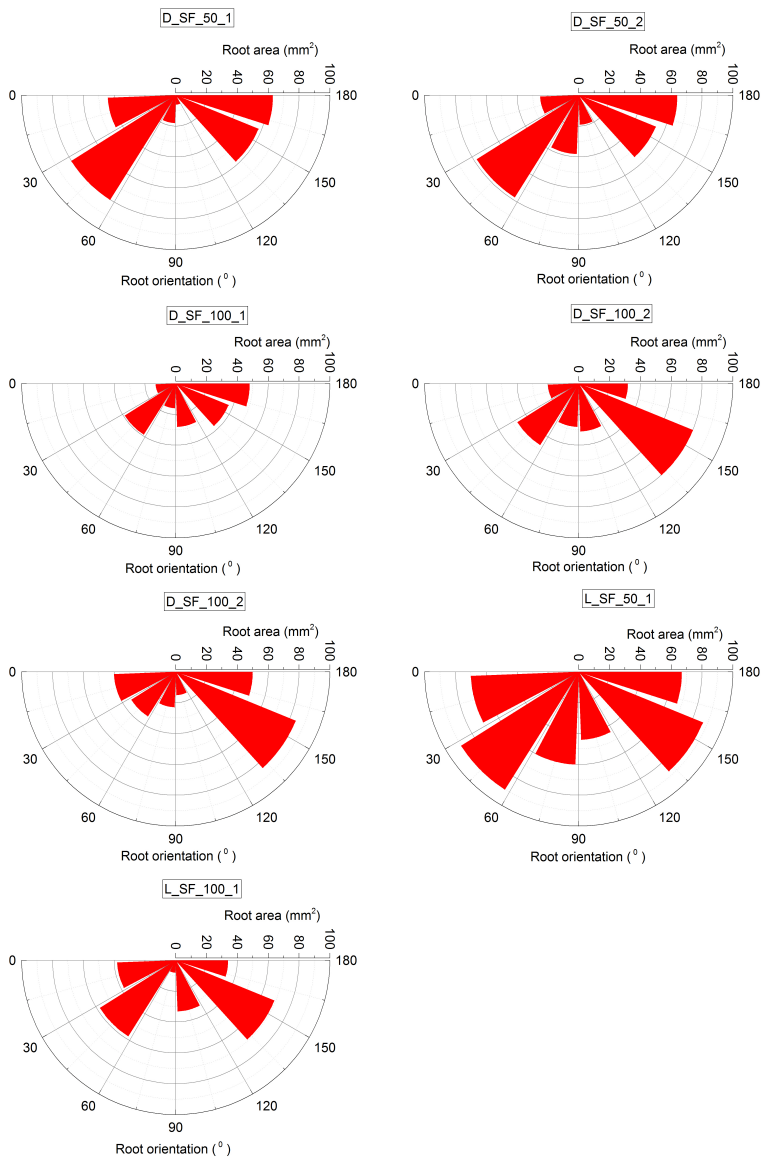


Figure 2.21: Root distribution of SF at different orientations. The first section on the title depicts the control (D for displacement controlled, L for load controlled), the second section depicts the vegetation type (SF for *Salix fragilis* L.), Third section depicts the normal load applied (100 for 100kg, 50 for 50kg, 200 for 200 kg), fourth section depicts the repetition number.

## REFERENCES

- [1] A. Evette, S. Labonne, F. Rey, F. Liebault, O. Jancke, and J. Girel, *History of bioengineering techniques for erosion control in rivers in western europe*, Environmental management **43**, 972 (2009).
- [2] L. Waldron, *The shear resistance of root-permeated homogeneous and stratified soil*, Soil Science Society of America Journal - SSSAJ **41** (1977), 10.2136/sssaj1977.03615995004100050005x.
- [3] S. Mickovski, P. Hallett, F. Bransby, M. Davies, R. Sonnenberg, and A. Bengough, *Mechanical reinforcement of soil by willow roots: Impacts of root properties and root failure mechanism*, Soil Science Society of America Journal - SSSAJ **73** (2009), 10.2136/sssaj2008.0172.
- [4] K. Loades, A. Bengough, F. Bransby, and P. Hallett, *Planting density influence on fibrous root reinforcement of soils*, Ecological Engineering **36**, 276 (2010).
- [5] M. Ghestem, G. Veylon, A. Bernard, Q. Vanel, and A. Stokes, *Influence of plant root system morphology and architectural traits on soil shear resistance*, Plant and Soil **377** (2014), 10.1007/s11104-012-1572-1.
- [6] B. Docker and T. Hubble, *Quantifying root-reinforcement of river bank soils by four australian tree species*, Geomorphology **100**, 401–418 (2008).
- [7] C.-C. Fan and Y.-W. Chen, *The effect of root architecture on the shearing resistance of root-permeated soils*, Ecological Engineering - ECOL ENG **36**, 813 (2010).
- [8] E. Comino, P. Marengo, and V. Rolli, *Root reinforcement effect of different grass species: A comparison between experimental and models results*, Soil and Tillage Research **110**, 60 (2010).
- [9] A. Yildiz, F. Graf, C. Rickli, and S. Springman, *Determination of the shearing behaviour of root-permeated soils with a large-scale direct shear apparatus*, Catena **166**, 98 (2018).
- [10] C. Zhang, L.-H. Chen, Y.-P. Liu, X.-D. Ji, and X. Liu, *Triaxial compression test of soil–root composites to evaluate influence of roots on soil shear strength*, Ecological Engineering **36**, 19 (2010).
- [11] F. Graf, M. Frei, and A. Böll, *Effects of vegetation on the angle of internal friction of a moraine*, For. Snow Landsc. Res **82**, 61 (2009).
- [12] M. Schwarz, D. Cohen, and O. D., *Root-soil mechanical interactions during pull-out and failure of root bundles*, Journal of Geophysical Research **115** (2011), 10.1029/2009JF001603.
- [13] A. S. R. A. Dias, *The effect of vegetation on slope stability of shallow pyroclastic soil covers*, Ph.D. thesis (2019).

- [14] T. Wu, W. III, and D. Swanston, *Strength of tree roots and landslides on prince of wales island, alaska*, Canadian Geotechnical Journal - CAN GEOTECH J **16**, 19 (1979).
- [15] N. Pollen and A. Simon, *Estimating the mechanical effects of riparian vegetation on stream bank stability using a fiber bundle model*, Water Resources Research **41** (2005), 10.1029/2004WR003801.
- [16] R. Thomas and N. Pollen-Bankhead, *Modeling root-reinforcement with a fiber-bundle model and monte carlo simulation*, Ecological Engineering - ECOL ENG **36**, 47 (2010).
- [17] D. Muir Wood, A. Diambra, and E. Ibraim, *Fibres and soils: A route towards modelling of root-soil systems*, Soils and Foundations **56**, 765 (2016).
- [18] M. Schwarz, A. Rist, D. Cohen, F. Giadrossich, P. Egorov, D. Büttner, M. Stolz, and J.-J. Thormann, *Root reinforcement of soils under compression*, Journal of Geophysical Research: Earth Surface **120** (2015), 10.1002/2015JF003632.
- [19] Q. NGHIEM, H. NAKAMURA, and K. Shiraki, *Analysis of root reinforcement at slip surface*. Journal of the Japan Landslide Society **40**, 302 (2003).
- [20] M. Acharya, *Analytical approach to design vegetative crib walls*, Geotechnical and Geological Engineering **36** (2018), 10.1007/s10706-017-0342-5.
- [21] G. Hunter and N. Khalili, *A simple criterion for creep induced failure of over-consolidated clays*, (2000).
- [22] J.-L. Briaud and R. Gibbens, *Behavior of five large spread footings in sand*, Journal of geotechnical and geoenvironmental engineering **125**, 787 (1999).
- [23] A. Whittle and J. Pestana, *Time effects in the compression of sands*, Geotechnique **48**, 695 (1998).
- [24] A. Segalini, G. Giani, and A. M. Ferrero, *Geomechanical studies on slow slope movements in parma apennine*, Engineering Geology **109**, 31 (2009).
- [25] J. Norris, A. Stokes, S. Mickovski, E. L. Cammeraat, R. Beek, B. Nicoll, and A. Achim, *Slope Stability and Erosion Control: Ecotechnological Solutions* (2008).
- [26] C. Phillips and C. Daly, *Willows or natives for stream bank control: a survey of usage in new zealand regional councils*, Motueka Integrated Catchment Management (Motueka ICM) Programme Report Series. Landcare Research, Lincoln (2008).
- [27] D. Delyser and W. Kasper, *Hopped beer: The case for cultivation*, Economic Botany **48**, 166 (1994).
- [28] R. Kneen, *Small scale and organic hops production*, Kneen, Left Fields, British Columbia, <http://www.crannogales.com/HopsManual.pdf> (ET, 21 Mart 2012) (2003).

- [29] H. Poorter, F. Fiorani, M. Stitt, U. Schurr, A. Finck, Y. Gibon, B. Usadel, R. Munns, O. Atkin, F. Tardieu, and T. Pons, *The art of growing plants for experimental purposes: A practical guide for the plant biologist*, *Functional Plant Biology* **39**, 821–838 (2012).
- [30] G. Veylon, M. Ghestem, A. Stokes, and A. Bernard, *Quantification of mechanical and hydric components of soil reinforcement by plant roots*, *Canadian Geotechnical Journal* **52**, 150428143438008 (2015).
- [31] A. Stokes, J. Norris, L. Beek, T. Bogaard, E. L. Cammeraat, S. Mickovski, A. Jenner, A. Di Iorio, and T. Fourcaud, *How vegetation reinforces soil on slopes*, (2008) pp. 65–118.
- [32] A. Dey and P. Basudhar, *Applicability of burger model in predicting the response of viscoelastic soil beds*, (2010) pp. 2611–2620.
- [33] A. Singh and J. Mitchell, *General stress-strain-time function for soils*, *J Soil Mech ASCE* **94**, 21 (1968).
- [34] K. J. Fridley, R. Tang, and L. A. Soltis, *Creep behavior model for structural lumber*, *Journal of Structural Engineering* **118**, 2261 (1992).
- [35] N. Yazdani, E. Johnson, and S. Duwadi, *Creep effect in structural composite lumber for bridge applications*, *Journal of Bridge Engineering* **9**, 87 (2004).
- [36] P. Georgiopoulos, E. Kontou, and A. Christopoulos, *Short-term creep behavior of a biodegradable polymer reinforced with wood-fibers*, *Composites Part B: Engineering* **80**, 134 (2015).
- [37] S. Springman, C. Jommi, and P. Teysseire, *Instabilities on moraine slopes induced by loss of suction: a case history*, *Géotechnique* **53**, 3 (2003).
- [38] J. Prabakar and R. Sridhar, *Effect of random inclusion of sisal fibre on strength behaviour of soil*, *Construction and Building materials* **16**, 123 (2002).
- [39] M. Schwarz, P. Lehmann, and D. Or, *Quantifying lateral root reinforcement in steep slopes—from a bundle of roots to tree stands*, *Earth Surface Processes and Landforms: The Journal of the British Geomorphological Research Group* **35**, 354 (2010).
- [40] P. Commandeur and M. Pyles, *Modulus of elasticity and tensile strength of douglas-fir roots*, *Canadian Journal of Forest Research* **21**, 48 (2011).
- [41] M. Schwarz, D. Cohen, and D. Or, *Pullout tests of root analogs and natural root bundles in soil: Experiments and modeling*, *Journal of Geophysical Research: Earth Surface* **116** (2011).
- [42] N. Pollen, *Temporal and spatial variability in root reinforcement of streambanks: accounting for soil shear strength and moisture*, *Catena* **69**, 197 (2007).
- [43] V. Operstein and S. Frydman, *The influence of vegetation on soil strength*, *Proceedings of the Institution of Civil Engineers-Ground Improvement* **4**, 81 (2000).

- [44] J. C. Ekanayake and C. J. Phillips, *A method for stability analysis of vegetated hillslopes: an energy approach*, Canadian Geotechnical Journal **36**, 1172 (1999).
- [45] R. L. Michalowski and A. Zhao, *Failure of fiber-reinforced granular soils*, Journal of geotechnical engineering **122**, 226 (1996).
- [46] A. Kamath, W. Gard, and J.-W. Van de Kuilen, *Biodynamic timber sheet pile walls: vegetation retaining structure*, European Journal of Wood and Wood Products **78**, 1045 (2020).
- [47] J. Zornberg, *Discrete framework for limit equilibrium analysis of fibre-reinforced soil*, Géotechnique **52**, 593 (2002).
- [48] K. S. Heineck, M. R. Coop, and N. C. Consoli, *Effect of microreinforcement of soils from very small to large shear strains*, Journal of geotechnical and geoenvironmental engineering **131**, 1024 (2005).
- [49] N. C. Consoli, M. A. Vendruscolo, A. Fonini, and F. Dalla Rosa, *Fiber reinforcement effects on sand considering a wide cementation range*, Geotextiles and Geomembranes **27**, 196 (2009).
- [50] F. H. Ali and N. Osman, *Shear strength of a soil containing vegetation roots*, Soils and Foundations **48**, 587 (2008).
- [51] D. H. Gray and H. Ohashi, *Mechanics of fiber reinforcement in sand*, Journal of geotechnical engineering **109**, 335 (1983).
- [52] R. Jewell, *Some factors which influence the shear strength of reinforced sand* (University of Cambridge, Department of Engineering, 1980).
- [53] D. Bull, I. Sinclair, F. Pierron, T. Roose, and J. Smethurst, *Understanding the mechanisms of root-reinforcement in soils: soil shear tests using x-ray computed tomography and digital volume correlation*, in *E3S Web of Conferences*, Vol. 92 (2019).
- [54] M. R. Hausmann, *Engineering principles of ground modification* (1990).
- [55] S. Cola and G. Cortellazzo, *The shear strength behavior of two peaty soils*, Geotechnical & Geological Engineering **23**, 679 (2005).
- [56] Y. Kong, A. Zhou, F. Shen, and Y. Yao, *Stress–dilatancy relationship for fiber-reinforced sand and its modeling*, Acta Geotechnica **14**, 1871 (2019).



# 3

## ROOT MECHANICAL STRENGTH CHARACTERIZATION

*"The important thing is not to stop questioning. Curiosity has its own reason for existing"*  
Albert Einstein



### 3.1. ABSTRACT

Vegetation is known to increase the stability of stream banks against shear failure. Generally, roots mechanical properties resemble those of a cable, i.e. high tensile strength and, in case of thin roots, no appreciable bending, shear or compression stiffness. Thus, the combination of roots and soil are seen to have better mechanical properties than soil alone due to the contribution of the tensile strength of the roots.

In this chapter, tension strength of *Humulus lupulus* L. (HL) and *Salix fragilis* L.(SF) are determined for two different soil moisture conditions. Tensile strength was observed to vary with diameter. Power law was observed to estimate volume-effect and fit all the tensile strength-diameter variations. Comparison of tensile strength in dry and wet conditions revealed that significant difference in tensile strength was observed for SF while no significant difference in tensile strength was observed for HL.

Load-controlled tests were conducted on fresh root samples of HL. Burger model and power law model shows promise to be able to capture the strain-time behavior of root samples reasonably well. The application of results of load-controlled tests are demonstrated using a simple but realistic power law model to predict time to failure of roots. While creep-failure of roots may not be of concern, significant deformations can occur which needs to be accounted in the current root-soil composite models.

### 3.2. INTRODUCTION

Vegetation reinforces soil, protecting the soil against erosion and shallow landslides. Several studies have focused on the removal of water from the soil by vegetation and subsequent hydrological reinforcement provided by the presence of roots ([1–3]). Apart from hydrological reinforcement, the mechanical reinforcement plays a major role on the stabilization of slopes against shallow landslides. Generally, roots mechanical behaviour resemble those of a cable, i.e. high tensile strength and stiffness, but not any appreciable any bending, shear or compression capacity because of their slenderness. Thus, the combination of roots and soil are seen to have better mechanical properties than soil alone due to the contribution of the tensile strength of the roots. The load acting on the soil along a shearing failure surface is transferred to the roots of the vegetation. [4, 5] proposed one of the earliest analytical models for estimating shear strength of root-soil composite based on root-soil interactions and force equilibrium. The tensile strength and the cross-section area of the roots at the shear surface were the governing factors in quantifying the mechanical contribution of roots. The model has been widely studied and used in the last few decades. When soil-root composite undergoes shear, roots are elongated due to the deformations occurring in the shear zone placing the roots under tensile stress [6, 7]. Therefore, tensile strength of roots plays a significant role in estimating the ability of roots to increase the mechanical strength of soil, provided that the roots are well anchored and do not pull out.

Studies reported in literature have focused on evaluating the tensile strength of variety of species from grasses [8] to mountainous trees [9]. A number of factors like age, diameter, type of root, soil type, root 3D pattern, season of sampling, soil density, waterlogging, among others, are associated with the variability in root tensile strength. The root diameter significantly influences the root tensile strength [10–13]. A negative power law relationship has been used to describe the variation of tensile strength with diameter and Young's modulus with diameter [12, 14]. As in wood, the composition of roots also changes with increasing diameter. While [15] attributed the decrease in strength with increasing diameter to decrease in cellulose content of the roots as diameter increases, [16] suggested the decrease in strength is due to lignin/ cellulose ratio with increase in diameter. Recently, a number of experimental studies on roots of woody species argued that the negative power-law relationships may not hold for all species [9, 17, 18].

The top few centimeters of the soil along the banks of canals and especially in summer larger parts of the banks would be relatively dry compared to winter conditions. [19] suggested that root tensile strength varies widely with changes in moisture. The root tensile strength was shown to increase with drying of roots [20]. The variation of Young's modulus with root moisture variation has been barely studied with few exceptions [9].

This study was conducted in the context of understanding the effect of the root strength variation on a timber sheet pile-vegetation earth retaining system for protecting canal banks [21]. The tensile strength variation during winter (saturated conditions) and summer (dry conditions) provides an understanding on the load sharing between the root-soil system and the timber sheet pile. In the timber sheet pile-vegetation system, as time progresses the timber sheet pile will undergo slow decay and the roots of the vegetation can take over the load on the stream bank. Thus, the roots of the vegetation will be subjected to long term loading to support the banks of the streams. This load might be well

below the peak tensile load that the roots can sustain, but will be acting on the roots for longer period of time. However, to the best knowledge of the author, there has been no study focused on the root mechanical behavior under sustained loading.

In this study the tensile strength of two species, *Salix fragilis* L. (SF) and *Humulus lupulus* L. (HL), is investigated. The experimental study presented here has the following objectives:

- (i) characterizing the root tensile strength and Young's modulus of the selected vegetation;
- (ii) study the variation in root tensile strength and Young's modulus under different soil moisture conditions;
- (iii) characterize behavior of roots under sustained loading conditions below the peak strength;
- (iv) attempt a practical approach to estimate the time to failure of roots under sustained tension.

### 3.3. MATERIALS & METHODS

#### 3.3.1. TESTING OVERVIEW

Two different types of tests were conducted to investigate the tensile strength of roots: (i) displacement-controlled test, which is the traditional testing method ; and (ii) step wise-load-controlled test, which allows a deeper understanding of how the root behaves when subjected to long term loading. The displacement-controlled test was performed on roots in two different moisture conditions: (a) wet (saturated conditions) correspondent to the winter period; and (b) dry (unsaturated conditions) correspondent to the summer period. However, note that the load-control tests were only performed in wet conditions and on one of the species (HL) due to the time-consuming nature of the test (Table.3.1).

Table 3.1: Overview of the methods and moisture conditions of the tensile strength testing.

| Testing methods     | Displacement-control (i)        | Load-control (ii) |
|---------------------|---------------------------------|-------------------|
| Moisture conditions | Saturated (a) , Unsaturated (b) | Saturated (a)     |
| Species             | HL, SF                          | HL                |

#### 3.3.2. GROWING CONDITION

*Humulus lupulus* L. and *Sagris fragilis* L. were grown in wooden boxes of sizes 500mm\*500mm \* 400mm (width\*length\*depth) in which only one individual plant was present per box. The boxes were placed in Botanical garden of TU Delft (52.0077°N, 4.3710°E), in the Netherlands. The plants were kept in the open space with no interference of buildings or other vegetation on the growth conditions. The climate in this region is temperate maritime with summer temperature during the growth period between 12°-36°C and winter temperature between 0°-9°C. Annual rainfall is about 700 millimeters; however, the plants were irrigated once every three days on average during the summer months from May-October. The growing medium is SM according to USCS classification.

Table 3.2: Summary of the root sampling and soil moisture adopted for each root

| Moisture conditions | Saturated                               | Unsaturated                    |
|---------------------|---|--------------------------------|
| Average suction     | <1 Kpa                                  | 22 kPa                         |
| Testing period      | Winter                                  | Summer                         |
| Prior to excavation | Soil submerged for 24h                  | Soil moved in-doors            |
| Roots preservation  | Roots preserved in water in sealed bags | Roots preserved in sealed bags |

3

### 3.3.3. ROOT SAMPLING

A total of five individuals were excavated of HL and six of SF for collection of roots for tensile strength testing. The above ground biomass was cut off before excavation to allow for convenient excavation and to avoid any stress on the roots during excavation. Sharp garden cutting tool, pruning shear, was used to cut the roots to prevent any pre-stress of the fibres. During winter, the boxes were saturated by submerging them in water for 24 hours before root excavation (i) (a). The excavated roots were placed in sealed bags filled with water and tested immediately after excavation. Straight roots of constant diameter throughout the length were selected for the study on time dependent behavior of roots in saturated conditions. This required the excavation of four plants of HL, which was the only species to be subjected to this testing method. During summer, the boxes were moved into an indoor-environment to determine the roots' strength in dry conditions. The roots were excavated and preserved in sealed plastic bags to prevent any further water loss. The suction of the soil was measured during the excavation of the roots in summer (Table.3.2).

A total of 65 root samples each from HL with a range of diameters from 0.2 mm to 6 mm and 0.3 mm to 4.5 mm were selected for saturated soil (HLW) and dry soil (HLD) displacement-controlled testing, respectively. A total of 66 root samples each from SF with a range of diameters from 0.2 mm to 4.5 mm and 0.2 mm to 4 mm were selected for saturated soil (SFW) and dry soil (SFD) displacement-controlled tests, respectively. A total of 22 roots with average diameter of 2.16 mm and 18 samples of average diameter 3.6 mm of HL were sampled for sustained loading tests. The root samples were then cut into specimens with a length of 120 mm making sure the root did not present any irregularity caused by tortuosity or previous damage. Furthermore, any fine branch extruding from the root is cut off at a distance of 3 mm from the specimen root.

### 3.3.4. TENSILE TESTING

In a displacement-controlled test, a test is deemed successful if the root failed in tension and strictly at a minimum of 1/3 of the free length from the clamps. All the displacement-controlled tests were conducted at a uniform displacement rate of 0.05mm/minute. [22] reported no significant effect of strain rate on tensile strength of roots. Nevertheless, the chosen displacement rate is within the range reported for moderate to rapid landslides. Young's modulus was determined from the displacement reading between the clamps as direct mounting of extensometers on the specimens was not possible.

In a load-controlled test, the tests last for more than 30 minutes, which could result

in change in the moisture content of the root. Thus, in addition to the root being tested, a second specimen of similar dimensions was placed inside the testing chamber. This root acts as a control for measuring the change in moisture content of the tested root. The weight of this root is monitored to check for any loss in moisture during testing. Two to three load steps within the peak expected load was aimed per root sample. The load-controlled tests were conducted using the following protocol in the machine:

- (i) A controlled displacement rate of 0.05mm/sec is applied until the target load is reached;
- (ii) The apparatus is then automatically switched to load-controlled mode and the target load is kept constant. See (Fig.3.2);
- (iii) The root is stretched under the constant load for a predefined time period (3.000-6000 seconds);
- (iv) After the completion of the prescribed time period, the root is subjected to the next target load;

The load-controlled tests were conducted in a chamber with controlled temperature. As a first step temperature to be set for minimum evaporation is determined based on reducing the difference between maximum humidity ratio  $X_s$  of saturated air and humidity ratio of air  $X$ . For instance, with temperature 18°C and relative humidity 60% the humidity ratio  $X$  is (0.0078318 kg/kg).  $X_s$  for a temperature of 10°C is 0.007612 (kg/kg) and 0.01062 for 15°C. Thus, a temperature of 11°C was chosen as starting point for the temperature at which the test is conducted. A sample is placed inside the chamber for 30 minutes and the moisture change is measured, and the temperature is modified if necessary. In addition to minimize the moisture content loss from the surface of the root during load-controlled test, a moist tissue was wrapped around the root specimen as shown in (Fig.3.1b). The wrapper is sprayed at constant intervals with water.

### 3.3.5. RHEOLOGICAL MODELS

A physical model (Burger model) and an empirical model (power law model) were used to study the time dependent viscous behavior of roots. The software Origin Pro. 8 was used to obtain the parameters of the models with the non-linear curve fitting.

The Burger model is a visco-elastic approach. The generalized Burger model consists of linear Maxwell and Kelvin unit combined in series. Sometimes multiple linear Kelvin units are used for improved accuracy. The Maxwell spring accounts for the instantaneous deformation and the Maxwell dashpot for the linear viscous deformation. The visco-elastic deformation is the resultant of the Kelvin unit. The Burger rheological model has been employed to study the time-dependent behavior of soils [23–25] and has been implemented in a number of finite difference method software programs such as Flac 3D. The creep behavior of wood, that has the same basic components of roots, and wood fiber-polymer composites have also been fitted well with burger model or a modified version of the generalized burger model for mechanosorptive effects [26–28]. Hence, the Burger model can be considered as having potential to model root-soil composite. General Burger model is given by:

$$\varepsilon(t) = \sigma \left[ \frac{1}{E_m} + \frac{1}{E_k} \left[ 1 - \exp\left(\frac{-E_k}{\eta_k} t\right) \right] + \frac{\sigma}{\eta_m} t \right] \quad (3.1)$$

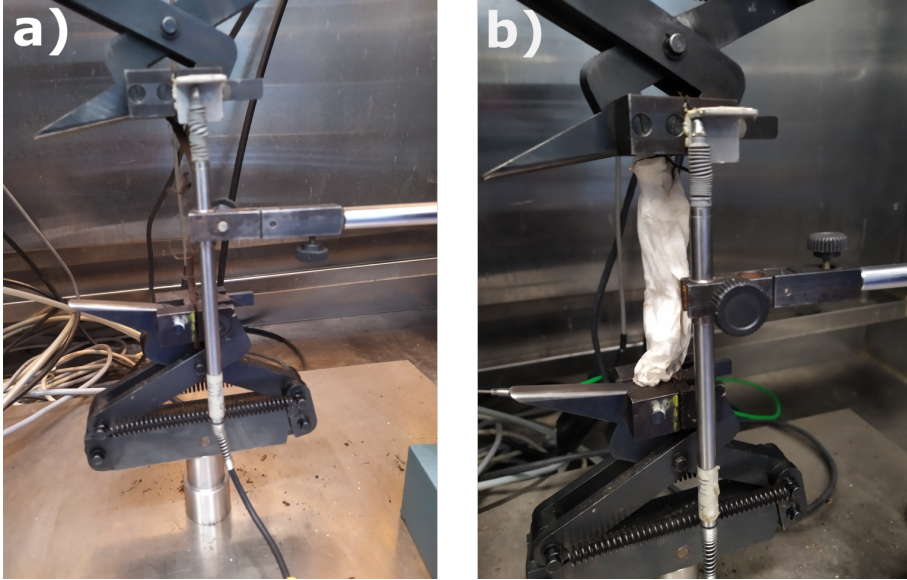


Figure 3.1: Testing setup: (a) root attached to the clamps and extensometer, and (b) wet tissue used to maintain the moisture content stable in the root during the load-control tests.

Where  $\varepsilon(t)$  is the creep strain,  $\sigma$  is the stress,  $t$  is the time,  $E_m$  and  $\eta_m$  are the elastic modulus of spring and viscosity of the spring and dash pot elements in the Maxwell unit respectively.  $E_k$  and  $\eta_k$  are the elastic modulus of the spring and viscosity of the dash pot in the Kelvin's unit respectively.

The power law model [26] used to simulate the time dependent viscous behavior of roots is given by:

$$\varepsilon(t) = \varepsilon_0 + At^n \quad (3.2)$$

Where  $A$  and  $n$  are the material constants and  $\varepsilon_0$  is the instantaneous strain at  $t=0$ .

As seen from the shear tests (Chapter 2), root-soil composite behavior resembles that of a ductile material. When the roots are used as a structural element as in a bio-engineered earth retaining systems [21], the serviceability failure criterion can be critical due to the large strains showed by the root-soil composite. The following estimation of time to failure is simplified and follows from the approaches on creep studies in soil [29, 30]. The rather crude analysis is shown for demonstrating the application of the tests on roots. Assuming the criterion for creep failure in a tension test as a critical strain, for e.g. 18% strain ( Note: this is arbitrary and can depend on the application) , the minimum time to creep failure can be estimated from the following power law equation:

$$\frac{s_f}{s_0} = \frac{s_f}{s_1} = \left( \frac{t_f}{t_1} \right)^N \quad (3.3)$$

Where  $s_f$  is the critical strain,  $s_0$  is the initial strain after loading at  $t=00$  minutes,  $s_1$  is the strain at the instant 1 minute.  $t_f$  is the time to failure  $t_1$  is the time corresponding

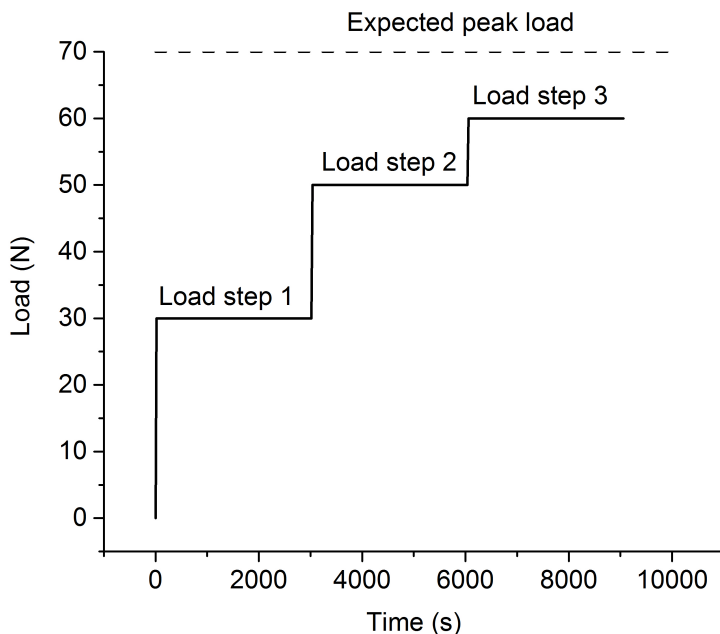


Figure 3.2: Illustration of the loading steps of the load-controlled test.

to  $s_1$ .  $s_0$  is approximated to  $s_1$  to adjust for the lag in test apparatus switching from displacement mode to load controlled mode. Assuming that creep failure can happen at any load level provided sufficient time is given to reach the critical strain and that the load level is proportional to the creep as in wood (validated from experiments shown in this study), time to creep failure depends on the parameter  $N$ . The  $N$  value is a material property and can be obtained as the slope of the straight part from the  $\log(s/s_1)$  versus  $\log(t/t_1)$  curve and will depend on the load level.

### 3.4. RESULTS

HLW and SFW tests show an elastic and a plastic nature, and are also characterized by failure at higher strain (Fig.3.3). HLD and SFD acted more rigid and stiffer, and failed at relatively lesser strain. Changing in behaviour from ductile to more brittle was observed when the water content of the soil decreased. The average above ground biomass in the HLD tests was 37 g and that of SFD 247 g.

#### 3.4.1. ROOT TENSILE STRENGTH WITHIN SPECIES

Root tensile strength of HLW and SFW was analyzed to determine the range of tensile strength values with the variation of the root diameter ( $D$ ). The tensile strength of both HLW and SFW decreased with diameter increase, see (Fig.3.4), (Fig.3.5). A power-

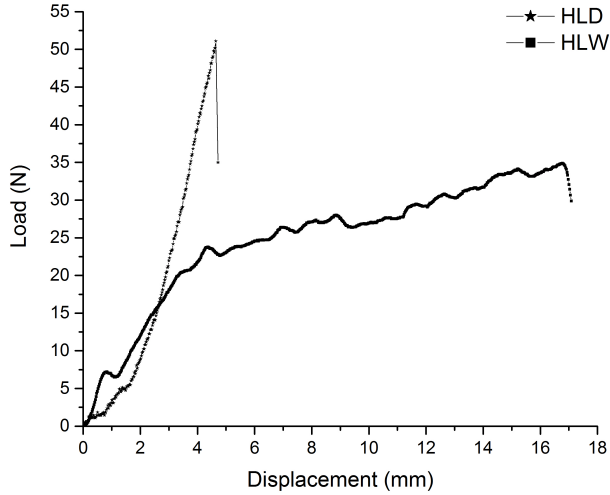


Figure 3.3: Representative load-displacement curve of dry and wet root samples, HLD-HLW

law relationship  $T_s = 10.9D^{-0.78}$  showed significant correlation (Adj. R-square = 0.60,  $p < 0.001$ ) between diameter and tensile strength. For SFW a power-law relationship was found significant,  $T_s = 29.8D^{-1.05}$  (Adj. R-square = 0.56,  $p < 0.001$ ) and an exponential fitting to the experimental data resulted in  $T_s = 17.0 + 268e^{-3.5D}$  (Adj. R-square = 0.56,  $p < 0.001$ ). After a root diameter of 1.5 mm, significant influence of diameter on strength is not observed for SF, while the tensile strength of HL was seen to further decrease within the tested diameter range but was less pronounced.

Box plots in (Fig.3.8) show the variation in tensile strength of HLW, SFW, HLD and SFD. HLD showed a power law variation with diameter given by equation  $T_s = 34.5D^{-0.395}$  (Fig.3.6) with a low Adj-R square (0.23), but significant. A power-law relationship ( $T_s = 56D^{-1.14}$ ) was used to describe the variation of tensile strength of SFD with diameter (Adj-R square=0.74;  $p < 0.001$ ). Roots of HLW and SFW were less strong than HLD and SFD respectively. However, the ANCOVA analyses using the root diameter as covariate shows that there is no significant difference in strength of HLW and HLD tests. Significant difference ( $p < 0.05$ ) was found in the average tensile strength between SFW and SFD. This implies that the drying of soil had an effect on the tensile strength of SF but had no significant influence on the HL tests. HLW tests resulted in values of Young's modulus ranging from 50 to 1455 MPa, with the majority of the samples (27 out of 30) having a Young's modulus below 400 MPa. The Young's modulus showed an increase with tensile strength and presented a linear relationship with tensile strength  $E = 0 + 21.4T_s$  (Adj. R-square=0.59  $p < 0.001$ ). The range of Young's modulus of SFW, HLD, SFD is shown in the box plot in (Fig.3.8). The variation of tensile strength with Young's modulus had a linear relationship for all the species. All the relationships are found to have a significance level  $p < 0.001$  except that of SFW. SFW had an Adj R-square of 0.26 with a significance level  $p < 0.05$ .

No significant difference exists in the tensile strength between HLW and SFW. How-

Table 3.3: Tensile strength of the different testing conditions and species (HLW, HLD, SFW, SFD): used equations, fitting parameters, coefficient of determination ( $R^2$ ), p-value,

|     | Equation          | Adj R-square | P      |
|-----|-------------------|--------------|--------|
| HLW | $20.9D^{-0.78}$   | 0.51         | <0.001 |
| HLD | $34.5*D^{-0.395}$ | 0.23         | <0.001 |
| SFW | $29.8D^{-1.05}$   | 0.56         | <0.001 |
| SFD | $56D^{-1.14}$     | 0.74         | <0.001 |

Table 3.4: Young's modulus of the different testing conditions and species (HLW, HLD, SFW, SFD): used equations, fitting parameters, coefficient of determination ( $R^2$ ), p-value,

|     | Equation       | Adj R-square | P      |
|-----|----------------|--------------|--------|
| HLW | $0+21.4*T_s$   | 0.59         | <0.001 |
| HLD | $15*T_s$       | 0.66         | <0.001 |
| SFW | $159+66.7*T_s$ | 0.26         | <0.05  |
| SFD | $93+12.6*T_s$  | 0.45         | <0.001 |

ever, after drying, significant difference is found in the tensile strength of HLD and SFD. This implies that roots of SF and HL reacted differently to soil drying. This could be due to different root composition and structure of SF and HL, which would have affected the water release from roots on soil drying.

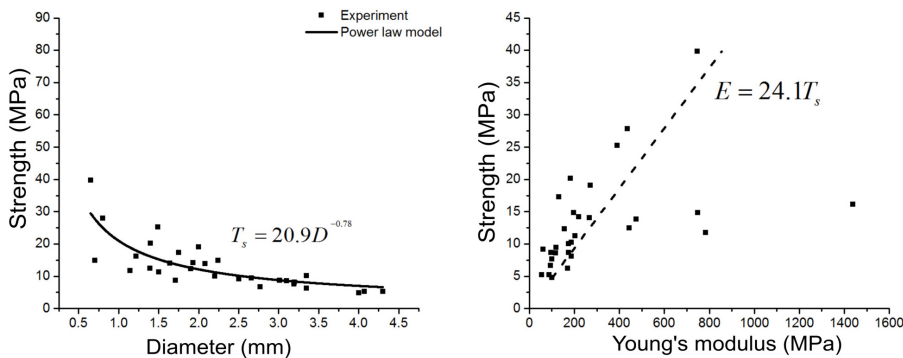


Figure 3.4: Variation of tensile strength and Young's modulus of HLW with diameter and tensile stress respectively.

### 3.4.2. VISCOUS BEHAVIOUR OF ROOTS

Three roots of a diameter of 2.16 mm (C-HL-1) were subjected to a total of six load steps (two load steps per root). Additional six roots of a diameter of 3.6 mm (C-HL-2) were subjected to a total of ten load steps. One root sample of each diameter was tested in a displacement-controlled tension test until failure. The displacement-controlled ten-

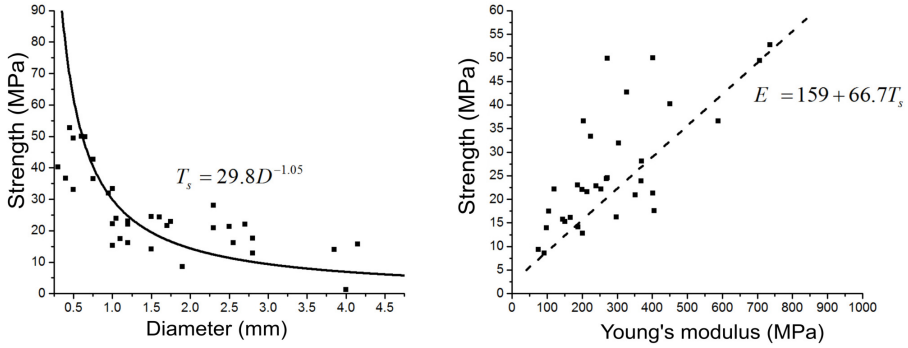


Figure 3.5: Variation of tensile strength and Young's modulus of SFW with diameter and tensile stress respectively.

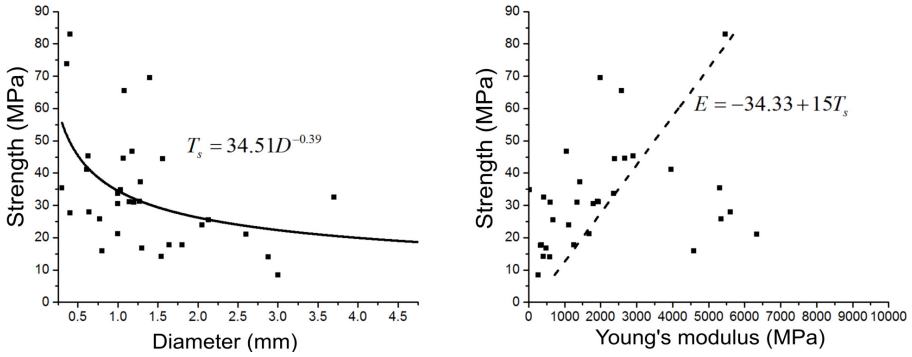


Figure 3.6: Variation of tensile strength and Young's modulus of HLD with diameter and tensile stress respectively.

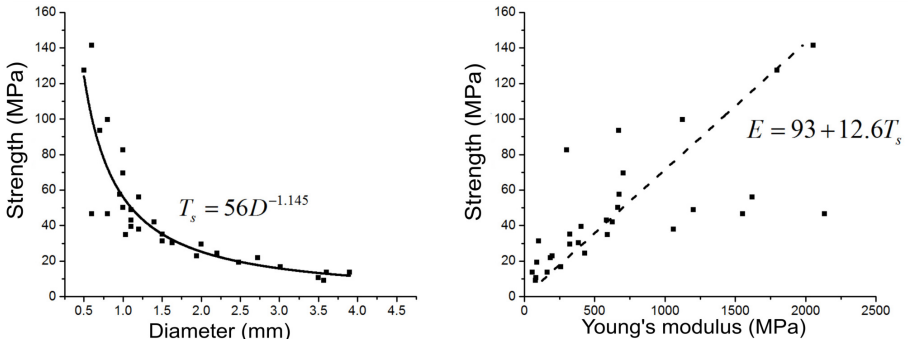


Figure 3.7: Variation of tensile strength and Young's modulus of SFD with diameter and tensile stress respectively.

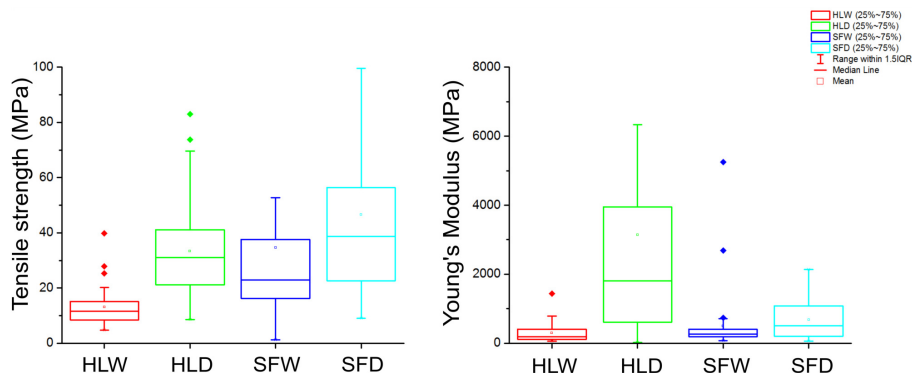


Figure 3.8: Box plots showing the variation in tensile strength and Young's modulus. The dots represent outliers, the Boxes represent the 25%-75% percentile variation.

sion tests show that a peak load of 61.7 N is resisted by 2.16 mm root and 70N by 3.6 mm root The load-displacement curves of load-controlled tests on root 2.16mm is given in (Fig.3.9 a) c) e)) and the corresponding  $\log(s/s_1)$  vs  $\log(t/t_1)$  is given in (Fig.3.9 b), d) e)).

The first root (Fig.3.9 a)) was subjected to a load of 10N and 20 N and then a load level of 60 N was attempted but failed in tension before reaching the final load. In the second root (Fig.3.9 c)), the load was held at 40N and 55 N for 3000 sec and in the third root (Fig.3.9 e) the load was held at 32 N and 50 N for 3000 and 5000 sec respectively. All the tests combined resulted in a range of load steps from 10N to 55N. The N value calculated as the slope of  $\log(s/s_1)$  vs  $\log(t/t_1)$  is reported in (Fig.3.12).

The Burger and Findley's power law model parameters used to fit the experimental data are presented in Table.3.5-Table3.8. Burger's model and power law model are able to capture time dependent behavior of the roots at sustained loading as seen in (Fig.3.14, Fig.3.15, Fig.3.16). The Burger's model is able to represent the instantaneous and visco-elastic strains better than the power law model. A general decrease in Burger's model parameters with increase in holding load is observed: (i) a progressively decrease in  $\eta_m$ , which represents the long-term non-recoverable deformation of the root, with increasing applied load shows the damage accumulation in the root; and (ii)  $E = E_m + E_k$ , representing the recoverable deformation also showed general decreasing trend which implies increasing damage. However,  $\eta_k$  showed an increase until about 50% of the peak load before decreasing. The increase in the n value in the power law model reflecting long term creep also increased with increasing load, which shows damage and increase in deformation with increasing constant load. The decrease in the parameter 'A', reflecting short term creep, was also observed. The parameters represented are for the best fit and negative values close to zero are included in equation though compression during tension test is not expected. These observations are in line with the physical observations of increasing strain for each load step during the test as given in the load-displacement curves.

Table 3.7: Burger model parameters 3.6 mm root

| Root number | Load (N) | $E_m$ (N/m <sup>2</sup> ) | $E_k$ (N/m <sup>2</sup> ) | $\eta_k$ (N/m <sup>2</sup> ) | $\eta_m$ (N/m <sup>2</sup> ) | $R^2$ |
|-------------|----------|---------------------------|---------------------------|------------------------------|------------------------------|-------|
| 1           | 53       | 334                       | 84                        | 1.8E6                        | 2E8                          | 0.80  |
| 2           | 67       | 696                       | 124                       | 6953                         | 57838                        | 0.99  |
| 2           | 35       | 3917                      | 161                       | 31087                        | 1.2E6                        | 0.97  |
| 3           | 35       | 340                       | 198                       | 36881                        | 1.13E6                       | 0.98  |
| 4           | 65       | 1.36E7                    | 4E6                       | 8E20                         | 32641                        | 0.98  |
| 4           | 5        | 261                       | 1026                      | 147905                       | 3.64E6                       | 0.87  |
| 5           | 60       | 2852                      | 399                       | 563286                       | 994927                       | 0.99  |
| 5           | 50       | 361                       | 370                       | 336968                       | 1.4E6                        | 0.99  |
| 5           | 40       | 998                       | 482                       | 159019                       | 1.26E6                       | 0.99  |
| 6           | 67       | 281                       | 152                       | 124983                       | 1.6E6                        | 0.99  |

Table 3.5: Burger model parameters 2.16 mm root

| Root number | Load (N) | $E_m$ (N/m <sup>2</sup> ) | $E_k$ (N/m <sup>2</sup> ) | $\eta_k$ (N/m <sup>2</sup> ) | $\eta_m$ (N/m <sup>2</sup> ) | $R^2$ |
|-------------|----------|---------------------------|---------------------------|------------------------------|------------------------------|-------|
| 1           | 10       | 32473                     | 419                       | 140374                       | 2.39E6                       | 0.93  |
| 1           | 20       | 2.8E19                    | 216                       | 14546                        | 927032                       | 0.96  |
| 3           | 32       | 672                       | 353.32                    | 159787                       | 1.89E6                       | 0.98  |
| 2           | 40       | 219                       | 194                       | 66158                        | 768912                       | 0.99  |
| 3           | 52       | 262                       | 83                        | 46593                        | 639286                       | 0.99  |
| 2           | 55       | 3479                      | 14.4                      | 105422                       | 95980                        | 0.98  |

Table 3.6: Power law model parameters 2.16 mm root

| Root number | Load (N) | A       | N    | $\epsilon_0$ | $R^2$ |
|-------------|----------|---------|------|--------------|-------|
| 1           | 10       | 3.2E-4  | 0.29 | 1E-4         | 0.97  |
| 1           | 20       | 7.22E-4 | 0.27 | 0.001        | 0.92  |
| 3           | 32       | 6.7E-4  | 0.27 | 1E-5         | 0.97  |
| 2           | 40       | 0.00198 | 0.23 | 4.9E-4       | 0.99  |
| 3           | 52       | 4.8E-4  | 0.4  | 0.00481      | 0.96  |
| 2           | 55       | 2.34E-5 | 0.96 | 1.04E-4      | 0.98  |

The N value determined from the slope of  $\log(s/s_1)$  versus  $\log(t/t_1)$  of all the tests is shown in Fig.3.12. A clear trend of increase in N with load is observed. After 90% of the peak load, a significant increase in N occurs. No failure happened in any test below 90% of the peak load within the tested time frame. However, creep failure is likely to occur when a critical strain is reached that can either be estimated from the displacement-

Table 3.8: Power law model parameters 3.6 mm root

| Root number | Load | A       | N      | $\epsilon_0$ | R2   |
|-------------|------|---------|--------|--------------|------|
| 1           | 53   | 0.7     | 0.002  | -0.7         | 0.59 |
| 2           | 67   | 0.0015  | 0.39   | 0            | 0.99 |
| 2           | 35   | 0.121   | 0.011  | -0.125       | 0.96 |
| 3           | 35   | 0.146   | 0.0093 | 0.147        | 0.99 |
| 4           | 65   | 2.7E-6  | 1.38   | 0.00112      | 0.99 |
| 4           | 5    | 0.007   | 0.03   | -0.00387     | 0.87 |
| 5           | 60   | 3.54E-5 | 0.6    | -2E-4        | 0.99 |
| 5           | 50   | 3.16E-4 | 0.37   | -0.0018      | 0.99 |
| 5           | 40   | 4.3E-4  | 0.3    | -1.3         | 0.98 |
| 6           | 67   | 0.0042  | 0.1753 | -0.005       | 0.99 |

controlled tests to reach the estimated peak stress or could be selected based on a serviceability condition with a maximum allowed strain of the structure or slope. In this crude analysis a peak strain is selected based on an approximate serviceability criterion. Rather than the possibility of creep failure, long term deformation due to the creep of roots will be investigated here. A critical strain of 18% is selected on arbitrary here for the purpose of demonstration of time to failure by creep deformation of roots. The following analysis is to show the practical implications of root creep. Load levels and their strain at  $t=0$  minutes are identified on the load-displacement curves in Fig.3.10, Fig.3.11. A value of N of 0.04 is selected here for demonstration. Vegetation's roots are still not being considered as structural elements in slope stability design; hence the selected critical strain is arbitrary. However, the above methodology can be adopted to estimate the time required for the critical strain to be reached. The time to failure predicted is given in Fig.3.13. For the chosen N value and load level, failure by creep is not reached. However, significant deformations at lower load levels are observed even for a shorter period of time for instance 1000 days. Please note that the x- and y-axis represent normalized values in terms of peak stress and critical strain in Fig.3.13.

### 3.5. DISCUSSION

No universally accepted testing protocol exists for root tensile testing. The ideal methodology in terms of clamping, testing speed and acceptance of a test as success or failure is debatable. Thus, it is worth mentioning the 'lessons learned' in this study briefly. The universal testing machine (UTM) is the most widely used for displacement-controlled tensile tests on roots [15, 31, 32] though other alternative equipment, such as adapting a direct shear device has been reported in literature [33]. A UTM with an adapted clamping system and controls for applying constant load was used in this study. Assessing the quality of the results and validity of the tests has been ambiguous and matter of debate among researchers [34]. Success rate is defined as the ratio of valid tests by the total number of tests conducted per test type. The strict protocol followed in this

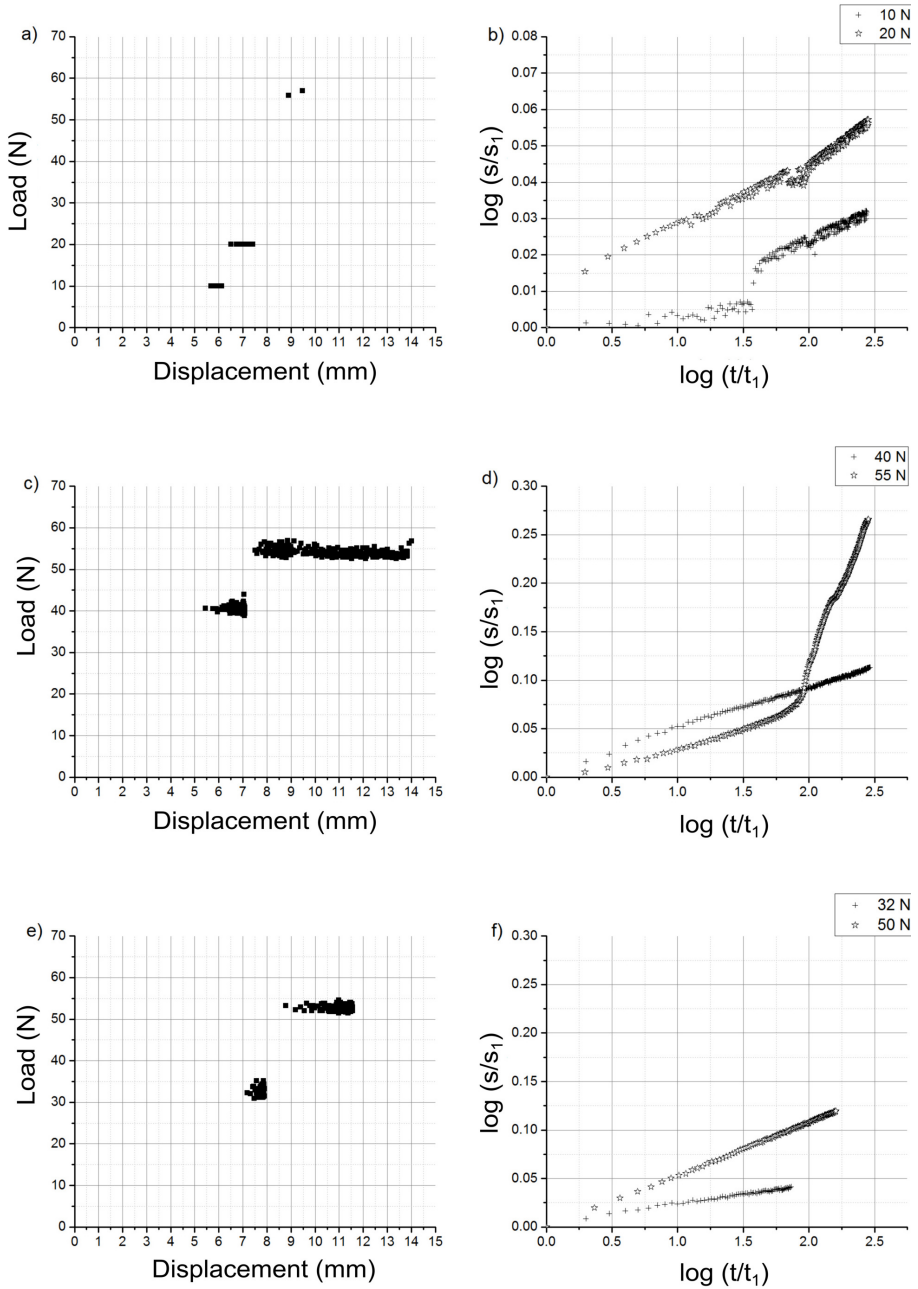


Figure 3.9: Load-displacement (left end side) and  $\log(t/t_1)$  versus  $\log(s/s_1)$  (right end side) in load-controlled tests on roots with a diameter of 2.16mm. a) and b) for root number 1, c) and d) for root number 2, e) and f) for root number 3.

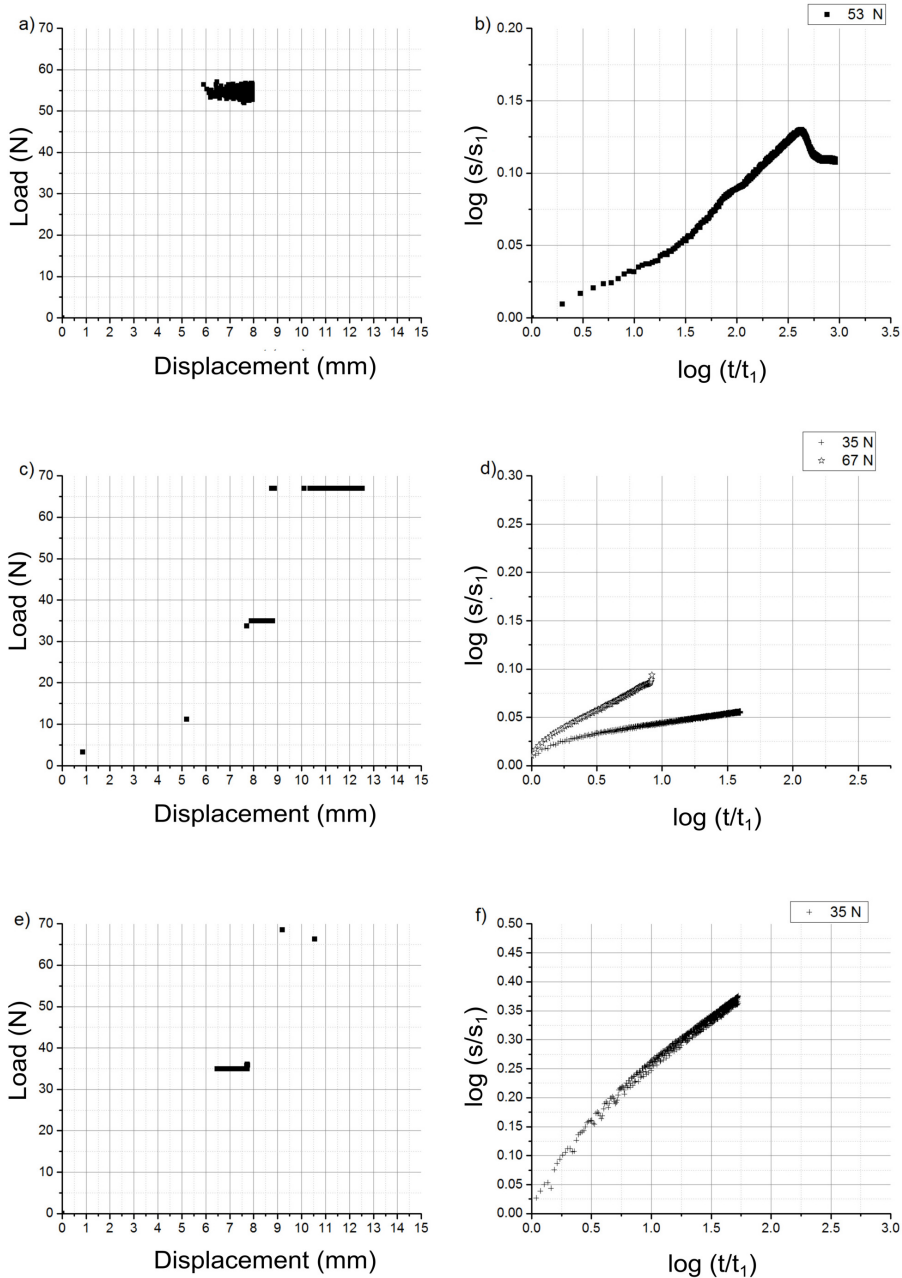


Figure 3.10: Load-displacement (left end side) and  $\log(t/t_1)$  versus  $\log(s/s_1)$ (right end side) in load-controlled tests on roots with a diameter of 3.6mm. a) and b) for root number 1, c) and d) for root number 2, e) and f) for root number 3.

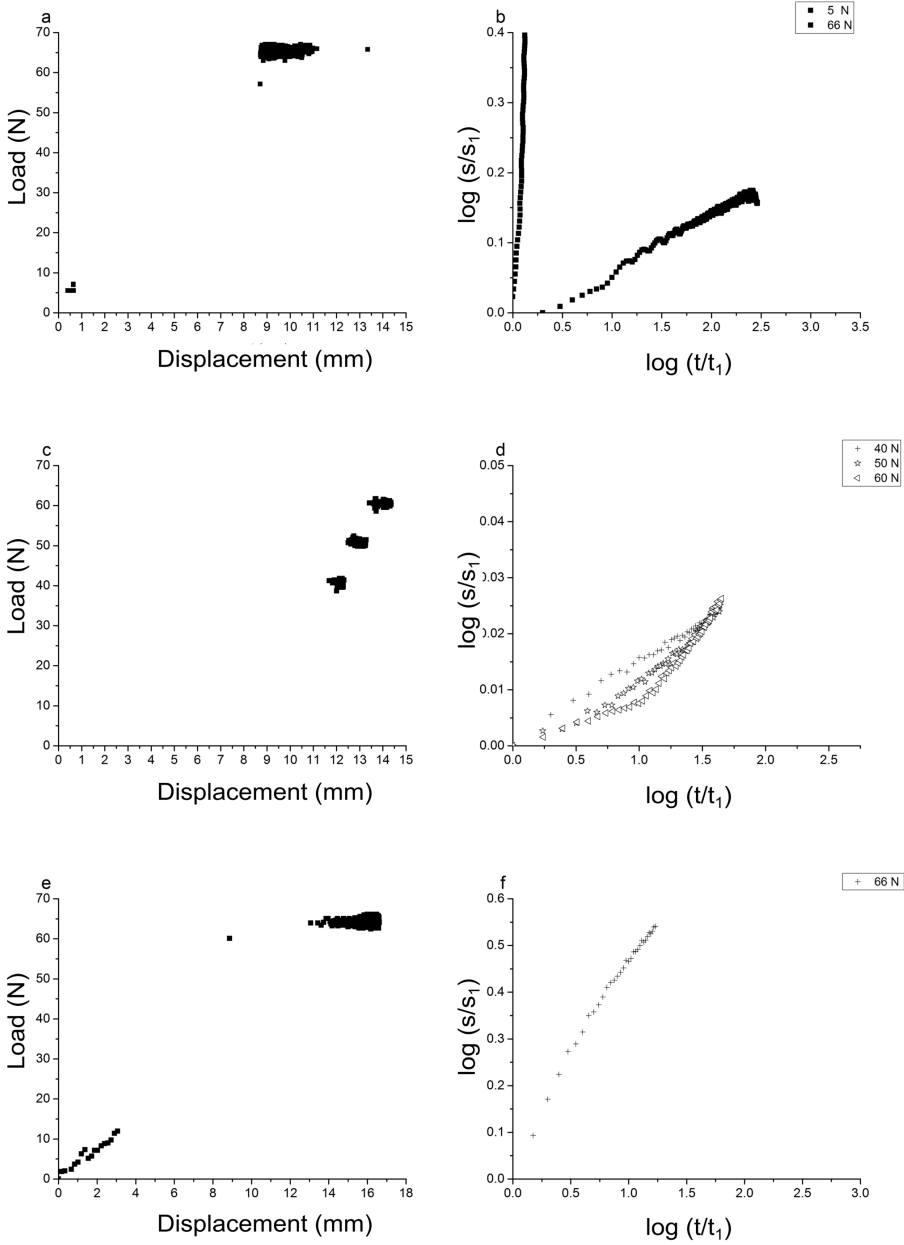


Figure 3.11: Load-displacement (left end side) and  $\log(t/t_1)$  versus  $\log(s/s_1)$  (right end side) in load-controlled tests on roots with a diameter of 3.6mm. a and b for root number 4, c and d for root number 5, e and f for root number 6.

study resulted in a success rate of testing of less than 50%. HLW and SFW had a suc-

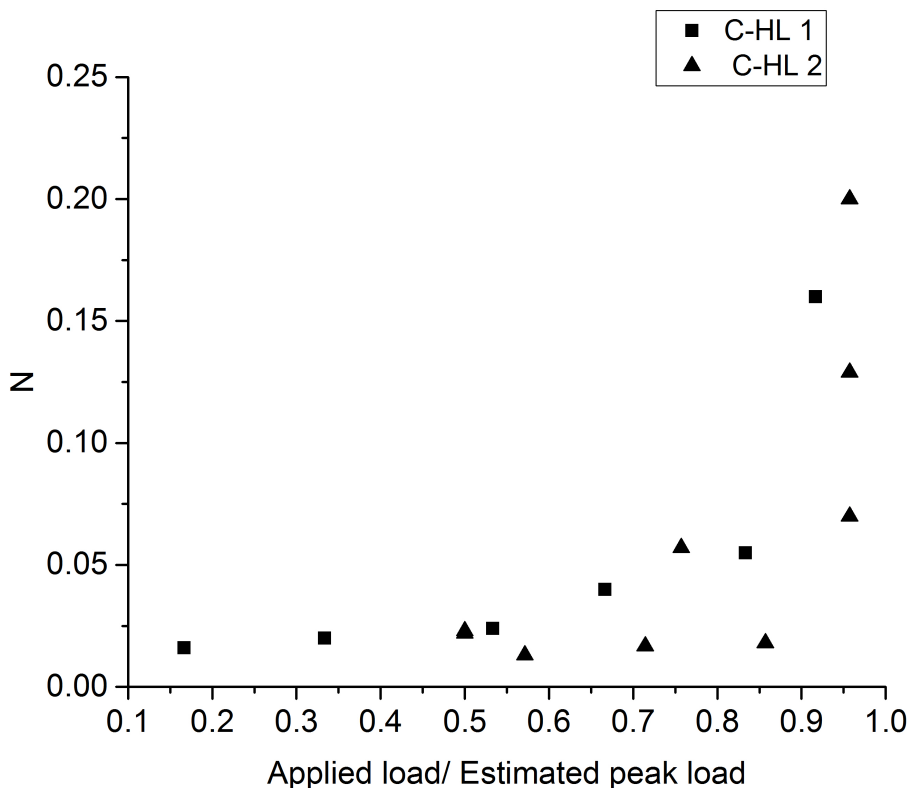


Figure 3.12: N value vs stress level.

cess rate of 48% and 52% respectively, indicating that dry roots have considerable higher strength and clamping may lead to premature failure. Low success rates in tensile tests on roots have been identified and reported in literature, eg. [6]. The check for the validity of the test results in this study was according to [35–37] which resulted in rejecting tests in which roots broke inside or near the clamps. [34] pointed out that a conservative approach as mentioned above has the drawbacks of time, cost and valid test being rejected. In addition, it was pointed that this could possibly result in a biasing the strength to higher ends of tensile strength. However, our observation during testing of roots of same diameter, length and moisture conditions multiple times shows a clear influence of clamping on any tests, which failed near the clamps.

No standardized clamping system exists for testing of roots. Hence, a variety of techniques are used by researchers, for instance screw clamps with sand paper attached to the screws were used by [13], a stone and epoxy mixture was applied at end of roots by [38], among others. Various techniques are reported in detail in [34]. Two different types of clamping techniques were attempted before using the jaw clamps mentioned here. A screw clamp with the root fixed to the clamp using extra strong epoxy made of a mixture of was used as a first trial. The second technique was using a drill bit to hold the roots



load step the tests equipment switched to the next load without the displacement mode being activated. Nevertheless, the tests were deemed successful, since the objective of the study was to study the viscous behavior at the chosen load level.

### 3.5.1. TENSILE STRENGTH AND YOUNG'S MODULUS VARIATION

The tensile strength of SF and HL roots in both moisture conditions followed a power-law relationship with the root diameter. A power-law is widely used to show the relationship between root tensile strength and root diameter ([6, 13]. Chemical composition of roots (lignin-cellulose ratio) could explain the variation of strength with diameter [15, 16]. Thicker roots have a smaller lignin-cellulose ratio compared to thinner roots. The positive correlation of lignin-cellulose ratio with tensile strength of roots implies that the root tensile strength would decrease with diameter [15, 39]. Thus, our results are in line with the previous studies showing that a power-law relationship can describe the variation of tensile strength with diameter.

The Young's modulus and tensile strength were significantly correlated in the present work. The Young's modulus is rarely reported in the literature with few exceptions [9, 18]. However, as seen in the shear (Chapter 2), the stiffness of root soil composite is different from that of bare soil, which cannot be explained or analysed without knowledge of the Young's modulus of roots. The increase in roots' stiffness observed with the reduction in soil moisture has implications on the global behavior of the root-soil composite. Dry roots will have a higher Young's modulus, which implies that a peak strength will be observed at smaller displacements due to higher mobilization of stresses [18]. The same roots in wet condition will exhibit a lower Young's modulus and strength, but maximum strength will most probably be reached at a higher displacement. Thus, the Young's modulus of roots has implications on strength mobilized at different displacements during the soil shearing. More importantly, the most recent models to estimate the reinforcement of the soil provided by the roots [40, 41], take into account the root-soil interactions that depend on the Young's modulus of the roots. Being able to estimate the stress-strain behaviour of the root allows more complex models to be adopted. The fact that the soil and the roots have different stiffness and their strength is mobilized at different strains, allows a better understanding of the stress-strain data of root-permeated soil.

### 3.5.2. EFFECT OF DRYING OF ROOTS

The soil moisture had no significant effect on the strength of HL roots while significant differences ( $<0.001$ ) were observed for SF roots. The reason for the different effect of the moisture conditions (or season) of the different species might be associated to the above ground biomass and to the type of plant. In the summer when the roots were excavated, the above ground biomass of HL was 35 g with no noticeable green leaves, while SF had an above ground biomass of 248 g with relatively greener leaves. The predominantly sandy soil used in this study might not reach the necessary negative water potential levels required to drive the water out of the roots. The SF is a woody plant and HL is an herbaceous climbing plant. The HL presented very little above ground biomass, showing evidence that the plant had died, for which the plant was not able to regulate the water exchanges with the atmosphere and soil. Therefore, the water content in the roots of HL was controlled by the moisture conditions of the soil. In contrast, SF had more

above ground biomass so that the atmosphere in summer could exert high negative water potential. The increase in strength of roots with drying in woody plants (which is the case of SF in this study) was reported by [20, 42]. The decrease in strength of the bonds between organic polymers in cells was seen as the reason for the difference in saturated roots and dry roots, similar to wood [43, 44]. HL being herbaceous, larger proportion of cortex tissues and less vascular tissues is expected [42] and a different moisture retention and hence the strength relationship with moisture would be observed.

## 3

### 3.5.3. VISCOUS BEHAVIOUR OF ROOTS

Though vegetation roots are known to increase the strength of soil, there has been no study looking into the time-dependent behavior of the soil reinforcement by roots. Even when creep failure is not of concern, large deformation when roots are under tension could be of interest to engineers and geologists. The results reported in the present study were not compared to similar tests on roots due to the fact that no other studies like this one were found. Therefore, the viscous behavior of roots is compared with other natural materials like wood and soil. Both wood and roots showed a dependency on the load level as both materials show an increase of the strains with higher load level. At loads higher than 90 %, an abrupt increase in of the N value is observed.

The reduction of the parameter  $\eta_m$ , in Burger's model depicting long term deformation, indicates higher mobility of the molecular chain in the root. When the serviceability conditions play a significant role in the design of engineering structures, such as a bio-engineered earth retaining system (BEERS), the evaluation the deformation characteristics of roots with time is necessary due to the ductile properties of the root-permeated soil. The power-law model used in this study was chosen deliberately to provide a preliminary assessment of the deformation of roots with time. A high stress level and a high N value was observed to be required for the roots to fail in tension due to creep. However, significant deformations (>20% of peak strain) are possible in a lower stress level (50% of peak load level) if enough time has passed. Such deformations might need to be taken into account in the design of service life of structures.

### 3.5.4. IMPLICATIONS FOR PRACTICAL APPLICATIONS

Tests on completely dry roots that have been reported in literature [9] give an understanding of the range of variation of tensile strength combined with tensile tests on saturated roots. However, the tensile strength of dry roots might never be used in engineering slope stability problems due to the possibility of overestimation of the resulting reinforcement provided by the roots. In a Bio-engineered earth retaining structure, such as a wooden sheet pile-vegetation system, the load acting on the wooden sheet pile plays a significant role on the service life of the system. The testing of dry roots provides an opportunity to estimate the extra load that could be supported by the vegetation in summer conditions, which would have implications on the service life. The saturation of roots subsequent to sampling could represent an appropriate condition (Conditions where positive root effects are needed), assuming that minimal transpiration occurs when there are high rainfall conditions in the winter. [36] pointed out that large differences in tensile strength exist among fresh, saturated and live roots. In the displacement-controlled tests in this study, there was minimal time between the excava-

tion and testing of roots, thus representing conditions close to the behavior that may be expected under embankment conditions. Currently, slope stability of vegetated slopes is analyzed in wet conditions subsequent to rainfall, which is generally the worst-case scenario. The roots are expected to help supporting the slope during this period, so the applied stresses on the roots will be at their highest. If the acting tensile load on the roots are well below their peak, and the root soil interaction does not fail, it is considered safe. Recently developed root reinforcement models take into account the progressive failure of roots [40, 45] where redistribution of stresses is taken into account.

### 3.6. CONCLUSIONS

Tensile strength of *Humulus lupulus* L. and *Salix fragilis* L. were determined at conditions representative of winter and summer soil moisture contents. It is observed that coarse grained soil may not reach negative water potential which are sufficient to drive water out of the roots in *Humulus lupulus* L. *Salix fragilis* L. showed significant difference in the tensile strength when tested in different moisture conditions. Burger model was observed to be able to predict the strain-time behavior of roots when tested in load-controlled tests for the time spans tested. At stresses which are lower than 0.9 times peak tensile strength of the roots, no roots were observed to fail after creep loading for more than 3000 seconds. However, they might undergo significant deformations which could be detrimental to Bio-engineered earth retaining structures.

### 3.7. APPENDIX A: STRAIN TIME EXPERIMENTAL CURVES FITTED WITH BURGER AND POWER LAW MODEL

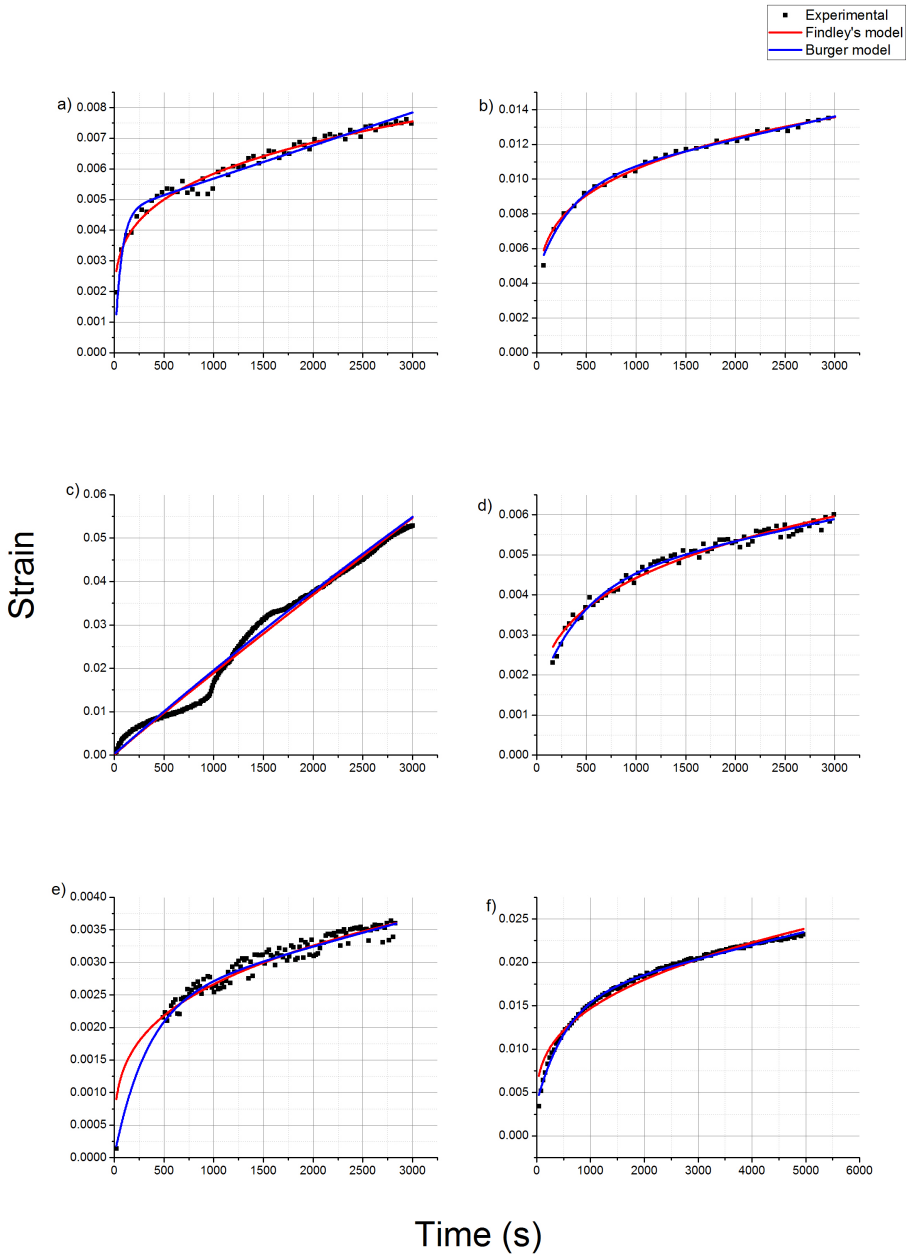


Figure 3.14: Burger and power law model fitted to experimental strain-time curves of root of diameter 2.16 mm. a) and b) for root 1, b) and c) for root 2, e) and f) for root 3.

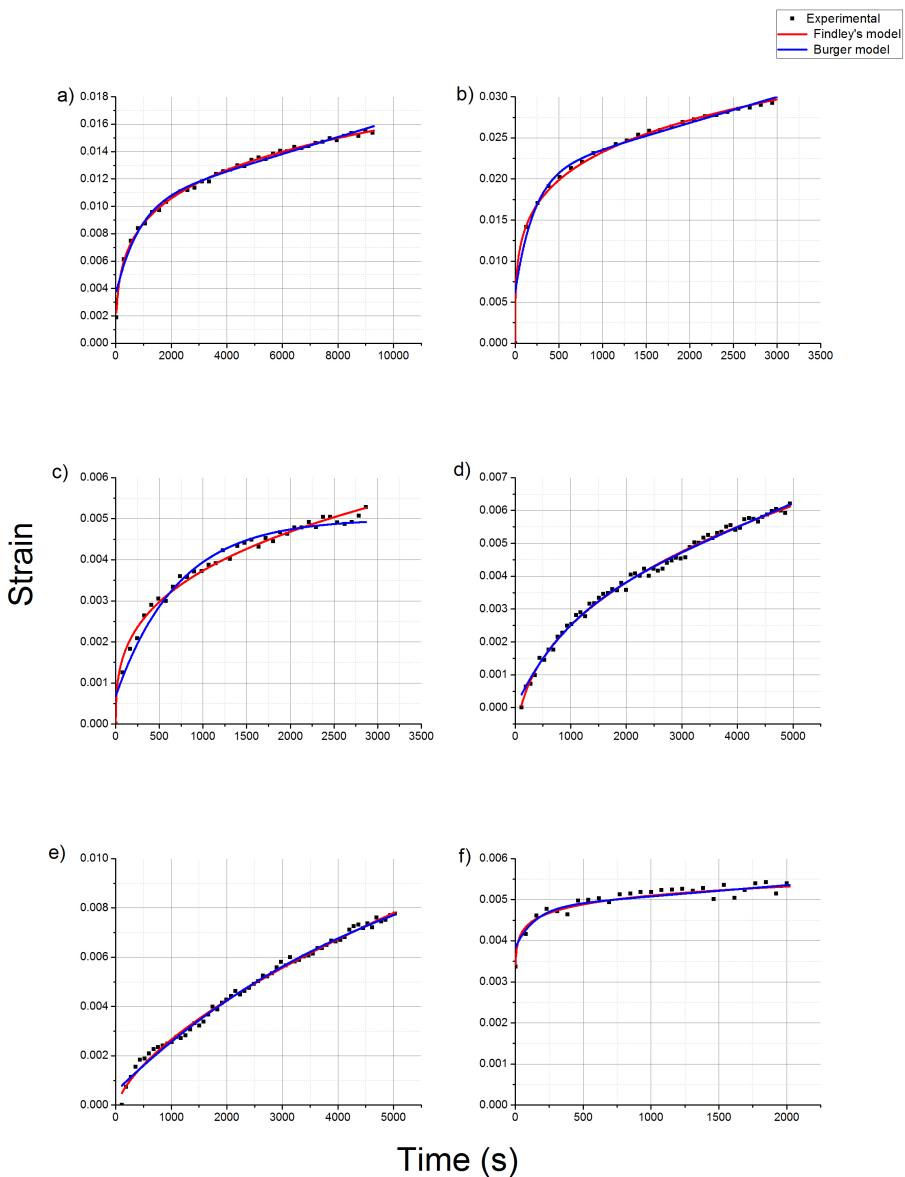


Figure 3.15: Burger and power law model fitted to experimental strain-time curves of root of diameter 3.6 mm. a) for root 1, b) and c) for root 2, d) for root 3, e) and f) for root 4.

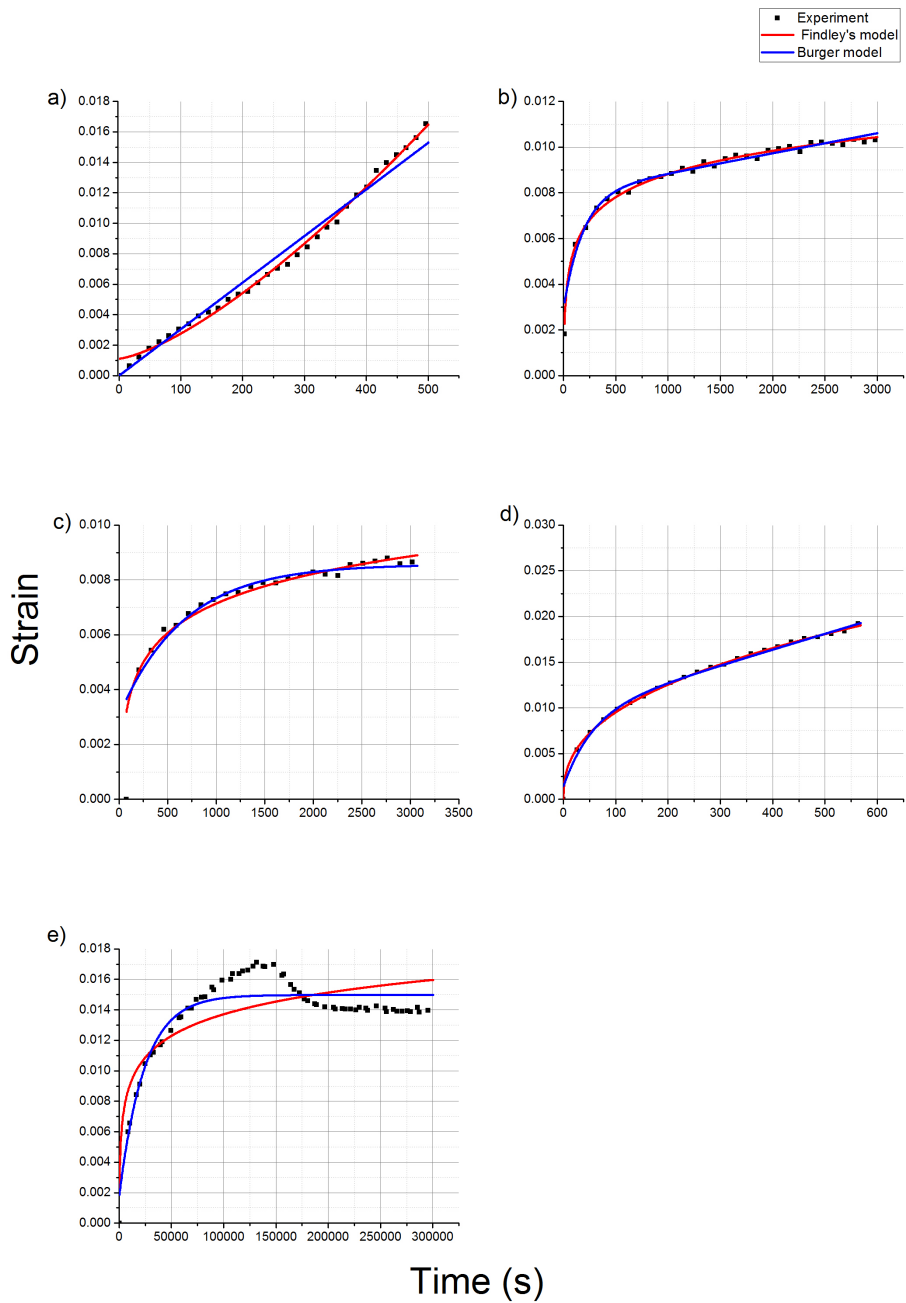


Figure 3.16: Burger and power law model fitted to experimental strain-time curves of root of diameter 3.6 mm. a), b), c) for root 5, d) for root 5. One extra root test loaded for 300000 s is shown.

## REFERENCES

- [1] J. Ni, A. K. Leung, C. W. W. Ng, and W. Shao, *Modelling hydro-mechanical reinforcements of plants to slope stability*, *Computers and Geotechnics* **95**, 99 (2018).
- [2] N. Pollen-Bankhead and A. Simon, *Hydrologic and hydraulic effects of riparian root networks on streambank stability: Is mechanical root-reinforcement the whole story?* *Geomorphology* **116**, 353 (2010).
- [3] D. Boldrin, A. K. Leung, and A. Bengough, *Correlating hydrologic reinforcement of vegetated soil with plant traits during establishment of woody perennials*, *Plant and Soil* **416**, 437 (2017).
- [4] L. Waldron, *The shear resistance of root-permeated homogeneous and stratified soil*, *Soil Science Society of America Journal* **41**, 843 (1977).
- [5] T. H. Wu, *Investigation of landslides on prince of Wales Island, Alaska* (Ohio State University, 1976).
- [6] Y. Yang, L. Chen, N. Li, and Q. Zhang, *Effect of root moisture content and diameter on root tensile properties*, *PLoS One* **11**, e0151791 (2016).
- [7] J. J. Roering, K. M. Schmidt, J. D. Stock, W. E. Dietrich, and D. R. Montgomery, *Shallow landsliding, root reinforcement, and the spatial distribution of trees in the oregon coast range*, *Canadian Geotechnical Journal* **40**, 237 (2003).
- [8] N. S. Nilaweera and D. Hengchaovanich, *Assessment of strength properties of vetiver grass roots in relation to slope stabilization*, (1996).
- [9] D. Boldrin, A. K. Leung, and A. G. Bengough, *Effects of root dehydration on biomechanical properties of woody roots of ulex europaeus*, *Plant and Soil* **431**, 347 (2018).
- [10] A. Stokes, J. E. Norris, L. Van Beek, T. Bogaard, E. Cammeraat, S. B. Mickovski, A. Jenner, A. Di Iorio, and T. Fourcaud, *How vegetation reinforces soil on slopes*, in *Slope stability and erosion control: ecotechnological solutions* (Springer, 2008) pp. 65–118.
- [11] G. B. Bischetti, E. A. Chiaradia, T. Epis, and E. Morlotti, *Root cohesion of forest species in the italian alps*, *Plant and Soil* **324**, 71 (2009).
- [12] Z. Mao, L. Saint-Andre, M. Genet, F.-X. Mine, C. Jourdan, H. Rey, B. Courbaud, and A. Stokes, *Engineering ecological protection against landslides in diverse mountain forests: choosing cohesion models*, *Ecological Engineering* **45**, 55 (2012).
- [13] S. De Baets, J. Poesen, B. Reubens, K. Wemans, J. De Baerdemaeker, and B. Muys, *Root tensile strength and root distribution of typical mediterranean plant species and their contribution to soil shear strength*, *Plant and soil* **305**, 207 (2008).
- [14] C.-C. Fan and C.-F. Su, *Role of roots in the shear strength of root-reinforced soils with high moisture content*, *Ecological engineering* **33**, 157 (2008).

- [15] M. Genet, A. Stokes, F. Salin, S. B. Mickovski, T. Fourcaud, J.-F. Dumail, and R. Van Beek, *The influence of cellulose content on tensile strength in tree roots*, Plant and soil **278**, 1 (2005).
- [16] C.-B. Zhang, L.-H. Chen, and J. Jiang, *Why fine tree roots are stronger than thicker roots: The role of cellulose and lignin in relation to slope stability*, Geomorphology **206**, 196 (2014).
- [17] Z. Mao, Y. Wang, M. L. McCormack, N. Rowe, X. Deng, X. Yang, S. Xia, J. Nespoulous, R. C. Sidle, D. Guo, *et al.*, *Mechanical traits of fine roots as a function of topology and anatomy*, Annals of botany **122**, 1103 (2018).
- [18] D. Boldrin, A. K. Leung, and A. Bengough, *Root biomechanical properties during establishment of woody perennials*, Ecological Engineering **109**, 196 (2017).
- [19] F. Preti and F. Giadrossich, *Root reinforcement and slope bioengineering stabilization by spanish broom (*spartium junceum L.*)*. Hydrology & Earth System Sciences **13** (2009).
- [20] T. C. Hales and C. F. Miniati, *Soil moisture causes dynamic adjustments to root reinforcement that reduce slope stability*, Earth Surface Processes and Landforms **42**, 803 (2017).
- [21] A. Kamath, W. Gard, and J.-W. Van de Kuilen, *Biodynamic timber sheet pile walls: vegetation retaining structure*, European Journal of Wood and Wood Products **78**, 1045 (2020).
- [22] C. Zhang, L. Chen, J. Jiang, and S. Zhou, *Effects of gauge length and strain rate on the tensile strength of tree roots*, Trees **26**, 1577 (2012).
- [23] A. Dey and P. Basudhar, *Applicability of burger model in predicting the response of viscoelastic soil beds*, in *GeoFlorida 2010: Advances in Analysis, Modeling & Design* (2010) pp. 2611–2620.
- [24] A. Segalini, G. Giani, and A. M. Ferrero, *Geomechanical studies on slow slope movements in parma apennine*, Engineering Geology **109**, 31 (2009).
- [25] A. Singh and J. Mitchell, *General stress-strain-time function for soils*, J Soil Mech ASCE **94**, 21 (1968).
- [26] K. J. Fridley, R. Tang, and L. A. Soltis, *Creep behavior model for structural lumber*, Journal of Structural Engineering **118**, 2261 (1992).
- [27] N. Yazdani, E. Johnson, and S. Duwadi, *Creep effect in structural composite lumber for bridge applications*, Journal of Bridge Engineering **9**, 87 (2004).
- [28] P. Georgiopoulos, E. Kontou, and A. Christopoulos, *Short-term creep behavior of a biodegradable polymer reinforced with wood-fibers*, Composites Part B: Engineering **80**, 134 (2015).

- [29] G. Bi, S. Ni, D. Wang, Y. Chen, J. Wei, and W. Gong, *Creep in primary consolidation with rate of loading approach*, Scientific reports **9**, 1 (2019).
- [30] G. Bi, Z. Li, Q. Wang, and D. Jiang, *An examination of creep failure criterion based on a strain threshold identified with a power law model*, Mechanics of Time-Dependent Materials **26**, 195 (2022).
- [31] S. Mickovski and L. Van Beek, *Root morphology and effects on soil reinforcement and slope stability of young vetiver (*Vetiveria zizanioides*) plants grown in semi-arid climate*, Plant and soil **324**, 43 (2009).
- [32] D. Kim, S. H. Lee, E. A. Combalicer, Y. Hong, and S. Im, *Estimating soil reinforcement by tree roots using the perpendicular root reinforcement model*, International Journal of Erosion Control Engineering **3**, 80 (2010).
- [33] M. Tosi, *Root tensile strength relationships and their slope stability implications of three shrub species in northern apennines (italy)*, Geomorphology **87**, 268 (2007).
- [34] F. Giadrossich, M. Schwarz, D. Cohen, A. Cislighi, C. Vergani, T. Hubble, C. Phillips, and A. Stokes, *Methods to measure the mechanical behaviour of tree roots: a review*, Ecological engineering **109**, 256 (2017).
- [35] M. Genet, N. Kokutse, A. Stokes, T. Fourcaud, X. Cai, J. Ji, and S. Mickovski, *Root reinforcement in plantations of cryptomeria japonica d. don: effect of tree age and stand structure on slope stability*, Forest ecology and Management **256**, 1517 (2008).
- [36] G. B. Bischetti, E. A. Chiaradia, T. Simonato, B. Speziali, B. Vitali, P. Vullo, and A. Zocco, *Root strength and root area ratio of forest species in lombardy (northern italy)*, in *Eco-and ground bio-engineering: The use of vegetation to improve slope stability* (Springer, 2007) pp. 31–41.
- [37] B. Abernethy and I. D. Rutherford, *The distribution and strength of riparian tree roots in relation to riverbank reinforcement*, Hydrological processes **15**, 63 (2001).
- [38] V. Operstein and S. Frydman, *The influence of vegetation on soil strength*, Proceedings of the Institution of Civil Engineers-Ground Improvement **4**, 81 (2000).
- [39] C. Lü and L. Chen, *Relationship between root tensile mechanical properties and its main chemical components of typical tree species in north china*, Transactions of the Chinese Society of Agricultural Engineering **29**, 69 (2013).
- [40] M. Schwarz, P. Lehmann, and D. Or, *Quantifying lateral root reinforcement in steep slopes—from a bundle of roots to tree stands*, Earth Surface Processes and Landforms: The Journal of the British Geomorphological Research Group **35**, 354 (2010).
- [41] G. J. Meijer, D. Muir Wood, J. A. Knappett, G. A. Bengough, and T. Liang, *Analysis of coupled axial and lateral deformation of roots in soil*, International Journal for Numerical and Analytical Methods in Geomechanics **43**, 684 (2019).

- [42] C. Zhang, X. Zhou, J. Jiang, Y. Wei, J. Ma, and P. D. Hallett, *Root moisture content influence on root tensile tests of herbaceous plants*, *Catena* **172**, 140 (2019).
- [43] T. Van der Put, *Theoretical explanation of the mechano-sorptive effect in wood*, *Wood and fiber science* **21**, 219 (2007).
- [44] T. Van der Put, *B. 1. deformation and damage processes in wood*, (1989).
- [45] N. Pollen and A. Simon, *Estimating the mechanical effects of riparian vegetation on stream bank stability using a fiber bundle model*, *Water Resources Research* **41** (2005).

# 4

## PHYSICAL MODELLING OF TIMBER SHEET PILE-VEGETATION SYSTEM

*"Innovation is not the product of a logical thought, even though the final product is tied  
to a logical structure"*  
Albert Einstein



## 4.1. ABSTRACT

A comparison was conducted between an unreinforced stream bank and stream bank reinforced using plant root analogue in terms of displacement of the sheet pile, failure pattern and failure pressure. The results of 1g scale tests on a newly developed physical model of a stream bank protected by a combination of a timber sheet pile wall and vegetation root analogue is reported in this chapter. A 3D model of *Humulus lupulus* L. root system was 3D printed and used as root analogues. A total of three physical tests are conducted, one unreinforced and two reinforced by root analogues. System failure was induced by removing the retaining water pressure on the stream side. Further, finite element analysis of the model stream bank using Plaxis 3D was done with objective of prediction of failure. A parametric analysis was performed with the objective of investigating the influence of the increase in cohesion due to the presence of roots and the spatial pattern of roots on the bending moment and displacements developing in the timber sheet pile.

The presence of plant root analogue influenced the failure pattern in terms of the volume of soil area which needs to be mobilized for failure. The vegetation root analogues, when present in an efficient spatial pattern are able to support the stream bank up to twice the drawdown pressure than the unreinforced bank. Higher initial displacements were observed for stream bank reinforced by root analogue when compared to non-vegetated embankment. More interestingly, the parametric analysis revealed that the forces acting on the timber sheet pile are influenced by the spatial pattern of roots rather than the quantity of additional cohesion that the roots provide. This observation has implications at practical scale and research scale. Therefore, species which have more spatial rooted area are more beneficial for the safety of a bank than species which have a higher number and stronger roots. On the other hand, this begets the need for controlled lab shear tests and calls for more field scale shear tests capable of providing data regarding the extend of the root reinforcement in the vertical and lateral directions.

## 4.2. INTRODUCTION

Shear strength back analysis of failed soil slopes has been employed to study the failure mechanism and to obtain the shear strength parameters at the slope scale [1–5]. The limitations of this method are that it requires that the slope has failed and that the pore water pressure distribution at the time of failure is known, which results in a small number of available case-studies. Geotechnical centrifuge modelling offers the ability for researchers to produce stresses similar to those acting on a real slope by using a smaller prototype and increasing its acceleration over that of gravity. Due to its reliability, cost efficiency and relative ease of performance, geotechnical centrifuge testing has been used to study a variety of soil engineering problems, such as foundations [6], seismic soil-structure interactions [7], heat migration in soil [8]. The centrifuge allows more control over the testing conditions, which makes it a more attractive option to researchers [9] than field tests under uncontrolled conditions [10]. 1g physical models to analyse geotechnical structures are often time consuming and expensive [11]. Nevertheless, researches have resorted to conduct 1g scale physical modelling [10, 12–14] and full scale field testing [15, 16].

As pointed out by [11], few centrifuge modellings tests have been conducted on vegetated slopes, possibly due to limited access of bio-engineering researchers to the equipment. [17] was one of the first studies that used centrifuge models to analyse the reinforcement of the soil by roots. They used young willow trees grown for 290 days to reinforce the slope in the prototype. Centrifuge tests with model plant roots using Viton O-ring rubber and wood which represented lower and higher bound of stiffness of real roots revealed that roots failed primarily by pullout and axial tension was mobilized with smaller displacement [18]. [19] studied three types of vegetation reinforcement (grass planting, fascines and staking) of a slope through centrifuge testing, where failure was induced by increasing the water level. Using centrifuge modelling it was suggested that the presence of roots can result in a reduction of crack formation at surface level and an increase in time for infiltration of rainfall and thereby an increase in time to failure of slopes [20, 21]. Furthermore, roots can result in a higher initial movement of the slope, which is the movement required to mobilize tensile stresses in roots [22]. [23], in their centrifuge tests, found that vegetated soil also improves the seismic performance of a slope and suggested a limiting height of the slope for a certain root depth for effective increase of stability due to roots. [24] used different artificial root systems in the centrifuge tests capable of inducing suction in the soil and suggested that heart-shaped root system was the most effective in increasing the transpiration induced suction and thereby increasing the stability of slopes in case of rainfall.

The above-mentioned studies were performed using live plants to investigate the mechanical reinforcement of the soil provided by roots [17, 19, 20, 22] have the inherent drawback of overestimation of root reinforcement in the centrifuge [25]. This is because the tensile strength of roots varies with diameter. For instance, a thin root at model scale would represent a thicker root at prototype scale but would have the same tensile strength as the thinner root, which results in overestimation of tensile strength of the roots. [25] suggested the use of more juvenile plants and an acceleration of 15g in order to simulate a mature root system and morphology. However, in such conditions, realistic representations of root biomass with depth cannot be achieved. [25] 3D printed the

roots using ABS (a material that has similar axial young's modulus and tensile strength of typical roots), which resulted in a realistic representation of root system shape.

In this study, a timber sheet pile-vegetation system to protect stream banks was investigated. It is hypothesized that when vegetation is used in combination with a timber sheet pile, the system would have higher stability, thereby reducing the resistance required from the timber sheet pile alone. A physical model was developed and tested with bare and rooted soil. Plant root analogues were 3D printed using PLA. A finite element analysis of the physical model was conducted using Plaxis 3D. Further, the effect of the variation in cohesion and rooted area was investigated through a parametric analysis.

## 4.3. MATERIALS AND METHODS

### 4.3.1. *Humulus Lupulus* L. 3D MODEL ROOT

Repeatability of tests with plants of same root architecture is a major challenge in the physical modelling of slopes reinforced with vegetation. Natural vegetation presents a natural variability in growth and root occupied volume even in controlled conditions. 3D printing provides an alternative to the use of natural roots because the model roots can be made according to the desired architecture and size, while still being representative for a natural root geometrical system. The root architecture printed in this study was based on the root architecture of *Humulus lupulus* L. A detailed description of root architecture of *Humulus lupulus* L. was provided by [26], who excavated *Humulus lupulus* L. plant after its fifth yield year in the beginning of flowering (Fig.4.1). The distance between the plants were 1.6 m in row and 3.2 m between the rows.

- Vertical roots which accounted for a cuboid like structure and going as deep as 1.7 m. These were thick perennial roots and young white roots;
- A third-row type roots were identified which grew in horizontal and vertical directions concentrated in the top few mm of soil.
- Horizontal roots, which were young and perennial, formed a cylinder-like shape with a radius of 1.6 m;

A 3D root architecture model was made in AutoCAD based on the [26] and the root architecture observed in chapter-2. The root was modelled as cylinders formed using extrusions (Fig.4.2). Root cross sectional area of the model root with depth is given in (Fig.4.3). In addition to straight elements tortuous roots were also modelled using spline function and extrusion. The minimum diameter of the roots was 1 mm which is the limit to distinguish the root from the support structure. The DWG of the model can be found in the repository (10.5281/zenodo.4555335) . The model roots were printed using PLA filaments. The properties of PLA and *Humulus lupulus* L. roots are given in Table.4.1. The Autocad file is converted to a STL (stereolithography) file to be used for rapid prototyping and 3-D printing. Ultimaker 3, manufactured by Ultimaker BV, the Netherlands was used for printing the model root in PLA. The machine prints a support structure of lighter density which can be easily broken and separated from the model root. The model and support structure rest on a hot plate, from which the model can be

trimmed off after printing. Due to size limitation the roots were printed in two halves and later joined together using a commercially available PLA pen and super glue.

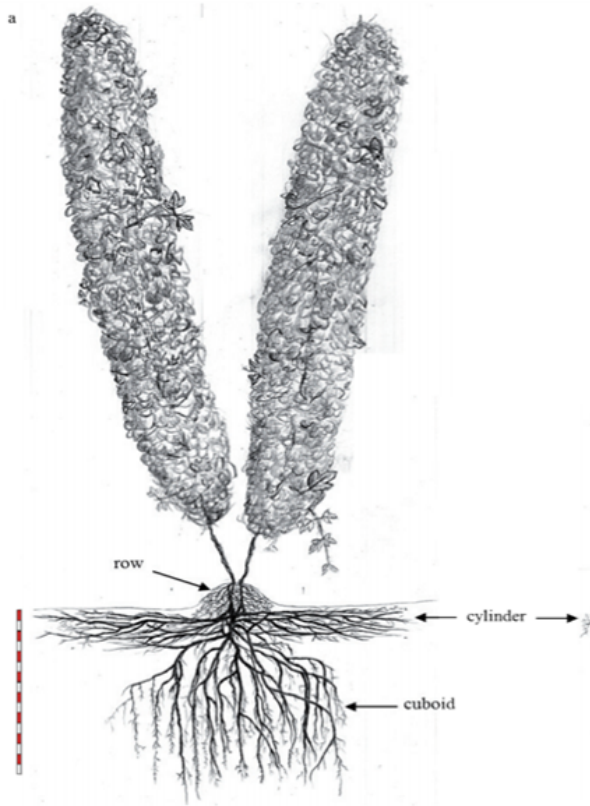


Figure 4.1: Three different zones of roots in a *Humulus lupulus* L. plant [26]

Table 4.1: Mechanical properties of PLA and *Humulus lupulus* L.

| Material                           | Tension strength | Young's modulus | Source          |
|------------------------------------|------------------|-----------------|-----------------|
|                                    | (MPa)            | (MPa)           |                 |
| PLA                                | 36-55            | 3500            | Material Manual |
| <i>Humulus lupulus</i> L.<br>roots | 4 -80            | 50-1000         | Chapter 3       |

#### 4.3.2. PHYSICAL MODELLING

The physical model was built at the Biobased structures and Materials Laboratory of TU Delft. Plywood with a thickness of 18 mm was used to built the box taking into

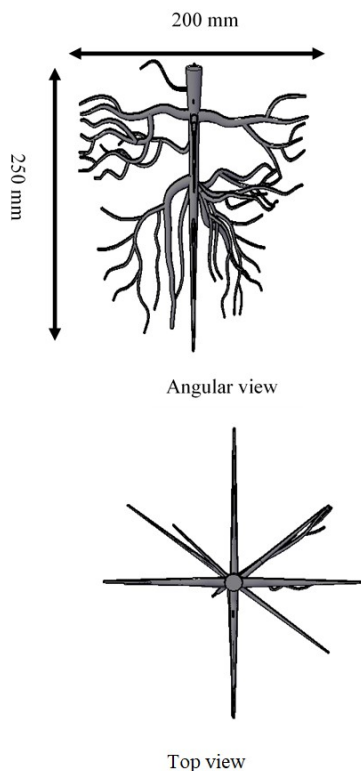


Figure 4.2: Root architecture of *Humulus lupulus* L. modelled in AutoCAD. The DWG file can be obtained from the repository [10.5281/zenodo.4555335](https://zenodo.org/record/4555335)

account the maximum forces that are expected. Extra vertical reinforcement bars were installed on the walls of the boxes in order to prevent any lateral deformations. One of the lateral walls, perpendicular to the sheet pile, was made of Plexiglass with the intent of allowing the tracking of soil movement using particle image volumetry (PIV). The box had a height of 650 mm, a width of 700 mm and a length of 1000 mm. The box could contain a retaining soil of length 700mm and the embedment length of 282 mm (Fig.4.4).

The design of the model retaining height, so that a failure condition was reached during testing, was made using calculations for required embedment depth for the sheet pile. Moreover, two physical real scale prototypes were tested to optimize the model dimensions reported here. The box is designed to be watertight by using a sealant on all corner edges. The sheet pile was made of Birch wood with a thickness of 18 mm. The embankment side would simulate the stream bank and the embedment side would simulate the canal. Water and soil particle movement from the embankment side to the stream side is arrested using thin rubber sheets used at the edges of the wooden sheet pile. Petroleum jelly was used at the edges of the sheet pile to eliminate friction between the sheet pile and the walls of the box. Thus, the sheet pile can move and rotate freely

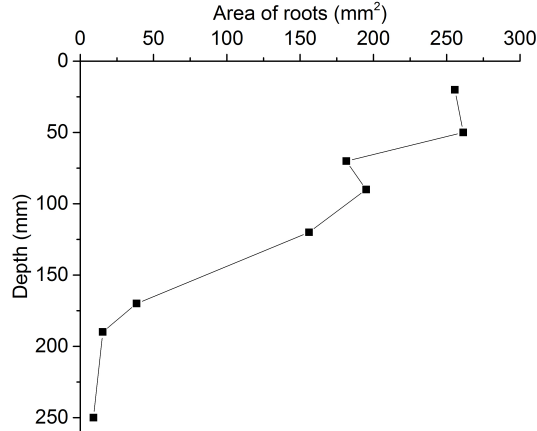


Figure 4.3: Area of roots of the model root with depth. The area of roots is the sum of the cross-section area of all roots crossing a horizontal plain at a given depth

4

when loads are gradually increasing and failure is imminent. The canal side is equipped with a water pump to induce drawdown. Provisions were made for a rigid platen of size 700 mm \* 700 mm to be placed on top of the embankment to apply surcharge if required after complete drawdown. The soil is filled in the embankment side in three layers with compaction applied uniformly to achieve the desired dry bulk density of  $\approx 1.2 \text{ g/cm}^3$ . A good contact between layers was ensured by scarifying the top of each layer with a steel rod before compacting the following layer. The sheet pile was fixed using clamps during preparation of the model until the commencement of the testing. The embedment side was built by the compaction of a single layer at the same density. A number of trials were conducted to find the best method to place the roots inside the soil. First trial involved pushing the roots into the soil at the desired location, which was not successful because the fine roots broke when pushed to required to push the root to reach the desired depth. Pouring soil as a slurry after placing the root was done as a second trial, which also failed due to the difficulty in achieving the soil required density. In the third trial, the roots were installed in a trench and the soil was carefully compacted around the roots using a small tamper to achieve the required density. The third trial was deemed successful since the roots were in the desired location and the required soil density was achieved as well. However, this technique was intensive with respect to time and effort required for careful tamping in between and around the roots. Manual placement of model roots was also done by [18] in their centrifuge model.

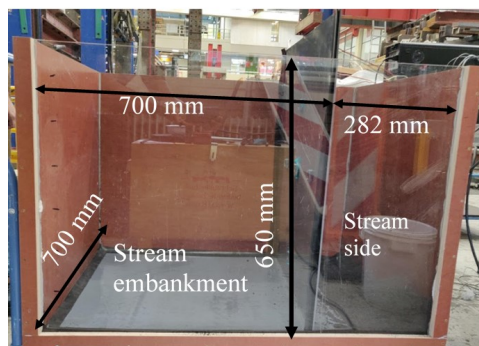


Figure 4.4: Dimensions of the physical model container and positioning of the sheet pile.

#### 4.3.3. INSTRUMENTATION

The physical model was equipped with the instrumentation to measure the horizontal displacement of the wooden sheet pile, the vertical displacement of the embankment, soil matric suction to ensure saturation, and verify the pressure acting on the sheet pile during water drawdown. The soil displacements and failure surface were captured through the plexiglass wall. A suction probe was installed at a depth of 200 mm and at a distance of 500 mm from the sheet pile in the embankment side. Draw wire sensors (FDMK30, accuracy  $\pm 0.001$  mm, range 0-50 mm) were placed at either ends of the sheet pile at the top height of the embankment. The average displacement of these two sensors could be used to measure the displacement of the sheet pile during the test. The sensors were placed on a custom-made rail and the wires were hooked on to the sheet pile (Fig.4.5). Single conditioned silicon pressure sensors (MPXHZ6130AC6U) were used to measure the pressure on the wooden sheet pile at five different locations. The pressure sensors are water resistant and were placed in a PVC casing filled with silicon oil which transfers the applied pressure on to the sensor. A linear variable potentiometer (LVDT) was placed on the top of the embankment at a distance of 150 mm from the sheet pile. The LVDT is a spring return type and measures the vertical settlement of the embankment. The LVDT was placed on a 3 mm thick plate which is in contact with the soil, thereby ensuring contact with the embankment throughout the testing. Digital images were captured using a Pentax k-70 DSLR camera at a rate of 3 frames per second. The resolution of the images were 6000\*4000 pixels. Two LED lights were used to illuminate the embankment cross-section and to reduce the reflections. Patch matching technique was used to track the change in displacement of the soil particles. Patches were placed on the plexiglass at a grid of 50mm \* 50 mm throughout the length and till the depth of 450 mm on the embankment side. Images were processed using GeoPIV-RG algorithms developed by [27]. A shower head and a mechanical water pump form the hydraulic part of the system. A commercially available shower head was used to fill the embankment side with water. The mechanical pump was manually controlled and operated at the desired rate of pumping.

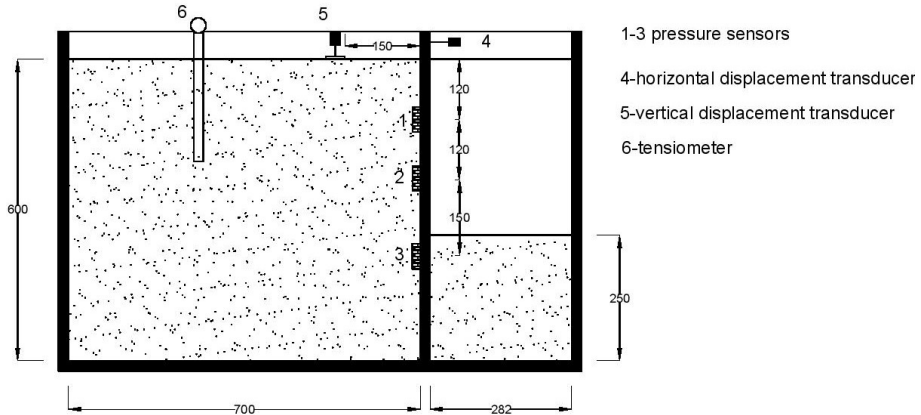


Figure 4.5: Sensors used in the physical model and dimensions of the embankment.

4

#### 4.3.4. TESTING METHOD AND PROTOCOL

Three different types of tests were planned, one with bare soil and two with model root inclusions. The first model with root inclusions had a total of three model root (Root pattern 1) and second model had a total of five model roots (Root pattern 2), see Fig.4.6. Three tests were conducted with no repetition due to high cost, time and effort required for conduction such real scale tests, however a strict protocol was followed for all the reported tests. The tests were conducted by removal of supporting water column on the streamside See, (Fig.4.7).

The embedment and the embankment were filled in the same manner for all the tests as mentioned above. The following protocol was adopted for each test to bring it to failure:

- After preparation of the embankment and the streamside, the box is filled with water to the top on the streamside. If the water level goes down during the following 60 minutes, the box is refilled and the process is repeated till the water level is stable at the required level.
- Water was poured on top of the embankment by switching on the showerhead for a period of ten minutes or until a ponding was observed on the top of the embankment.
- Step (ii) is repeated until the impoundment water level remains stable and the suction level reading is as close to zero as possible ( $\ll 1$  kPa). An average of six hours was taken to form the impoundment of water on the embankment side. The system was left to stabilize for a period of 18 hours.
- The water level was inspected to ensure it is remaining stable. In case of water level drop is noticed, steps (ii) and (iii) are repeated. The water level in all the three tests were kept stabilized for a period of 36 hours.
- The showerhead is removed and the sensors are installed.

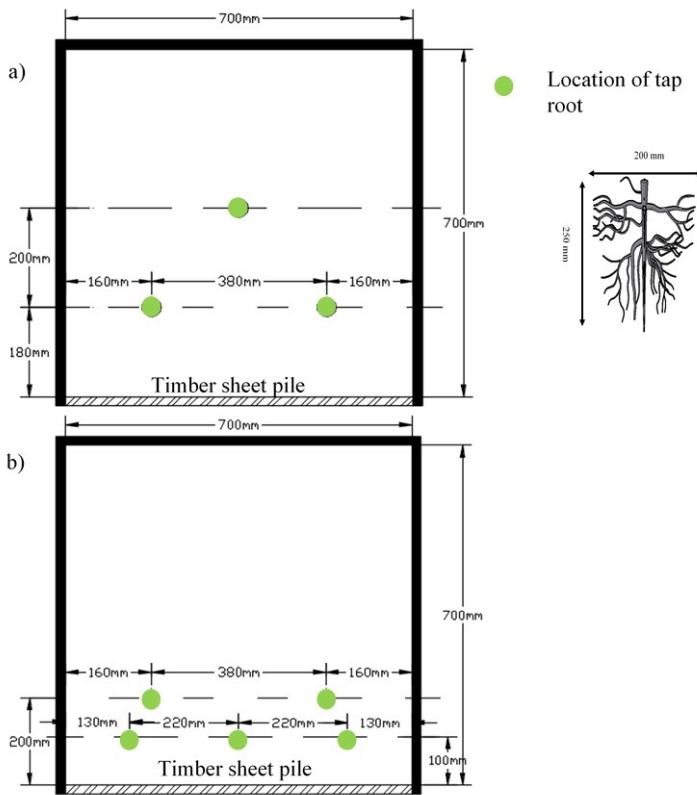


Figure 4.6: Plan view of the stream embankment. Location of tap root within the embankment according to the root placement geometry 1 (Root pattern 1) (a) and geometry 2 (b) (Root pattern 2)

- The water is removed from the streamside at a rate of 4.2 litre/minute until failure.
- After completion of the tests, the roots are excavated to see the mode of failure.

## 4.4. RESULTS

### 4.4.1. BARE SOIL

The horizontal displacement of the top of the sheet pile with drawdown depth is shown in Fig.4.8. The sheet pile started to move towards the streamside until a drawdown depth of 120mm. After a drawdown depth of 120 mm a significant horizontal movement of the sheet pile was observed followed by failure. The failure was characterized by a wedge failure behind the sheet pile with a depth of about 200 mm and a width of 100 mm. The evolving failure wedge with depth can be seen in Fig.4.21. The formation of

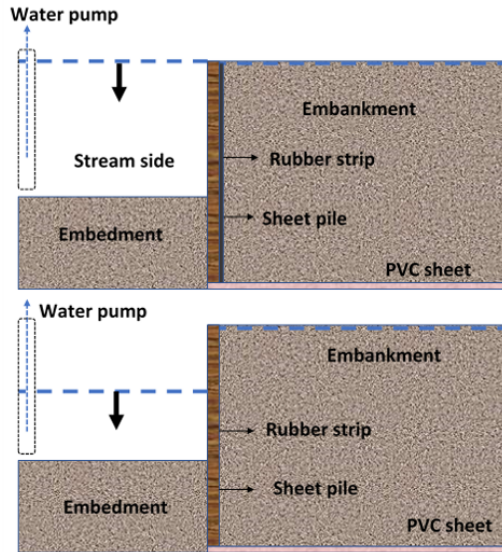


Figure 4.7: Testing method used in the physical model

wedge crack can be observed in Fig.4.21 b), at 100 mm drawdown. With further draw-down, the horizontal displacement increased at the depth below the area where the initial wedge crack was observed. Thus, failure was initiated at the top edge and propagated with depth and width finally forming the wedge failure as seen in Fig.4.10.

The vertical displacement recorded was negligible until a drawdown depth of 100 mm. This shows the localization of displacements near the sheet pile for displacements up to 100 mm. With further drawdown, larger wedge area was mobilized. The vertical displacement was measured behind the failure wedge at a distance of 150 mm from the sheet pile. Abrupt increase in vertical displacement could be observed at 135 mm draw-down, implying that failure happened between 125 and 140 mm of drawdown. The vertical and horizontal displacements and the PIV data are coherent with respect to the surface failure propagation observed, see Fig.4.8, Fig.4.9. For instance, localized horizontal displacements and initiation of failure were observed in the PIV at 100 mm drawdown, and can also be observed in the progressive increase of the horizontal displacement of the sheet pile until about 90 mm and minimal movement in the vertical direction. More interestingly, the sheet pile movement at the top showed a plateau until 125 mm draw-down and the PIV, at that moment, shows the progression of the failure wedge vertically and horizontally inwards into the embankment. The increase in vertical displacement reinforces this progressive failure wedge evolution. An approximation of the failure wedge observed in the bare soil test has a slope of  $63.40^\circ(\theta)$ , as observed in Fig.4.10.

From [28], the observed angle is related to shear strength angle at constant volume ( $\phi_{cv}$ ) as,  $\theta = (\frac{\pi}{4} + \frac{\phi_{cv}}{2}) \Rightarrow \phi_{cv} \approx 36^\circ$ , which is similar to the critical friction angle obtained in the shear tests (Chapter 2). The load sensor results are not reported here due to leakage of silicon oil and full contact of sensors to soil body could not be ensured once the displacement of the sheet pile started.

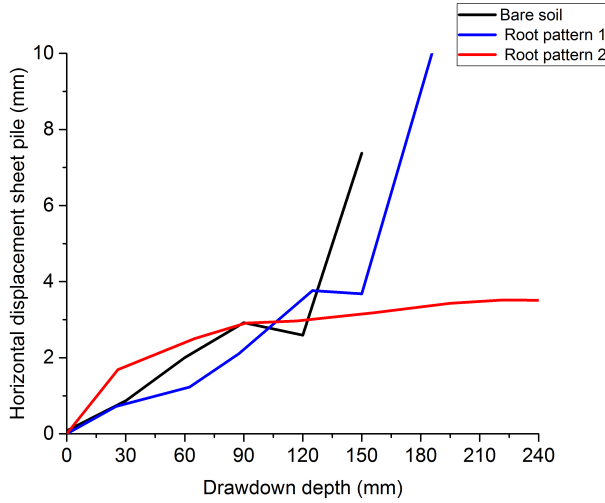


Figure 4.8: Horizontal displacement of sheet pile with drawdown depth.

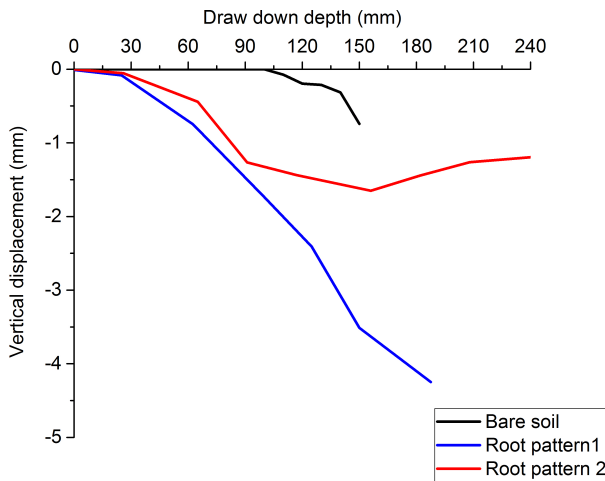


Figure 4.9: Vertical displacement measured at a distance of 150 mm from the timber sheet pile in the stream embankment.

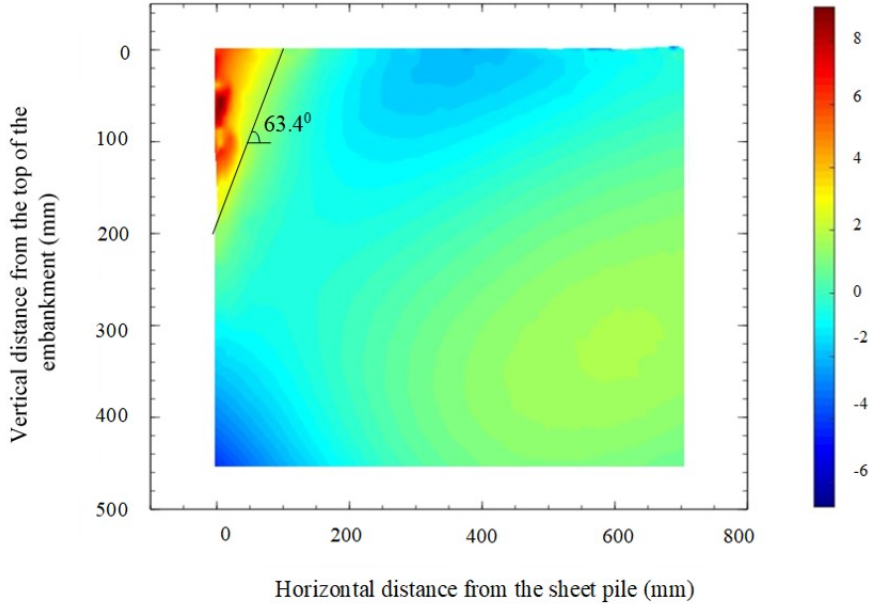


Figure 4.10: Horizontal displacement of soil particles in the stream embankment in bare soil test, obtained from PIV)

#### 4.4.2. ROOT PATTERN 1

The horizontal movement of the sheet pile at the top follows the same displacement trend of the bare soil. The horizontal displacement of the sheet pile during the initial drawdown of up to 30 mm is the same as in bare soil, beyond which the displacements are smaller but increasing until about 125 mm of drawdown, Fig.4.8. Abrupt displacements are observed at a drawdown depth of 155 mm. The PIV images show the progressive initiation of displacements of the rooted zone with drawdown Fig.4.22. Larger vertical displacements are observed in tests with root pattern-1 than in bare soil. A larger area is being mobilized in the rooted model than in bare soil, which moves inwards into the embankment. The failure wedge observed in the rooted soil is deeper than that in the bare soil test, reaching a depth of about 300 mm and a width of about 120 mm shown by the measurements from the top. A plateau in the horizontal displacement of the sheet pile is observed as in the bare soil. This could be explained as the attempt to mobilize a larger area of the embankment, before failure, which could be observed in the progression of displacements seen in PIV, Fig.4.22. Clearly, an improvement over bare soil is observed with respect to drawdown depth required to initiate the failure.

The total number of roots intersecting the failure surface is 11 corresponding to root area of  $58 \text{ mm}^2$ . Only 40 mm length of these roots are in the failure wedge. The failure mode of all roots was identified as being pull out of the soil. Another peculiarity of failure wedge of rooted soils can be observed in Fig.4.11. Rather than having a linear failure surface as in bare soil, towards the top of the embankment a curvature could be observed, which could possibly be due to the engagement of roots, which increases the influence

area.

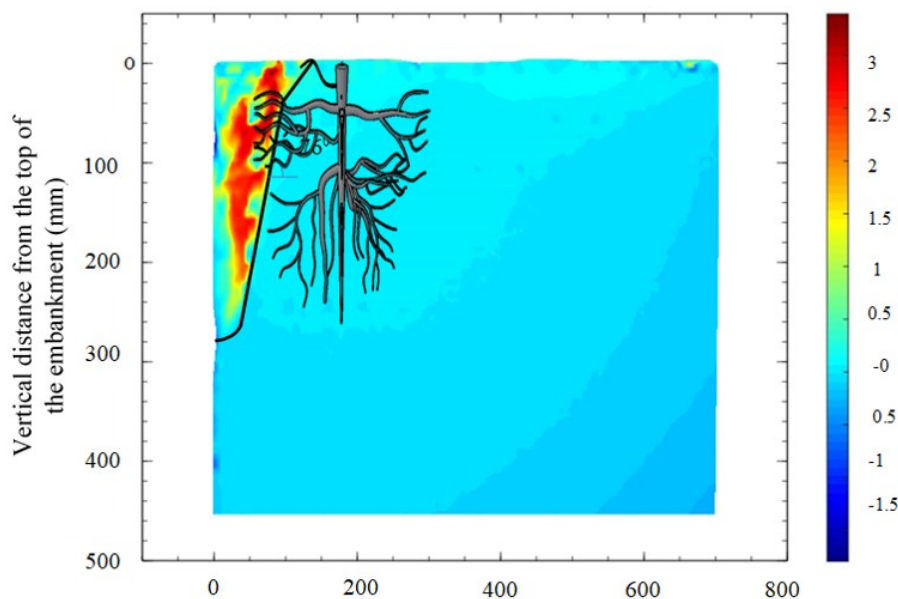


Figure 4.11: Horizontal displacement of soil particles in the stream embankment in the root pattern-1 test, obtained from PIV.

#### 4.4.3. ROOT PATTERN 2

The soil with testing root pattern 2 was significantly more reinforced (total of 5 model roots) compared to root pattern 1. A larger initial horizontal displacement of the sheet pile is observed for the initial 25 mm drawdown, after which the rate of displacement reduces. With further drawdown until 250 mm, the movement of the sheet pile is minimal ( $<1$  mm) and never reaches an abrupt increase in displacement as observed in the bare soil and in the root pattern 1 test. The initial higher displacement observed with the root pattern 2 in this study are in line with the observation of faster initial movements of vegetated slopes reported in [29]. This implies that the effect of root reinforcement is obtained after an initial displacement, indicating reinforcement effect might be similar to reinforced concrete. This is also in line with the shear test results reported in Chapter 2, where the rooted samples required a higher displacement to reach the peak shear strength. Nevertheless, the roots showed a higher peak strength compared to bare soil. Vertical displacements similar to the ones observed in the root pattern 1 test was observed for the initial drawdown after which the rate of vertical displacements also reduced and stabilized with further drawdown. No failure plane development could be observed in the PIV (Fig.4.23) which shows that the soil body is stable.

#### 4.4.4. SUMMARY OF TESTS

The observations from the physical model tests are summarised below:

- Presence of root analogues improve the stability of the timber sheet pile-vegetation system. This is evident from the higher drawdown depth required for failure in root pattern 1 and absence of development of failure wedge in root pattern 2.
- Higher initial movement observed in root pattern 2 which - had larger number of roots close to the sheet pile (5 roots), shows that the reinforcing effect of roots come into play after a higher initial displacement. Nevertheless, the root pattern 2 showed higher stability than bare soil.
- The failure wedge developed in root pattern-1 was wider and deeper than that of bare soil, which shows that larger volume of soil is mobilized by root reinforced soils.

4

### 4.5. FINITE ELEMENT MODELLING

#### 4.5.1. MODEL

A 3D finite element numerical simulation was conducted using the finite element program PLAXIS 3D with primary goal of prediction of failure drawdown depth (bare soil, root pattern-1). The dimensions of the embankment, sheet pile and embedment are based on the dimension of the physical model tested. The soil elements are modelled as 10-node tetrahedral elements in 3D finite element mesh. A second order interpolation for displacements is provided by using the 10-node tetrahedral elements in PLAXIS 3D. The boundaries along the x-axis and y-axis (x-min, x-max and y-min, y-max) were normally fixed, allowing lateral displacements. The lower boundary of the z-axis (z-min) is fully fixed, while the upper boundary (z-max) is free to allow lateral and vertical displacements (Fig.4.12).

Sheet pile is modelled as a plate element with elastic perfectly plastic behaviour. The interface element between the sheet pile and soil was simulated as frictional and the strength reduction factor  $R_{inter}$  was assumed equal to 0.67 as proposed by [30] and [31] to simulate the non perfect contact between the sheet pile and soil.

The Mohr-Coulomb model was used to simulate the soil units. The best fit parameters for the bare soil test are given in Table.4.2. In finite element modelling of root reinforced slopes, the increase of the soil strength due to presence of roots is estimated as an additional cohesion term  $C_R$ , [11, 32, 33]. The cohesion of the soil is increased by  $C_R$  in the regions where the root's influence is present. The influence area of a root bundle is still subject of research and only limited knowledge is available in literature [11]. In slope stability problems, the root's influence is generally considered throughout the slope face in a uniformly distributed manner or the influence zone is based on actual boundaries of the roots. In this study, where the roots have variable diameters in different directions, the influence area of the roots on a planar scale was chosen to be the actual extreme boundary of the model roots (Fig.4.13). A constant value of  $C_R$  was attributed throughout the rooting depth. Thus, the zone where the model roots were present in the experiment was modelled in finite element method as cuboidal block of increased  $C_R$ , in addition to the properties of the soil. On the test on the root pattern-1,

a total area of roots of  $58 \text{ mm}^2$  was found to intersect with the failure surface around the wedge. Considering the total area of the surface of the wedge ( $0.22 \text{ m}^2$ ) and tensile strength of PLA to be  $37 \text{ MPa}$ , the estimated  $C_R$  to be used in the simulations was  $9.8 \text{ kPa}$ , according to the model developed by [34, 35].

$$C_R = T_S \times \frac{A_R}{A_S} \quad (4.1)$$

$$C_R = 36 \text{ MPa} \times \frac{58.2}{226100} = 9.8 \text{ kPa} \quad (4.2)$$

The estimation of  $C_R$  is based on the assumption that all the roots break, which was not the case observed in the experiment. The estimated  $C_R$  will thus represent the maximum reinforcement that the root would provide. The influence of this assumption on the simulation results will be shown later.

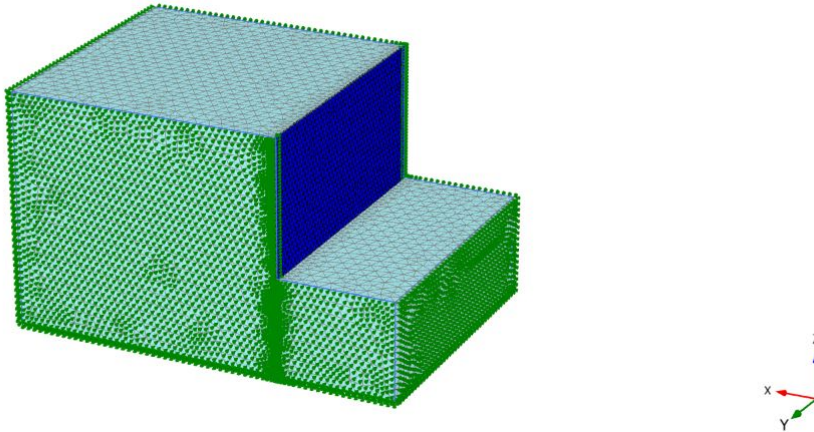


Figure 4.12: Node fixities and model mesh

Table 4.2: Input properties of soil and sheet pile used in the PLAXIS 3D modelling

| Parameter                    | Value                               |
|------------------------------|-------------------------------------|
| Soil unsaturated unit weight | 12 kN/m <sup>3</sup>                |
| Soil saturated unit weight   | 15.5 kN/m <sup>3</sup>              |
| Soil Stiffness               | 1200 kPa                            |
| Cohesion                     | 0 kPa                               |
| Friction angle               | 36 <sup>0</sup>                     |
| Dilatancy angle              | 0 <sup>0</sup>                      |
| Poisson's ratio of soil      | 0.26                                |
| Sheet pile stiffness         | 8x10 <sup>6</sup> kN/m <sup>2</sup> |
| Sheet pile thickness         | 18mm                                |

4

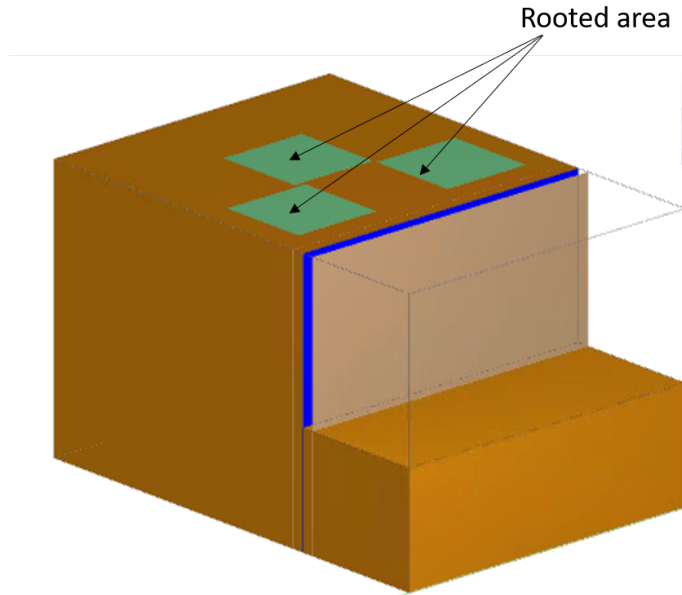


Figure 4.13: Location of rooted area in root pattern 1 in the model

#### 4.5.2. RESULTS

In addition to predicting the failure the parameters assessed for the monitoring of timber sheet pile-vegetation system were the horizontal displacement of the sheet pile, the vertical settlement in the embankment and the failure displacement contour. The model simulation and the experimental observation of the horizontal displacement of the sheet pile and vertical settlement of the embankment are presented in (Fig.4.14). Though, the horizontal displacement is overestimated in the simulation when compared to experimental results, the general trend of rate of increase of displacement in the sim-

ulation are in good agreement with the experimentally observed values. Nevertheless, the simulation reached a soil collapse level at 150 mm drawdown and the horizontal displacement at 140 mm drawdown is reasonably estimated. The failure wedge obtained in the simulations is shown in (Fig.4.16). The simulation show that the failure pressure can be reasonably predicted using these simulations.

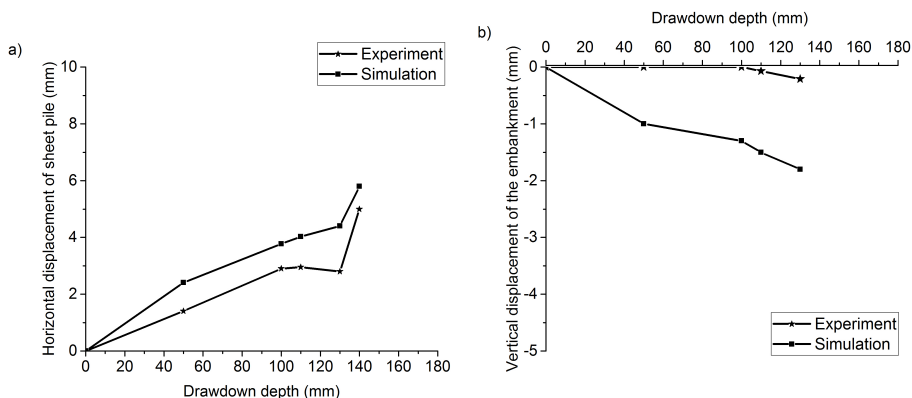


Figure 4.14: Comparison of experimentally measured and predicted a) horizontal displacement of the sheet pile, and b) vertical displacement in the embankment with bare soil.

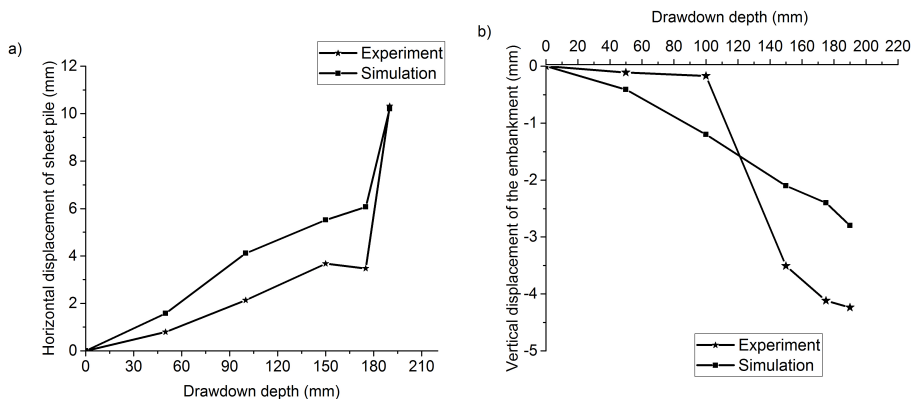


Figure 4.15: Comparison of experimentally measured and predicted a) horizontal displacement of the sheet pile, and b) vertical displacement in the embankment in the test with the root pattern-1

The horizontal displacement obtained from the simulations of root pattern-1 are also overestimated until failure, however the soil collapse in modelling occurs at the same drawdown depth as measured in the experiments (Fig.4.15). Contrary to horizontal displacements, the vertical settlement of the embankment is underpredicted after a drawdown depth of 60 mm. In the PLAXIS model of root pattern-1, the rooted zone is considered to have the same properties of soil but an increase of 9.8 kPa in cohesion. Based on the observation some behavior of rooted area could be speculated. In the simulations

the rooted zone seems to act like a reinforced soil providing a behaviour similar to but-  
tressing. Similar observation was also reported by [11], who suggested that the rooted  
zone might act as “soft retaining walls”. This also points to the possibility of soil arching  
occurring between the rooted zones [36]. These effects are observed in the simulations  
due to the approximation of the rooted zone area and modelling the root-soil matrix as  
an increase in cohesion term without changing any other parameters. For instance, the  
stiffness of rooted zone will be different from the adjacent embankment, but that was not  
taken into account. Nevertheless, the simulations show a general trend of displacements  
similar to that in the experimental observation. The but-  
tressing effect observed in the simulations interrupts the propagation of the failure wedge  
towards the embankment (Fig.4.17).

4

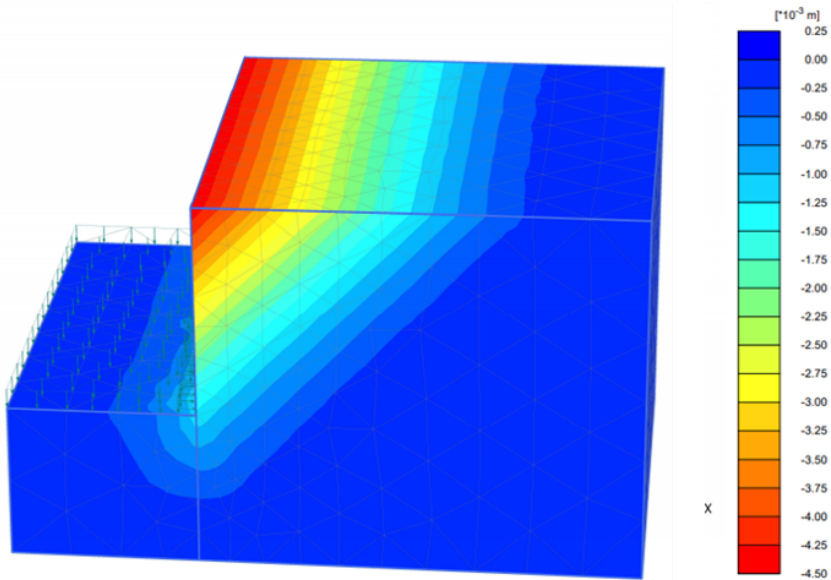


Figure 4.16: Horizontal displacement contour from the simulation of the bare soil test.

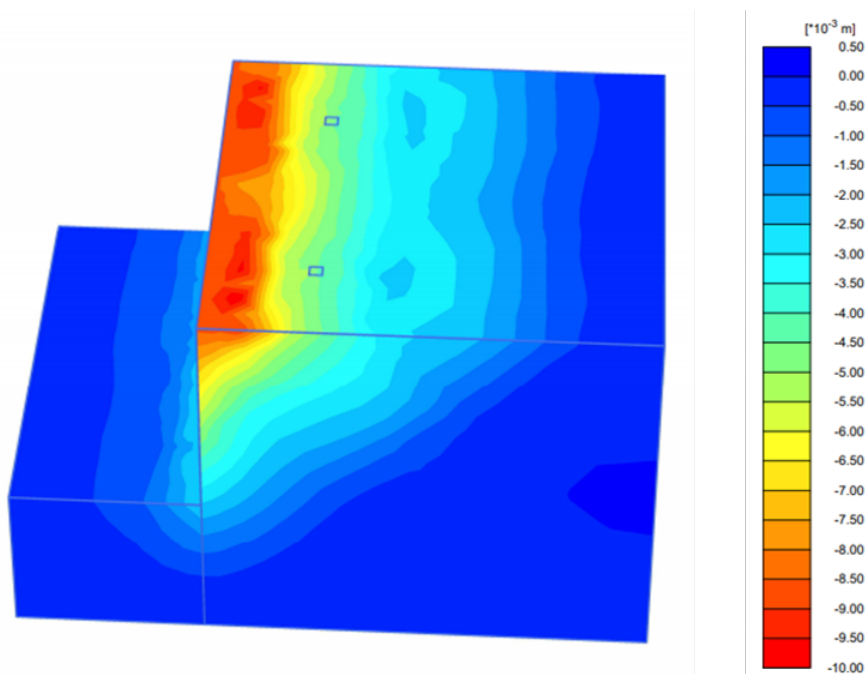


Figure 4.17: Horizontal displacement contour from the simulation of the root pattern-1 test.

Continuum finite element simulations were seen to be effective in simulating the global behavior of the timber sheet pile-vegetation system, where root analogues were used in place of real roots. The influence of the roots spatial configuration is complex and modelled through cohesion parameter adaption. Estimating the effect of roots as an increase in cohesion in the rooted zone is an oversimplified approach. Nevertheless, this approach provided a reasonable simulation of the observed experimental results. A consistent trend was observed in prediction of failure and the horizontal displacement of the timber sheet pile in experiments and simulations. It is to be noted that with such approximations the primary goal of this study was to predict the failure.

#### 4.6. PARAMETRIC ANALYSIS

A parametric analysis with four different Root Area Patterns (RAP) and four different cohesion distribution was conducted to further the insights gained from the physical modelling on an embankment of two meter soil retaining height. RAP refers to different zones where the root influence is present in a spatial configuration, (Fig.4.18). This analysis is aimed at providing a better understanding of:

- The location at which the roots would better perform on reducing the bending moment and soil displacements on the timber sheet pile;
- The effect of the increase in root cohesion to represent the reinforcement provided by the roots;

The maximum rooting depth of 1.5 m was chosen based on rooting depth reported for *Humulus lupulus* L. [26], where majority of the root volume was concentrated above 1.5 meters. The rooting depth is divided into three different zones, each providing different reinforcement to the soil ( $C_R$ ). Though very high root cohesion values ( $>50$  kPa, [37]) have been reported in literature, the maximum  $C_R$  considered in this study was 22 kPa, which is within the range of the majority of the  $C_R$  values reported in the field [38]. The four different root cohesion distribution (C1, C2, C3, C4) used in this study are given in (Table.4.3). The four different rooted area chosen are shown in (Fig.4.18), (Fig.4.19). From a practical perspective, two extreme root area patterns were chosen: (i) a RAP which consists of an area with four plants (Fig.4.18 a); and (ii) a RAP which consists of 3 meters adjacent to the sheet pile throughout the embankment as vegetated (Fig.4.19 d). Two root patterns in between the extremes were also investigated (Fig.4.18 b), (Fig.4.19 c)).

All the analyses were done on a 3D model of an embankment with a length of 7.0 m, width of 5.5 m with water table 1 m below the surface and embedment depth of 3.9 m. The input soil parameters and timber sheet pile parameters are given in (Table.4.4) and (Table.4.5).

Table 4.3: Cohesion distribution used in the parametric analyses

| Depth (m) | C1 (kPa) | C2 (kPa) | C3 (kPa) | C4 (kPa) |
|-----------|----------|----------|----------|----------|
| 0.0-0.5   | 2.5      | 5        | 10       | 15       |
| 0.5-1.0   | 5        | 10       | 20       | 22       |
| 1.0-1.5   | 4        | 8        | 12       | 16       |

Table 4.4: Soil properties for the soil model

| Parameter               | Value | Unit              |
|-------------------------|-------|-------------------|
| Saturated unit weight   | 17    | kN/m <sup>3</sup> |
| Unsaturated unit weight | 15    | kN/m <sup>3</sup> |
| Stiffness               | 2000  | kPa               |
| Cohesion                | 0     | kPa               |
| Friction angle          | 36    | Degree            |

Table 4.5: Timber sheet pile properties

| Retaining depth (m) | Unit weight(kN/m <sup>3</sup> ) | Thickness(mm) | MoE (N/mm <sup>2</sup> ) |
|---------------------|---------------------------------|---------------|--------------------------|
| 2                   | 12.2                            | 60            | 20000                    |

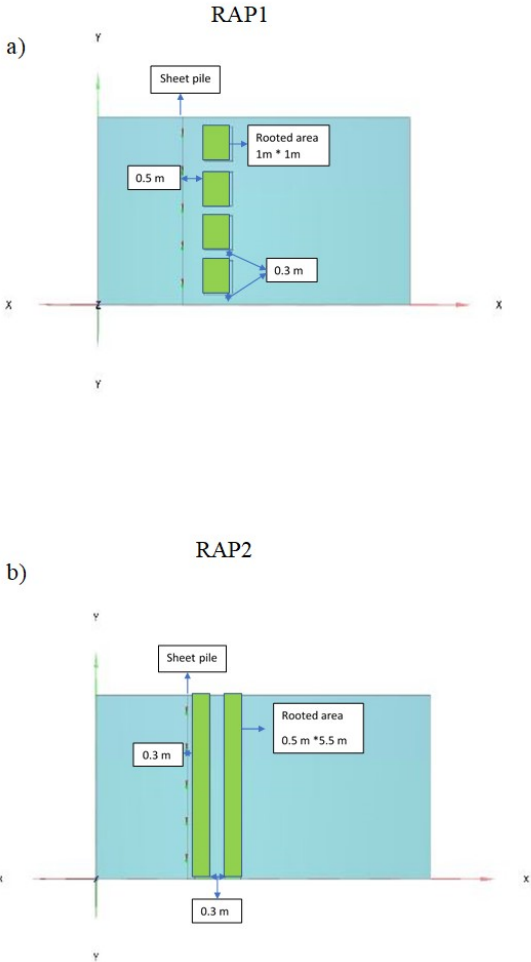


Figure 4.18: Top view of the root area patterns (RAP) evaluated in this study.

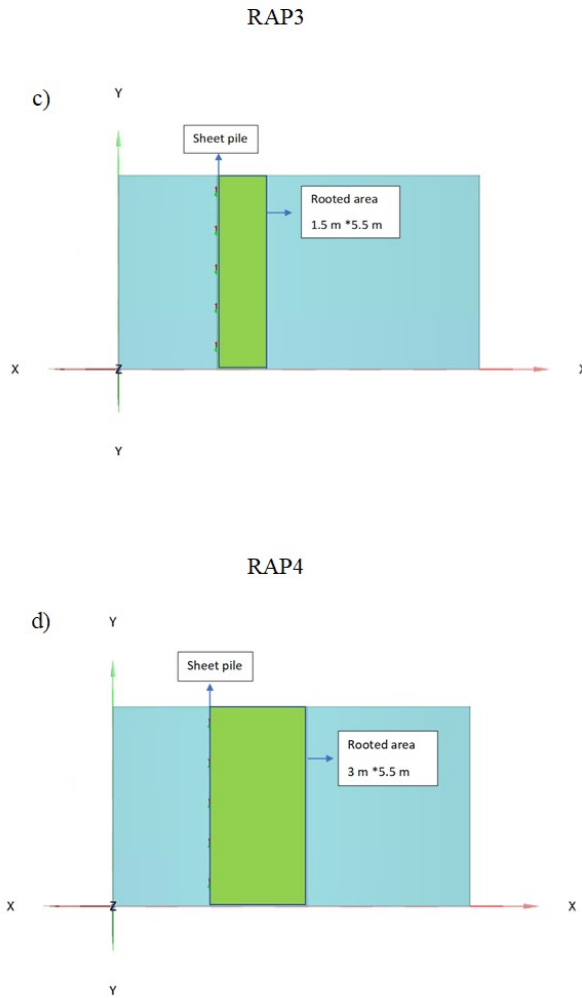


Figure 4.19: Top view of the root area patterns (RAP) evaluated in this study.

#### 4.6.1. EFFECT OF COHESION INCREASE DUE TO PRESENCE OF ROOTS

The cohesion due to presence of roots was varied within a wide range, from 2.5 kPa to 15 kPa on the top 0.5 m, 5 kPa to 22 kPa in the zone from 1.0 m to 1.5 m of depth, and 4 kPa to 16 kPa in from 1.0 m to 1.5 m of depth, in all the rooting patterns studied here. The changes in displacement and bending moment of the sheet pile with variation of cohesion are shown in (Fig.4.20). All the parameters are normalized with respect to the corresponding values of the bare soil. The presence of roots decreases the bending moment and displacement of the sheet pile, but it increases the factor of safety of the timber sheet pile-vegetation system. (Fig.4.20) shows that the variation of cohesion has negligible effect on the displacement and maximum bending moment. The difference in estimated displacements and bending moment when the two-extreme cohesion distributions, C-1 and C-4 areas used as the increase in cohesion due to the presence of roots is less than 1%. Similar observation was also recently reported by [38] in their studies on root reinforced slopes subjected to earthquake dynamic forces. The 3D analysis using different rooted area reinforces that the increase in root cohesion might have very little influence on timber sheet pile-vegetation system. Moreover, the effect of roots on the stream bank stabilization might be even less pronounced when used in fine grained soils which have intrinsic cohesion. The results previously mentioned are relevant to studies focused on measuring the increase in cohesion due to the presence of roots in the laboratory and field. The error associated to the estimation of the strength increase due to roots has lesser consequence on the stability. The advanced analytical models [39, 40] which require relatively large number of input parameters (which can also be difficult to acquire) need not necessarily present an advantage when used on a practical scale because the difference in bending moments acting on the timber sheet pile would be minimal.

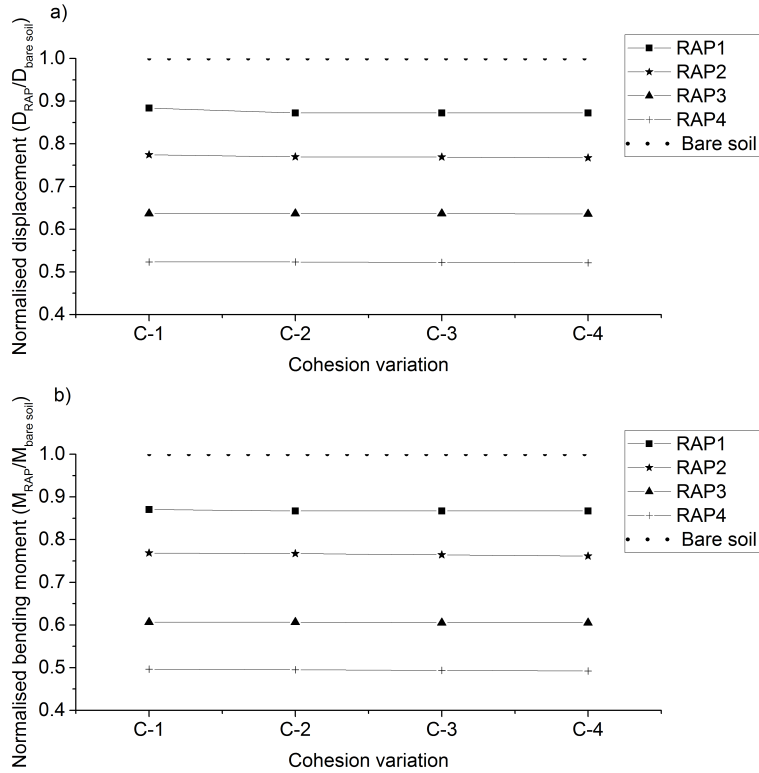


Figure 4.20: Normalised sheet pile displacement and bending moment with variation of cohesion for different root area pattern (RAP)

#### 4.6.2. EFFECT OF ROOT AREA PATTERN

Out of the four rooted area patterns used in this study, RAP4 was the best at reducing the maximum bending moment and displacement of the timber sheet pile. The beneficial effect due to the presence of roots increases as the rooted area also increases. The factor of safety associated to the bare stream bank was 1.33 for a retaining height of 2 m. When the case C-1 was used on a 2m slope, the factor of safety obtained for the RAP1 was 1.55, which increased to 2.01 when the RAP4 was used. A comparison of the RAP1 with RAP2 shows that the gaps between the rooted zones decrease the beneficial effect of presence of roots. [36] reported that an increase in spacing between the root system decreases the effect of vegetation on the slope stability. From the physical modelling reported above and based on this analysis, it can also be inferred that non-rooted zone can be detrimental to the stability. This in turn implies that, it would be beneficial to use vegetation that grows not only deep but also covers a wide spatial area. Species selection thus plays a crucial role in terms of stability to cover wider volumes than having stronger roots.

### 4.6.3. IMPLICATIONS FOR ON-GOING RESEARCH & PRACTICAL IMPLEMENTATION

**B**ased on the above discussion the following suggestions and questions are raised:

- Testing of shear strength of rooted soil: Given that the majority of the roots lie above 2 meters of depth maximum rooting depth possible which is generally below 2 meters, the increase in root cohesion has negligible influence on decreasing the displacements and bending moments on the sheet pile. a) The observations in the present study show that the focus should be on conducting tests which are quick and can provide the range of root cohesion, rather than conducting precise sophisticated tests. These findings are supported by [38]. b) Data on the variation of shear strength laterally is as relevant for practical application as vertical shear strength variations. This calls for more field scale test than lab tests where it is not practical to find the lateral extend of rooted strength increase. c) Shear tests on plants of varying age can be avoided, since the benefit of increase in cohesion, thereby increase in root area ratio might have negligible benefits.
- Selection of plant species: Rather than using roots which have favourable root orientation and quantity of roots, it is recommendable to use species which grow not only in depth but also spread their roots laterally.

## 4.7. CONCLUSIONS

**A** physical model of timber sheet pile-vegetation system is developed and tested for bare soil and rooted soils. Root analogues were 3D printed using PLA. Root analogues increase the stability of the system when compared to bare soil. Finite element analysis was conducted to validate and predict the failure of the system. Though the failure was reasonably predicted, the finite element analysis was over predicting the displacement of the sheet pile and vertical settlement of the embankment. The parametric analysis revealed that variation in root cohesion distribution had negligible effect on the bending moment and displacements of the sheet pile. It was also observed that non-rooted zones result in decreasing the stability of the system. The increase in root area resulted in decrease in bending moment and displacements of the sheet pile. Roots of species which occupy larger vertical and lateral area should be preferred over species whose roots predominantly grow in vertical direction.

## 4.8. APPENDIX A: PIV IMAGES

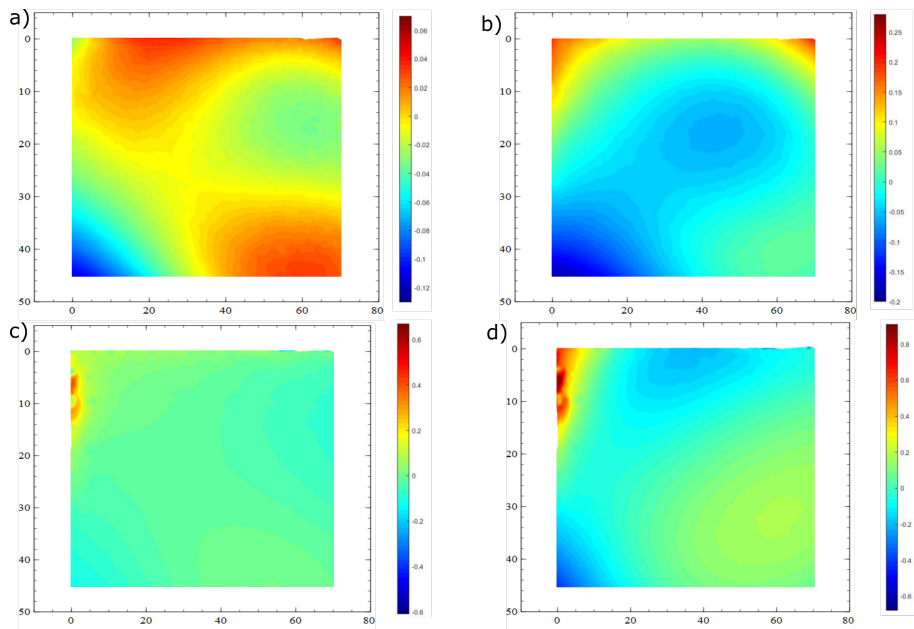


Figure 4.21: Failure wedge formation in bare soil a) 5cm drawdown b) 10 cm drawdown c) 12 cm drawdown d) 14 cm drawdown.

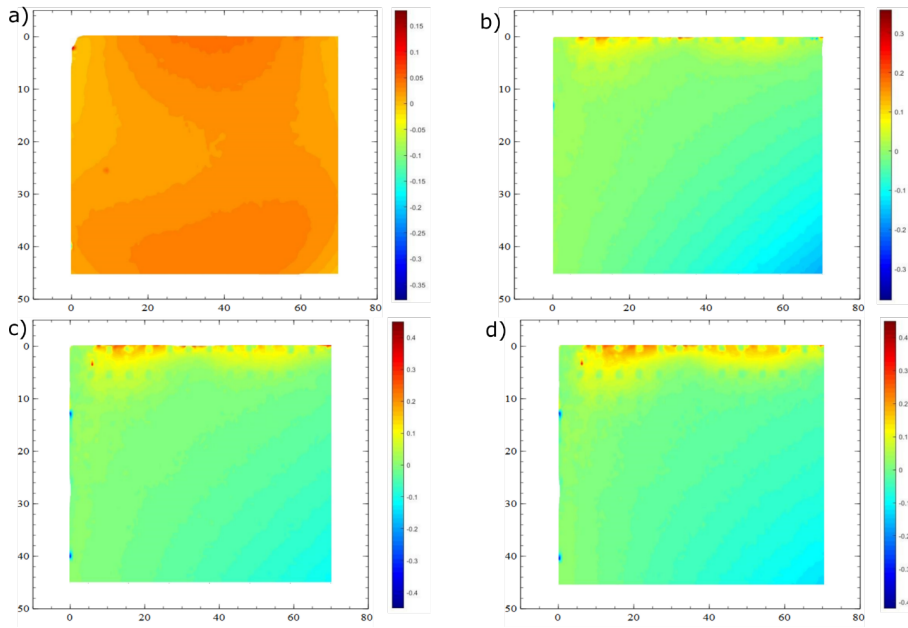


Figure 4.22: Failure wedge formation in root pattern-1 a) 5cm drawdown b) 10 cm drawdown c) 15 cm drawdown d) 17 cm drawdown.

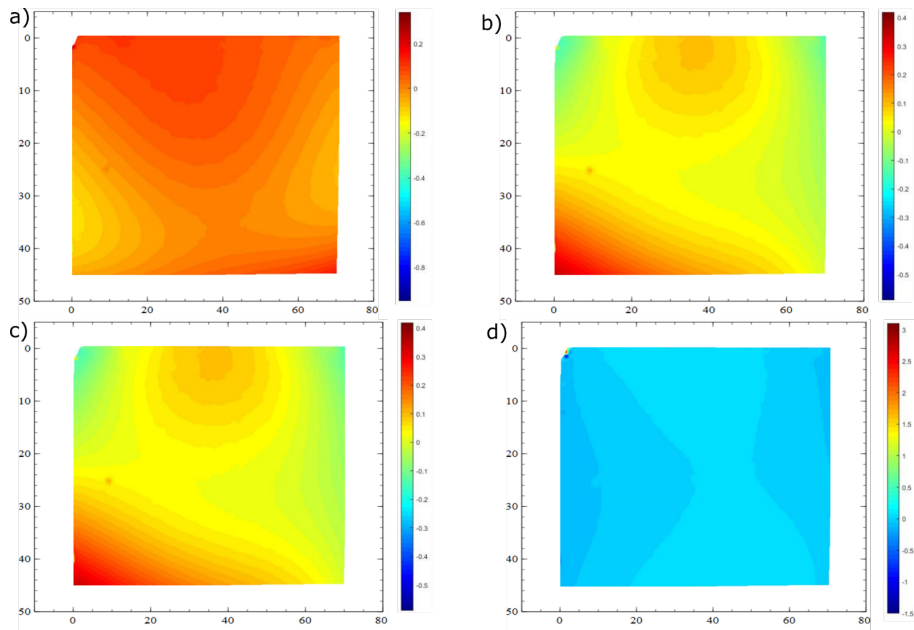


Figure 4.23: Failure wedge formation in root pattern-2 a) 5cm drawdown b) 10 cm drawdown c) 15 cm drawdown d) 25 cm drawdown.

## REFERENCES

- [1] D. M. S. Gerscovich, E. do Amaral Vargas Jr, and T. M. P. de Campos, *Back analysis of a landslide in a residual soil slope in rio de janeiro, brazil*, *Soils and Rocks* **34**, 139 (2011).
- [2] R. B. Gilbert, S. G. Wright, and E. Liedtke, *Uncertainty in back analysis of slopes: Kettleman hills case history*, *Journal of Geotechnical and Geoenvironmental Engineering* **124**, 1167 (1998).
- [3] B. Tiwari, T. L. Brandon, H. Marui, and G. R. Tuladhar, *Comparison of residual shear strengths from back analysis and ring shear tests on undisturbed and remolded specimens*, *Journal of Geotechnical and Geoenvironmental Engineering* **131**, 1071 (2005).
- [4] L. Wesley and V. Leelaratanam, *Shear strength parameters from back-analysis of single slips*, *Geotechnique* **51**, 373 (2001).
- [5] J. Zhang, W. H. Tang, and L. Zhang, *Efficient probabilistic back-analysis of slope stability model parameters*, *Journal of Geotechnical and Geoenvironmental Engineering* **136**, 99 (2010).
- [6] K. Horikoshi and M. Randolph, *Centrifuge modelling of piled raft foundations on clay*, *Geotechnique* **46**, 741 (1996).
- [7] B. Ghosh and S. Madabhushi, *Centrifuge modelling of seismic soil structure interaction effects*, *Nuclear Engineering and Design* **237**, 887 (2007).
- [8] S. Krishnaiah and D. Singh, *Centrifuge modelling of heat migration in soils*, *International Journal of Physical Modelling in Geotechnics* **4**, 39 (2004).
- [9] H. Takahashi, S. Sassa, Y. Morikawa, D. Takano, and K. Maruyama, *Stability of caisson-type breakwater foundation under tsunami-induced seepage*, *Soils and Foundations* **54**, 789 (2014).
- [10] W. Take and M. Bolton, *The use of centrifuge modelling to investigate progressive failure of overconsolidated clay embankments*, *Constitutive and Centrifuge Modelling: Two Extremes*, SM Springman, Lisse, AA Balkema, 191 (2002).
- [11] T. Liang, *Seismic performance of vegetated slopes*, Ph.D. thesis (2015).
- [12] A. Chueasamat, T. Hori, H. Saito, T. Sato, and Y. Kohgo, *Experimental tests of slope failure due to rainfalls using 1g physical slope models*, *Soils and Foundations* **58**, 290 (2018).
- [13] M. A. Heib, F. Emeriault, M. Caudron, L. Nghiem, and B. Hor, *Large-scale soil-structure physical model (1 g)-assessment of structure damages*, *International Journal of Physical Modelling in Geotechnics* **13**, 138 (2013).

- [14] Y. Kohgo, N. Tokoro, A. Togari, and M. Shimamura, *Simulation of behavior of a slope model with a shallow subsurface sand layer due to rainfall*, 5th Asia-Pacific Conference on Unsaturated Soils 2012 **2**, 613 (2012).
- [15] C. Jommi, D. Sterpi, T. de Gast, S. Muraro, E. Ponzoni, and H. van Hemert, *Coupled hydro-mechanical analysis of the pre-failure and the failure behaviour of a dyke on soft subsoil: Formulation and synthesis of results*, in *ICOLD International Benchmark Workshop on Numerical Analysis of Dams, ICOLD-BW* (Springer, 2019) pp. 645–665.
- [16] A. Askrinejad, F. Casini, P. Bischof, A. Beck, and S. Springman, *Rainfall induced instabilities: a field experiment on a silty sand slope in northern switzerland*, (2012).
- [17] R. Sonnenberg, M. Bransby, P. Hallett, A. Bengough, S. Mickovski, and M. Davies, *Centrifuge modelling of soil slopes reinforced with vegetation*, Canadian Geotechnical Journal **47**, 1415 (2010).
- [18] R. Sonnenberg, M. Bransby, A. Bengough, P. Hallett, and M. Davies, *Centrifuge modelling of soil slopes containing model plant roots*, Canadian Geotechnical Journal **49**, 1 (2012).
- [19] A. Takahashi, K. Nakamura, and S. Likitlersuang, *On the seepage-Induce failure of vegetationstabilised slopes*, in *Proceeding of the 8th International Conference on the Physical Modelling in Geotechnic* (2014) pp. 1233–1239.
- [20] K. H. Eab, S. Likitlersuang, and A. Takahashi, *Laboratory and modelling investigation of root-reinforced system for slope stabilisation*, Soils and Foundations **55**, 1270 (2015).
- [21] K. H. Eab, A. Takahashi, and S. Likitlersuang, *Centrifuge modelling of root-reinforced soil slope subjected to rainfall infiltration*, Géotechnique Letters **4**, 211 (2014).
- [22] A. Askarinejad and S. M. Springman, *Centrifuge modelling of the effects of vegetation on the response of a silty sand slope subjected to rainfall*, in *Computer Methods and Recent Advances in Geomechanics: Proceedings of the 14th International Conference of International Association for Computer Methods and Recent Advances in Geomechanics, 2014 (IACMAG 2014)* (Taylor & Francis Books Ltd, 2015) pp. 1339–1344.
- [23] T. Liang, J. A. Knappett, G. B. Anthony, and D. M. Wood, *On the role of vegetation in earthquake induced landslides*, in *1st International Conference on Natural Hazards & Infrastructure* (2016).
- [24] K. Viroon, *Effects of root geometry and transpiration on slope stability: centrifuge and numerical modelling*, Ph.D. thesis, The Hong Kong University of Science and Technology (2015).
- [25] T. Liang, J. Knappett, A. Bengough, and Y. Ke, *Small-scale modelling of plant root systems using 3d printing, with applications to investigate the role of vegetation on earthquake-induced landslides*, Landslides **14**, 1747 (2017).

- [26] T. Graf, M. Beck, M. Mauerner, D. Ismann, J. Portner, P. Doleschel, and U. Schmidhalter, *Humulus lupulus - the hidden half*, *BrewingScience* **67**, 161 (2014).
- [27] S. A. Stanier, J. Blaber, W. A. Take, and D. White, *Improved image-based deformation measurement for geotechnical applications*, *Canadian Geotechnical Journal* **53**, 727 (2016).
- [28] W. J. M. Rankine, *ii. on the stability of loose earth*, *Philosophical transactions of the Royal Society of London*, 9 (1857).
- [29] A. Askarinejad and S. M. Springman, *Rainfall induced instabilities in a silty sand slope: a case history in northern switzerland*, .
- [30] M. Khoiri and C.-Y. Ou, *Evaluation of deformation parameter for deep excavation in sand through case histories*, *Computers and Geotechnics* **47**, 57 (2013).
- [31] B.-C. B. Hsiung and S.-D. Dao, *Prediction of ground surface settlements caused by deep excavations in sands*, *Geotechnical Engineering* **46**, 111 (2015).
- [32] Z. Mao, F. Bourrier, A. Stokes, and T. Fourcaud, *Three-dimensional modelling of slope stability in heterogeneous montane forest ecosystems*, *Ecological Modelling* **273**, 11 (2014).
- [33] W. Wu, B. M. Switala, M. S. Acharya, R. Tamagnini, M. Auer, F. Graf, L. te Kamp, and W. Xiang, *Effect of vegetation on stability of soil slopes: numerical aspect*, *Recent advances in modeling landslides and debris flows*, 163 (2015).
- [34] L. Waldron, *The shear resistance of root-permeated homogeneous and stratified soil*, *Soil Science Society of America Journal* **41**, 843 (1977).
- [35] T. Wu, *Investigation on landslides on prince of wales island. alaska geotech. rpt. no 5, dpt*, Of Civil Eng., Ohio State Univ., Columbus, USA (1976).
- [36] C.-C. Fan and Y.-F. Lai, *Influence of the spatial layout of vegetation on the stability of slopes*, *Plant and soil* **377**, 83 (2014).
- [37] D. Zhang, J. Cheng, Y. Liu, H. Zhang, L. Ma, X. Mei, and Y. Sun, *Spatio-temporal dynamic architecture of living brush mattress: root system and soil shear strength in riverbanks*, *Forests* **9**, 493 (2018).
- [38] T. Liang, J. A. Knappett, A. K. Leung, and A. G. Bengough, *Modelling the seismic performance of root-reinforced slopes using the finite-element method*, *Géotechnique* **70**, 375 (2020).
- [39] M. Schwarz, P. Lehmann, and D. Or, *Quantifying lateral root reinforcement in steep slopes—from a bundle of roots to tree stands*, *Earth Surface Processes and Landforms: The Journal of the British Geomorphological Research Group* **35**, 354 (2010).
- [40] N. Pollen and A. Simon, *Estimating the mechanical effects of riparian vegetation on stream bank stability using a fiber bundle model*, *Water Resources Research* **41** (2005), 10.1029/2004WR003801.



# 5

## APPROACH TO THE DESIGN OF TIMBER SHEET PILE-VEGETATION SYSTEM

*"Knowledge like timber shouldn't be much use till they are seasoned"*  
Oliver Wendell Holmes



## 5.1. ABSTRACT

This chapter discusses the design approaches from practical application stand point of timber sheet pile-vegetation system to protect stream and canal banks. Two different design approaches, involving different perspectives with regards to the role of vegetation are considered.

In the system approach (SA), vegetation and timber sheet pile are considered as a single composite system in which the role of vegetation is to reduce the resistance required from the sheet pile. Thus including vegetation as a structural element would result in a reduction in resistance required from timber sheet pile that would reduce the damage accumulation on the timber sheet pile as well, thereby resulting in higher service life of the system as a whole. In the discrete approach (DA) the timber sheet pile and the vegetation are considered as mutually exclusive elements and the role of vegetation is to support the top layers of soil while the timber sheet pile undergoes decay. The timber sheet pile is less resistant to decay at the soil-water-air interface, thereby the vegetation, which has a rooting depth of approximately 1.5 to 2 m, would be able to take over the stream bank stability where timber sheet piles undergo decay.

The design approaches were illustrated on stream banks with 2 m and 3 m of retaining height. In both approaches (SA and DA), the effect of vegetation is considered as an increase in: (i) cohesion due to the presence of roots; and (ii) internal friction angle of the rooted area. The vegetation was seen to increase the service life of the stream bank protection by 6 years in the SA. On the other hand, the vegetation supported the stream bank after the decay of the top part of the sheet pile in the DA when analysed using plaxis 3D (Factor of safety > 1).

## 5.2. INTRODUCTION

Soil bio-engineering involves the use of live plants in combination with inert materials to protect and conserve soil. Plant roots are expected to provide mechanical reinforcement to the soil while the evapo-transpiration provides hydrological reinforcement. [1] used live plants in combination with wood to develop a dynamic soil bio-engineering scheme, which was validated on a slope stabilized by a crib wall and willow. [2] developed an integrated model taking into account the hydrological and mechanical effects of vegetation using easy to obtain input parameters. Different types of bio-engineered structures were analysed by [3], some 20 years after construction. The effect of riparian vegetation in stabilizing streambanks was quantified in the pioneering works of [4–6]. Timber sheet piles are often used as a stream bank protection structure. Timber sheet piles are considered environmentally friendly compared to other conventional solutions, such as concrete walls or steel sheet piles. Sometimes, tropical hardwoods which have better resistance to decay than softwoods may not be locally available, and have to be imported. For example, the Netherlands has about 2400 km of engineered timber sheet piles but very little exploitable tropical hardwoods [7]. Thus, there is a need for an alternative solution, which involves locally available materials and at the same time fits into the scope of ecological engineering. A timber sheet pile-vegetation composite stream bank protection structure is proposed in this chapter as an alternative to currently employed conventional methods.

The combination of timber sheet pile and vegetation is evaluated in two different design approaches in the present study: System approach (SA), and Discrete approach (DA), as described below.

In SA, the timber sheet pile (inert) and the vegetation (live) are considered as a single system in which the load is shared between the inert and the live parts. It is hypothesized that the load sharing would result in the reduction of the damage accumulation on the sheet pile. The damage on a timber sheet pile occurs not only due to biological degradation, but also due to the duration of the load effects. When vegetation is used in combination with the timber sheet piles, a reduction in duration of load effects can be expected due to the load sharing between the vegetation and the timber sheet piles. Thus, an increase of service life of the timber sheet pile, and thereby the whole system, is expected.

In DA, the vegetation and the sheet pile are considered as separate elements, each contributing to protect the stream bank on separate time frames. The part of the sheet pile below the stream bank is less susceptible to decay and has a longer service life. Thus, the vegetation has to be established on the top soil layers of stream bank, where the decay of the timber sheet pile occurs. The two approaches are schematically shown in (Fig.5.1).

In a real scenario, the timber sheet pile-vegetation system behavior will be a combination of both the approaches. The resistance required by the sheet pile would be less due to the presence of vegetation, which would decrease the damage accumulation on the sheet pile and as the decay of portion of sheet pile in the air-water-soil interface occurs the vegetation would support the top portion of the stream bank. Thus, both the approaches shown in the study can be considered conservative.

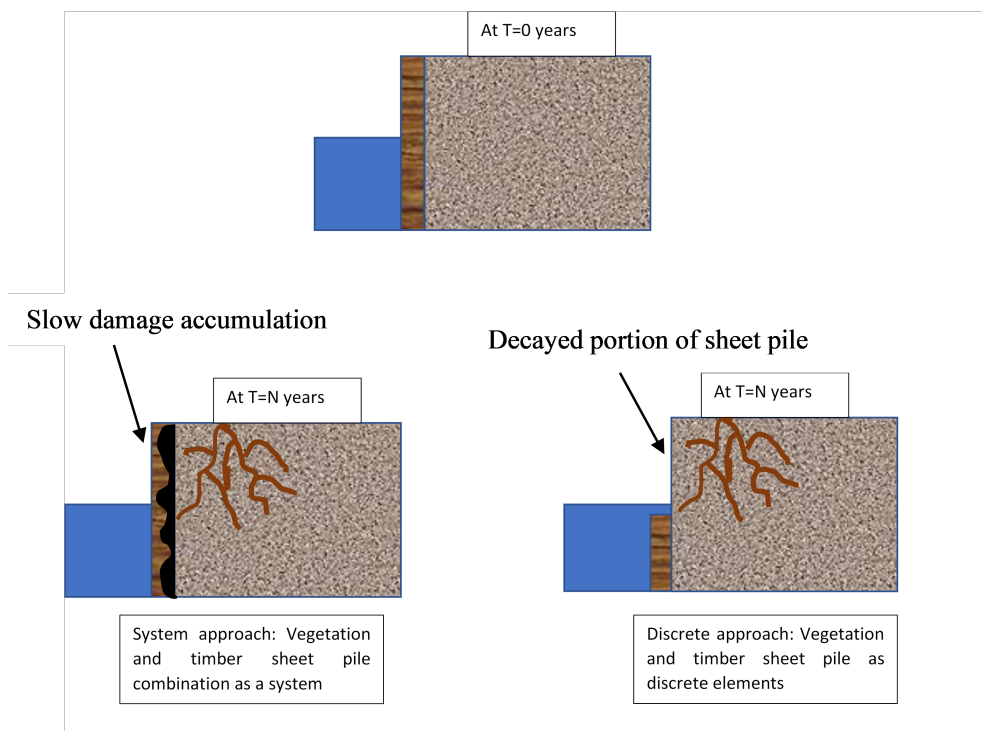


Figure 5.1: Approaches for design of timber sheet pile-vegetation system.

## 5.3. METHODS

### 5.3.1. SYSTEM APPROACH (SA): VEGETATION AND TIMBER SHEET PILE COMBINATION AS A SYSTEM

Timber service life modelling is generally conducted as a time-dependent structural safety evaluation. The prediction of the rate of decay of wooden members, and hence their structural strength, is key to any bio-engineered structure design. For an ideal bio-engineered structure, herein timber sheet pile-vegetation combination, the load transfer and the load sharing design depend on the ability to accurately predict the contribution of sheet pile to the system over time. Effects due to variation of load and resistance determine the time-dependent behaviour of the sheet piles. Timber service life models are also referred to as damage accumulation models and a number of approaches can be found in literature [8–10]. These models describe the development of the timber strength over time under the influence of a long-term load. In these models, the elements' cross sections do not change over time, for instance by assuming that the wood

material properties are not influenced by decay and the cross section is constant. A modification of the straightforward exponential damage model of [10] for changing material properties and cross sections can be found in [11] and [12] for deteriorating timber piles and cracked timber beams respectively. To include the time dependent reduction in load carrying capacity of the timber when physical and biological deterioration takes place, as given in equation (equation.5.1).

$$\frac{d\alpha}{dt} = \exp \left[ -a + \frac{b\sigma(t)}{f_s(t)} \right]. \quad (5.1)$$

Where  $d\alpha/dt$  is the rate of damage, in which  $\alpha$  can be any value from 0 to 1 (0 representing no damage and 1 representing structural failure),  $\sigma(t)$  represents the history of load variation (N or Nmm),  $f_s(t)$  represents the variation of the load carrying capacity with time (N or Nmm). Often, instead of plotting the development of  $\alpha$ ,  $1 - \alpha$  is plotted, indicating the residual load carrying capacity. The moment carrying capacity varies with time due to the reduction of cross-section, and also because the strength of the outer layers may be reduced because of biological decay. Thus, the total rate of change of the effective sectional moment of area  $\epsilon_I$  and change in effective cross-sectional area  $\epsilon_A$  resisting shear can be written as:

$$\epsilon_I(t) = \left(1 - \frac{2\delta}{b}\right) \left(1 - \frac{2\delta}{t}\right)^2 \quad (5.2)$$

$$\epsilon_A(t) = \left(1 - \frac{2\delta}{b}\right) \left(1 - \frac{2\delta}{h}\right) \quad (5.3)$$

Where  $\delta$  is the rate of decay (cross section) per year,  $b$  is the width, and  $h$  is the thickness of the sheet pile. Thus, the time dependent area ( $A_t$ ) and the moment of area ( $W_t$ ) could be written in terms of original area ( $A_0$ ) and original moment of inertia ( $W_0$ ) as:

$$W_t = W_0 \epsilon_I \quad (5.4)$$

$$A_t = A_0 \epsilon_A \quad (5.5)$$

For estimating the increase in service life due to the presence of vegetation the following two cases are analysed:

- Case -1: Stream bank with a retaining height of 3 m protected by a cantilever timber sheet pile.
- Case -2: Stream bank of retaining height 3 m protected by cantilever timber sheet pile and mature vegetation combination, see Fig.5.2 and Table 5.1. The mechanical reinforcement due to vegetation is taken from the direct shear tests conducted in Chapter 2. Two different analysis were conducted each with a different mechanical reinforcement due to vegetation. Firstly, the effect of vegetation is considered as increase in cohesion (CR) due to the presence of roots . In the second analysis, the effect of vegetation is as assumed to be an increase in the frictional component of the soil as estimated in Chapter 2.

Table 5.1: Summary of all the cases analysed in the system approach

| Case    | Effect of vegetation |
|---------|----------------------|
| Case -1 | Nil                  |
| Case-2  | $C_R=5$ kPa          |
| Case-3  | $\phi_R = 54^\circ$  |

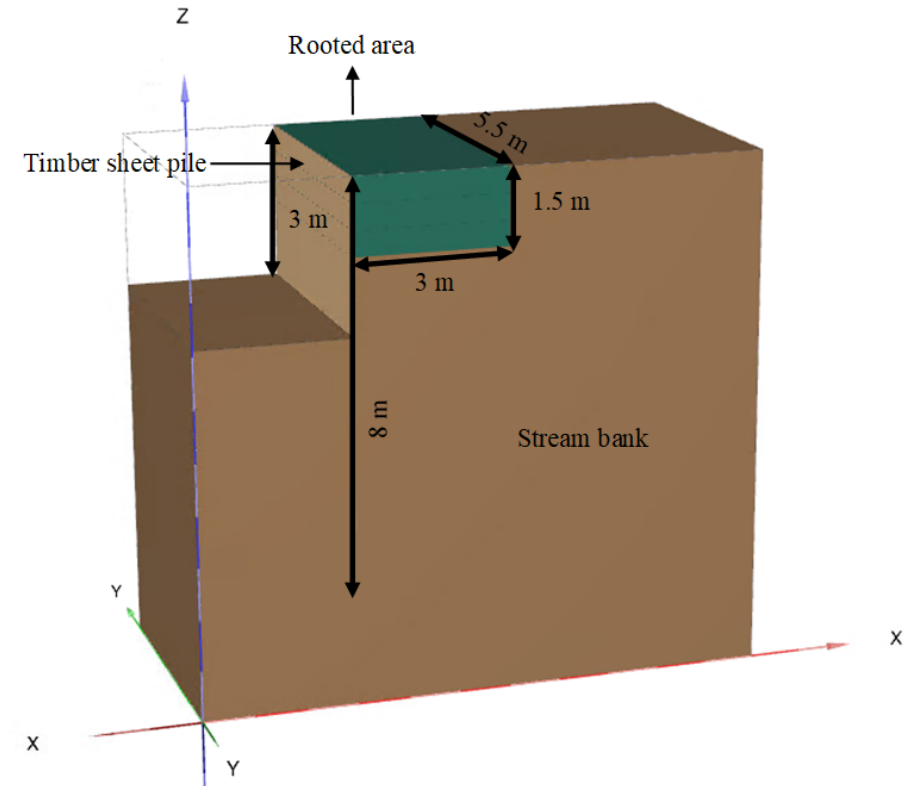


Figure 5.2: Dimensional characteristics of the timber sheet pile-vegetation system investigated in SA.

### 5.3.2. DISCRETE APPROACH (DA): VEGETATION AND TIMBER SHEET PILE AS DISCRETE ELEMENTS

Tropical hardwoods were traditionally used in stream bank structures owing to their higher resistance to decay and attack by fungi and marine organisms [13]. However, locally available wood used for the timber sheet pile systems undergoes high rates of decay, which is nonuniform throughout the timber sheet pile. The air-water-soil interface provides an environment for the decay to occur. This results in non-uniform decay with high concentration of decay at the part which is at and above the water table. The part

of the sheet pile below this water table is less prone to biological activity of decay and consequently higher serviceability. To tackle this issue twin-sheet pile walls which are a combination of tropical hardwoods and softwoods were introduced (Fig.5.3). The part of the sheet pile which is more prone to decay is made of tropical hardwoods and the part which is less prone to decay is made of less resistant softwoods. In DA, softwood is used



Figure 5.3: Twin-wood sheet pile, combination of tropical hardwood and softwood resulting in improved service life. (Taken from FORECO hout producten. <https://www.foreco.nl/nl/producten/twinwood>)

to make the timber sheet pile. Considering vegetation and softwood timber sheet pile as separate elements (DA), hypothesizes that the vegetation is able to support the stream bank in the parts where the softwood timber sheet pile has undergone decay. The increase of the soil strength through the mechanical reinforcement provided by the roots is estimated here based on the results reported in Chapter 2. As in the SA, the reinforcement provided by the roots is analyzed in two different ways: in the first analyses, the reinforcement is seen as an increase in cohesion ( $C_R$ ); and in the second analyses, the contribution is an increase of the frictional component of the soil strength as obtained in Chapter 2.

The minimum water level was assumed to be 1.25 m below the top of embankment, which implies that the top 1.25 m of the sheet pile is more exposed and consequently less resistant to decay. The water level in the canals/streams in the Netherlands are generally regulated, hence assuming a stable water level is valid. Stream banks with retaining heights of 2 m and 3 m were analysed.

A stream bank face with slope angle greater than friction angle of soil would be unstable when the soil has no cohesion. Hence an additional case was considered by designing stream bank with a face slope angle of 45°. The summary of all the cases are

presented in (Table5.2) and (Fig.5.4-Fig.5.7)

### 5.3.3. ASSUMPTIONS

The following assumption were made in both approaches:

- The maximum rooting depth is 1.5 meters.
- Influence of increase in reinforcement provided by the roots is observed to be minimum on reducing the loads on the wooden sheet pile (Chapter 4). A maximum cohesion increase due to presence of roots  $C_R$ , is assumed to be 5 kPa (average increase in  $C_R$  observed for *Humulus lupulus* L. in Chapter 2). Though very high values of  $C_R$  (>50kPa) is reported in literature [14], the majority of the reported results are below 50kPa.
- The variation of the reinforcement effect of roots with depth are not included, instead a uniform value for strength parameters ( $C_R$ ,  $\phi_R$ ) are used throughout the rooting depth.
- A time lag of two years is taken for the decay of the sheet pile to start. This assumption implies that the roots have developed enough to reinforce the soil mechanically.
- A length of 3 meters behind the timber sheet pile is considered as vegetated. In practical terms, this would correspond to two matured plants of *Humulus lupulus* L. for every 1.0-1.5 m in width.
- The water level is at 1 m below the top of the embankment and the suction above the water table is ignored.

Table 5.2: Summary of all cases analysed in the discrete approach. TSP-timber sheet pile

| Case       | Stream bank protection           | Sheet pile decay length (m) | Slope angle (°) | Retaining height (m) | Effect of vegetation |
|------------|----------------------------------|-----------------------------|-----------------|----------------------|----------------------|
| 2m:Case-1  | TSP<br>protected stream bank     | 0                           | 90              | 2                    | -                    |
| 2m:Case-2  | TSP and<br>vegetated stream bank | 0                           | 90              | 2                    | $C_R=5$ kPa          |
| 2m:Case-3  | TSP and vegetated stream bank    | 1.25                        | 90              | 2                    | $C_R=5$ kPa          |
| 2m:Case-4  | TSP and<br>vegetated stream bank | 0                           | 90              | 2                    | $\phi_R = 54^\circ$  |
| 2m:Case-5  | TSP and vegetated stream bank    | 1.25                        | 90              | 2                    | $\phi_R = 54^\circ$  |
| 2m:Case -6 | TSP                              | 0                           | 45              | 2                    | -                    |
| 2m:Case-7  | TSP and vegetated stream bank    | 0                           | 45              | 2                    | $\phi_R = 54^\circ$  |
| 2m:Case-8  | TSP and vegetated stream bank    | 1.25                        | 45              | 2                    | $\phi_R = 54^\circ$  |
| 3m:Case-1  | TSP<br>protected stream bank     | 0                           | 90              | 3                    | -                    |
| 3m:Case-2  | TSP and<br>vegetated stream bank | 0                           | 90              | 3                    | $C_R=5$ kPa          |
| 3m:Case-3  | TSP and vegetated stream bank    | 1.25                        | 90              | 3                    | $C_R=5$ kPa          |
| 3m:Case-4  | TSP and<br>vegetated stream bank | 0                           | 90              | 3                    | $\phi_R = 54^\circ$  |
| 3m:Case-5  | TSP                              | 1.25                        | 90              | 3                    | $\phi_R = 54^\circ$  |
| 3m:Case-6  | TSP                              | 0                           | 45              | 3                    | -                    |
| 3m:Case -7 | TSP and vegetated stream bank    | 0                           | 45              | 3                    | $\phi_R = 54^\circ$  |
| 3m:Case-8  | TSP and vegetated stream bank    | 1.25                        | 45              | 3                    | $\phi_R = 54^\circ$  |

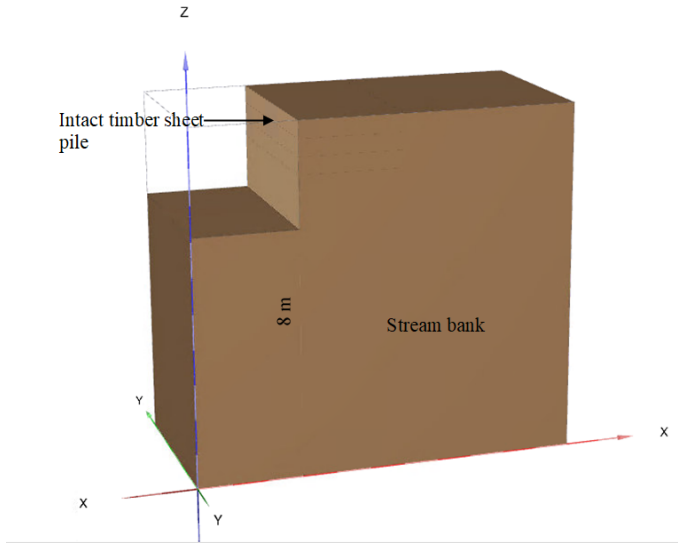


Figure 5.4: Illustration of a 2 m and 3 m retaining head without the presence of vegetation (2m: Case 1 and 3m: Case 2, respectively) in DA.

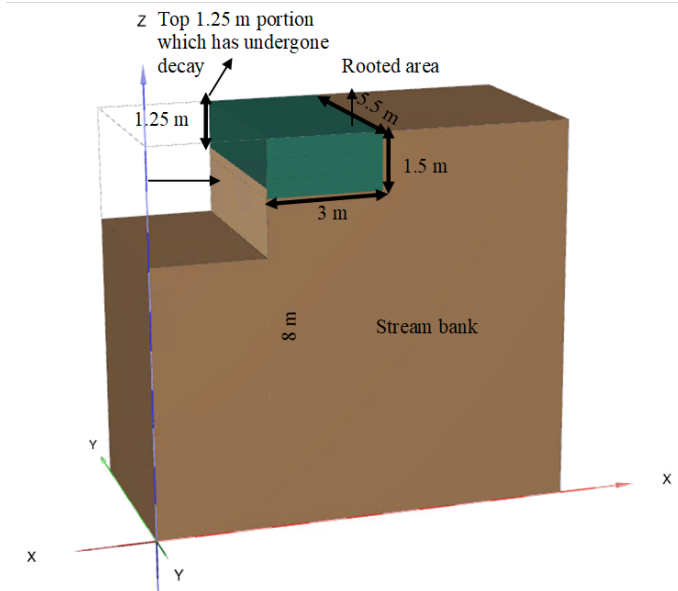


Figure 5.5: Illustration of 2m Case 3 and 3m Case 3 in DA

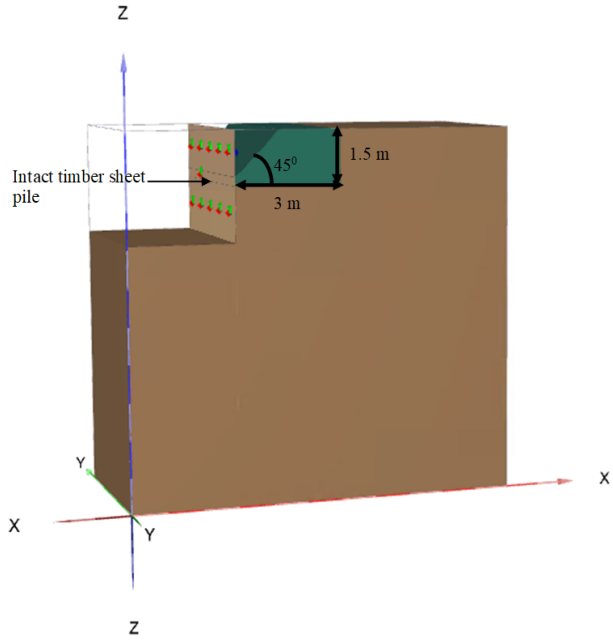


Figure 5.6: Illustration of 2m Case 6 and 3m Case 6 in DA

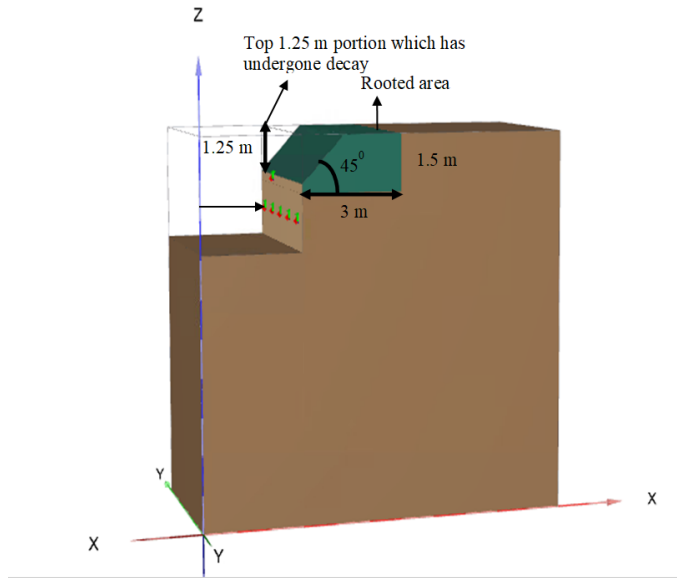


Figure 5.7: Illustration of 2m Case 8 and 3m Case 8 in DA

## 5.4. RESULTS

### 5.4.1. SYSTEM APPROACH

The input parameters of the soil and timber sheet pile are summarized in (Table5.3). The maximum bending moment and shear stress obtained from PLAXIS 3D are reported in (Table5.4).

Table 5.3: Input parameters to PLAXIS 3D.

| Parameter                     | Value             |
|-------------------------------|-------------------|
| Soil unsaturated unit weight  | 15 kN/ $m^3$      |
| Soil saturated unit weight    | 17 kN/ $m^3$      |
| Soil stiffness                | 2000 kPa          |
| Soil friction angle           | 36°               |
| Soil cohesion                 | 0                 |
| Modulus of elasticity of wood | 20000 N/ $mm^2/m$ |
| Thickness of sheet pile-3m    | 84 mm             |
| Unit weight of sheet pile     | 12.2 kN/ $m^3$    |

Table 5.4: Maximum bending moment and shear force acting on the timber sheet pile obtained from PLAXIS 3D

| Case    | Effect of vegetation | Max bending moment<br>(kNm-m) | Max shear force<br>kN-m' |
|---------|----------------------|-------------------------------|--------------------------|
| Case -1 | Nil                  | 21.82                         | 49.26                    |
| Case-2  | $C_R=5$              | 17.74                         | 26.47                    |
| Case-3  | $\phi_R = 54^0$      | 20.47                         | 27.89                    |

The maximum bending moment (M) acting on the sheet pile in case 1 was obtained from the outputs of the analysis on PLAXIS 3D, corresponding to the initial bending moment ( $M_0=21.82\text{kNm}$ ) experienced by the sheet pile before the growth of vegetation. Sheet piles are often made of wood species azobé (*Lophira alata*) which is assigned to the strength class D70 of European standard EN 338 [15]. This corresponds to a characteristic bending strength of  $f_m = 49.5\text{MPa}$ , after taking into account the safety factors of the material properties ( $\gamma_M = 1.3$  EC5,  $k_{ls}=1.15$ ) [7] modification factor and a shear strength of 15 N/mm<sup>2</sup>, but excluding the influence of long-term loading, as this is now incorporated in the damage model. The decay rate of the entire timber sheet pile was assumed to be -0.001 m/year (1 mm/year). The parameters of the timber damage accumulation model, a=21, b=24.63 were adopted for the estimation of the time to failure for timber beams [10]. The variation of damage accumulation ( $\alpha$ ) with time for all the cases in both bending and shear are shown in (Fig.5.8).

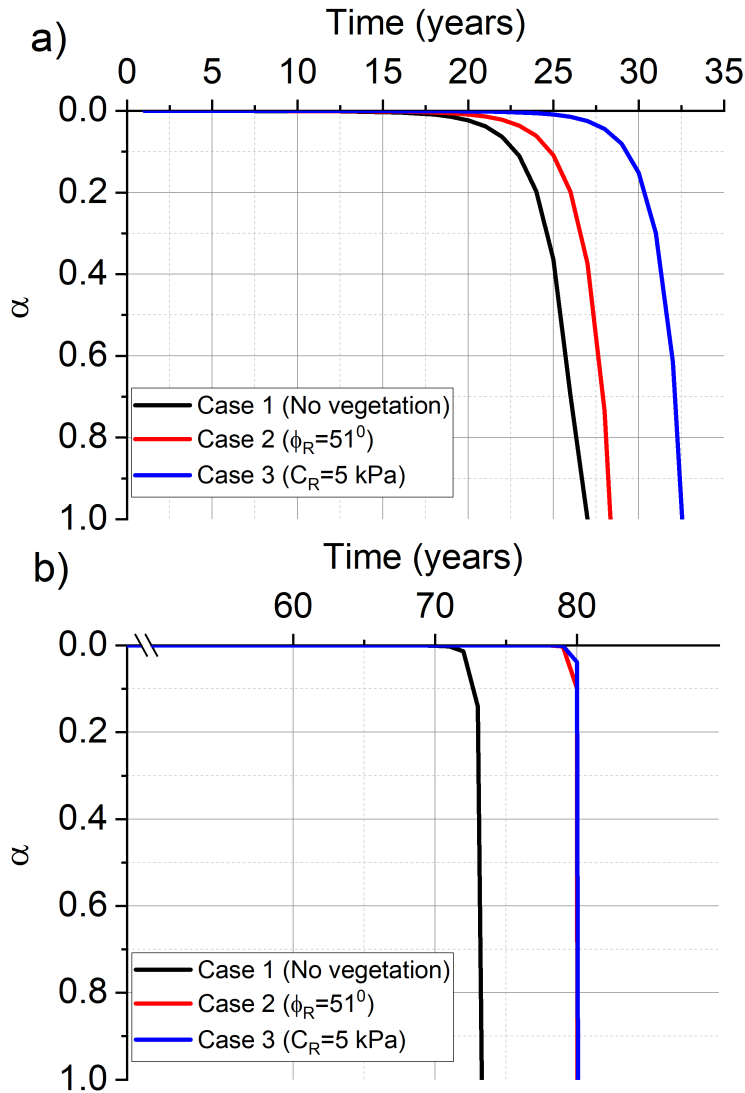


Figure 5.8: Damage accumulation a) in bending b) in shear

The presence of vegetation increased the time for complete damage of the sheet pile-vegetation system to occur. In Case -1, with no vegetation, the complete damage ( $\alpha$ ) occurs after 26 years. When the vegetation effects are included the service life of the timber sheet pile-vegetation system increases to 29 years (Case-2) and 33 years (Case-3). Thus, the effect of vegetation can be seen as an increase in service life of 3 years (11.5%) if the effects of vegetation are included as an increase in friction angle of the rooted zone and 7 years (27%) if effects of vegetation are included as an increase in cohesion in the rooted zone. As suggested in Chapter 3, at low confining pressures and high moisture

levels, the vegetation effects can be effectively considered as an increase in friction angle of the rooted area. Thus, it can be concluded that, a well-maintained vegetated stream bank with a retaining height of 3 meters would increase the service of the stream bank protection system (timber sheet pile-vegetation) at least by  $\approx 10\%$  year and maximum of  $\approx 30\%$  years for the parameters used.

#### 5.4.2. DISCRETE APPROACH

The input parameters used for the study are shown in (Table 5.5). The estimated factor of safety of all cases is presented in (Table 5.6).

Table 5.5: Soil and sheet pile properties used for safety analysis

| Parameter                                | Value                       |
|--|-----------------------------|
| Soil unsaturated unit weight             | 15 kN/m <sup>3</sup>        |
| Soil saturated unit weight               | 17 kN/m <sup>3</sup>        |
| Soil stiffness                           | 2000 kPa                    |
| Soil friction angle                      | 36°                         |
| Soil cohesion                            | 00                          |
| $C_R$ , additional cohesion due to roots | 5 kPa                       |
| Friction angle due to presence of roots  | 54°                         |
| Stiffness of sheet pile                  | 20,000 N/mm <sup>2</sup> /m |
| Thickness of sheet pile-2m               | 60 mm                       |
| Thickness of sheet pile-3m               | 100 mm                      |
| Unit weight of sheet pile                | 12.2 kN/m <sup>3</sup>      |
| Depth of sheet pile-2 m                  | 6 m                         |
| Depth of sheet pile-3 m                  | 8 m                         |

Table 5.6: Safety factors obtained for various cases analysed according to the DA.

| Case          | Sheet pile decay length (m) | Slope angle (°) | Retaining height (m) | Effect of vegetation | Factor of safety |
|---------------|-----------------------------|-----------------|----------------------|----------------------|------------------|
| 2m:<br>Case-1 | 0                           | 90              | 2                    | -                    | 1.355            |
| 2m:<br>Case-2 | 0                           | 90              | 2                    | $C_R = 5$            | 2.15             |
| 2m:<br>Case-3 | 1.25                        | 90              | 2                    | $C_R = 5$            | 1.32             |
| 2m:<br>Case-4 | 0                           | 90              | 2                    | $\phi_R = 54^\circ$  | 1.55             |
| 2m:<br>Case-5 | 1.25                        | 90              | 2                    | $\phi_R = 54^\circ$  | <1               |

Table 5.6: Safety factors obtained for various cases analysed according to the DA.

| Case        | Sheet pile decay length (m) | Slope angle (°) | Retaining height (m) | Effect of vegetation | Factor of safety |
|-------------|-----------------------------|-----------------|----------------------|----------------------|------------------|
| 2m: Case -6 | 0                           | 45              | 2                    | $\phi_R = 54^\circ$  | <1*              |
| 2m: Case-7  | 0                           | 45              | 2                    | $\phi_R = 54^\circ$  | 1.72             |
| 2m: Case-8  | 1.25                        | 45              | 2                    | $\phi_R = 54^\circ$  | 1.70             |
| 3m: Case-1  | 0                           | 90              | 3                    | nil                  | 1.28             |
| 3m: Case-2  | 0                           | 90              | 3                    | $C_R = 5$            | 1.6              |
| 3m: Case-3  | 1.25                        | 90              | 3                    | $C_R = 5$            | 1.31             |
| 3m: Case-4  | 0                           | 90              | 3                    | $\phi_R = 54^\circ$  | 1.58             |
| 3m: Case-5  | 1.25                        | 90              | 3                    | $\phi_R = 54^\circ$  | <1               |
| 3m: Case-6  | 0                           | 45              | 3                    | $\phi_R = 54^\circ$  | <1               |
| 3m: Case -7 | 0                           | 45              | 3                    | $\phi_R = 54^\circ$  | 1.60             |
| 3m: Case-8  | 1.25                        | 45              | 3                    | $\phi_R = 54^\circ$  | 1.60             |

The presence of vegetation in combination with the timber sheet pile increased the factor of safety of the stream bank (2m: Case-2, 2m: Case-4, 3m: Case-2, 3m: Case-4) when compared to the non vegetated timber sheet pile only case for both retaining heights investigated. When the vegetation effects were included as an increase in cohesion, the stream bank was observed to be stable (Factor of safety > 1) even after the decay of top 1.25 meters of the sheet pile had occurred (2m: Case-3, 3m: Case-3). The stream bank was not stable when the vegetation was responsible for an enhancement of the friction angle and the sheet pile had decayed in the top 1.25 m. When the face of the stream bank had a slope gradient of 45°, the stream bank was stable when the vegetation effect is included as an increase in friction angle even after the decay of the top 1.25 m portion of the timber sheet pile (2m Case-8, 3m: Case-8). However, the stream bank with a 45° gradient was unstable in the absence of vegetation, even when the timber sheet pile decay did not occur. Nevertheless, on inclusion of vegetation the stream bank was found to be stable (2m: Case-7, 3m: Case -7).

## 5.5. DISCUSSION & CONCLUSIONS

Bio-engineered earth retaining structures commonly involves combining materials which evolve with time and hence have varying contribution to support the load acting on it. [1] suggested that a methodology which takes into account the deterioration of materials involved and subsequent variation in load supporting capacity would be a useful tool for eco-engineers. This study demonstrates the use of a timber sheet pile-vegetation bio engineered earth retaining structure to be used for stream bank protection. Two contrasting processes, both conservative, taking into account the deterioration of timber sheet piles from a practical perspective and the increase in strength of the stream bank due to the presence of vegetation are combined into a single procedure for the analysis of structural capacity.

In SA an increase in service life was observed in both cases. The stream bank did not require a change in slope. An increase in stability of the stream bank is observed in DA approach when a timber sheet pile is used in conjunction with vegetation. When the reinforcing effects of vegetation are included as an increase in frictional angle of the rooted zone, the system seems to collapse when the decay of sheet pile occurs. However, when the slope of the face of the bank was reduced to  $45^\circ$ , the vegetation was found to be able to support the stream bank even after the decay of the sheet pile. When the effect of vegetation is considered as an increase in cohesion, the stream bank was stable even after the decay of the sheet pile. The SA is based on the superposition of the vegetation benefits onto the conventional timber engineering design principles. The SA approach would hamper the need for interim stability checks because the benefits of presence of vegetation is considered as an increase in service life. In other bio-engineered earth retaining structures the design methodology involved ensuring sufficient growth of vegetation to support the slope before the complete decay of wood occurred [1, 16]. However, the parametric analyses in chapter 4 shows that the full potential benefit of vegetation on the whole system is realized as soon as the initial stages of the growth of vegetation. Considering realistic data as used in this study, unlike other bio-engineered earth retaining structure (eg. cribwall-vegetation retaining structure) the design of timber sheet pile-vegetation system could be considered operational at a very early stage ( $< 1$  year), provided sufficient growth of vegetation occurs. The time lag required for decay to start depends on the natural durability of the timber used, for instance [1] used a time period of less than one year while [17] used a delay time of 5 years in their calculations. The assumed delay time depends on bio-physical circumstances, where air-water-soil exposure represents the worst possible case for decay of wood. The shear test results presented in chapter 2 showed an increase of shear strength of 6-10 kPa within a growth period of 1 year, which would be well above the shear strength increase used in the case study presented here.

The data required for both approaches can be obtained through field or laboratory testing of rooted specimens. The decay values used in this study are conservative [17]. The proposed approaches can be easily translated into conventional geotechnical analysis and included in sheet pile analysis software's like D-sheet piling which is widely used in the Netherlands.

In [3], it is suggested that the autochthonous developed vegetation have to ensure the stability of a bio-engineered earth retaining structure after the decay of the sheet

pile occurs. However, in the system approach adopted here vegetation is included as a structural element and the vegetation and sheet pile are considered to be in symbiosis throughout the service period. Thus, SA approach does not truly fit into the concept of an eco-engineering work where natural ecological succession is expected [1]. In contrast, DA approach will depend on a natural restoration of the stream bank. The SA approach leads to the possibility of designing timber sheet pile walls with smaller dimensions, or with less durable material. The structural safety of the 'combined' system of sheet pile and vegetation can be estimated using the proposed procedure. Thus, the SA approach involves conventional engineering approach while DA approach is more friendly to the flora and fauna usually found around the stream banks. It is to be noted again, that the real scenario would be a combination of both the approaches. More research is necessary for successful merging of both the approaches.

The widely used approach of including vegetation effects as a cohesion increase in the rooted zones is less conservative compared to the inclusion of vegetation effects as an increase in friction angle. In chapter 2 of this thesis, the roots of *Humulus lupulus* L. and *Salix fragilis* L. were found to increase the frictional component of the soil. Nevertheless, this chapter has considered both the scenarios. Since the factor of safety in DA approach and the increase in service life in SA approach differed significantly, when root effects were considered as an increase in cohesion of friction angle, the input parameters should be carefully chosen.

## REFERENCES

- [1] G. Tardío and S. B. Mickovski, *Implementation of eco-engineering design into existing slope stability design practices*, Ecological Engineering **92**, 138 (2016).
- [2] A. González-Ollauri and S. B. Mickovski, *Integrated model for the hydro-mechanical effects of vegetation against shallow landslides*, EQA-International Journal of Environmental Quality **13**, 37 (2014).
- [3] J. P. Fernandes and N. Guiomar, *Simulating the stabilization effect of soil bioengineering interventions in mediterranean environments using limit equilibrium stability models and combinations of plant species*, Ecological Engineering **88**, 122 (2016).
- [4] R. E. Thomas and N. Pollen-Bankhead, *Modeling root-reinforcement with a fiber-bundle model and monte carlo simulation*, Ecological Engineering **36**, 47 (2010).
- [5] A. Simon and A. J. Collison, *Quantifying the mechanical and hydrologic effects of riparian vegetation on streambank stability*, Earth Surface processes and landforms **27**, 527 (2002).
- [6] N. Pollen-Bankhead and A. Simon, *Enhanced application of root-reinforcement algorithms for bank-stability modeling*, Earth Surface Processes and Landforms **34**, 471 (2009).
- [7] J. W. G. Van de Kuilen and M. Van Der Linden, *Reliability based design of timber sheet pile walls*, NZ Timber Des J **11**, 11 (1999).
- [8] T. van der Put, *Reaction Kinetics of Bond Exchange of Deformation and Damage Processes in Wood: IUFRO S 5.02 Conference September 1986, Firenze, Italy* (Stevin Laboratorium van de Faculteit der Civiele Techniek de Technische . . . , 1986).
- [9] R. Foschi and Z. Yao, *Another look at three duration of load models*, in *Proceedings of IUFRO wood engineering group meeting, Florence, Italy, paper* (1986) pp. 19–9.
- [10] C. Gerhards and C. Link, *A cumulative damage model to predict load duration characteristics of lumber*, Wood and Fiber Science **19**, 147 (2007).
- [11] J. W. G. Van de Kuilen, *Service life modelling of timber structures*, Materials and Structures **40**, 151 (2007).
- [12] J. W. G. Van de Kuilen and W. F. Gard, *Residual service life estimation using damage accumulation models*, in *World conference on timber engineering, Auckland, New Zealand, 15-19 juli 2012* (2012).
- [13] W. F. Gard and J. W. G. van de Kuilen, *Micro-drilling resistance measurements of dense hardwoods for hydraulic structures*, in *WCTE 2018-World Conference on Timber Engineering* (World Conference on Timber Engineering (WCTE), 2018).

- [14] D. Zhang, J. Cheng, Y. Liu, H. Zhang, L. Ma, X. Mei, and Y. Sun, *Spatio-temporal dynamic architecture of living brush mattress: root system and soil shear strength in riverbanks*, *Forests* **9**, 493 (2018).
- [15] J. W. G. Van de Kuilen and H. J. Blaß, *Mechanical properties of azobé (lophira alata)*, *Holz als Roh-und Werkstoff* **63**, 1 (2005).
- [16] M. S. Acharya, *Analytical approach to design vegetative crib walls*, *Geotechnical and Geological Engineering* **36**, 483 (2018).
- [17] J. W. G. van de Kuilen and W. F. Gard, *Mechanical performance models*, in *Performance of Bio-based Building Materials* (Woodhead Publishing, 2017).

# 6

## CONCLUSIONS AND OUTLOOK

## 6.1. OBSERVATIONS AND CONCLUSIONS

The work presented in this thesis aims to advance the current knowledge on root permeated soils and its application to bio-engineered earth retaining structures. An analysis and design method for bio-engineered earth retaining structure to protect stream banks is proposed. It comprises a timber sheet pile-vegetation system, where the load-carrying capacity of an engineered sheet pile is combined with plant-systems that increase the shear resistance of the soil. The systems strength and reliability is based on both components: the timber and the plants.

A need for understanding the root-soil interaction from an application based realistic perspective. From this perspective, the insufficiency of conventional geotechnical laboratory scale testing to represent root-soil interactions was identified. A lack of knowledge on time dependent behavior of tensile strength of roots and root-soil matrix in shear was recognized. Hence, this necessity to conduct tests as close to realistic field situations was translated into the experimental campaign adopted in this study. Majority of the testing apparatus, large scale direct shearing apparatus (displacement controlled and load controlled), clamps and testing technique for tensile testing of roots, physical model of timber sheet pile-vegetation system, were developed from the outset at the Bio-based structures and Materials laboratory. A finite element analysis of the timber sheet pile-vegetation system modelled in laboratory and subsequent parametric analysis to study the influence of root contributions on to the stability of the system were conducted. Detailed conclusions drawn in this thesis with respect to mechanical behavior of roots, root-soil shear behavior and timber sheet pile-vegetation system are discussed below.

### *Relevance of realistic testing conditions and protocol*

- Vegetation roots are generally concentrated on the top 1 to 2 meters of soil. The confining pressures used to test the root soil matrix should be representative of the depths at which roots can grow. Since root failure mode depends on the moisture conditions of the soil, the moisture conditions of the tested soil-root matrix should be representative of the conditions at which root effects are most desired, and consequently cover the expected moisture variations over the year. In this study the range of confining pressure used were from 4.4 kPa to 10.4 kPa which is representative for the confining stresses expected on barely to heavily vegetated slopes. The Netherlands, with high water table especially along canal banks, saturated conditions under which shear tests were conducted simulate realistic conditions.
- The benefit of testing immediately after collection of roots avoided the search for a suitable preservation technique. This was a clear advantage as fresh roots could be tested in the desired moisture conditions (HLW and SFW).
- Interpretation of root breakage during tensile testing is a subject of debate. In this study, a conservative approach was followed. Roots that failed at a maximum of 1/3rd from the clamps were excluded from the analysis. Since there exist not universally accepted clamping system, three different clamps were prepared and the jaw clamp used in this study was selected based on highest success rate of tests.

However, even in this case the success rates of tests were low (<50 %) . Nevertheless, bias on determining if the roots slipped or broke were completely removed. Thus, it is recommended to conduct large number of tests and determine successful tests, which have the desired quality.

- To reduce the moisture loss of roots to the minimum a preliminary study to find the optimal temperature at which, in combination with the relative humidity in the lab undesirable changes in moisture content of the roots would take place was done. Continuous wetting of the outer layer of root and using a damp cloth around the root was found to prevent significant moisture loss during the testing period.
- The physical model developed in this study was tested at 1g scale, thus removing uncertainties with respect to scaling laws for root-soil interaction studied by centrifuge testing. 3D printing of model roots provided an opportunity to avoid any difference in root architecture, thus avoiding complications in analysis.

#### *Shear behavior of root permeated soils*

- Presence of roots of *Humulus Lupulus* L. and *Salix fragilis* L. were observed to increase the shear resistance of soil for all tested confining stresses. No favourable root orientations were observed in the tested displacement range. This could possibly be due to the existence of a critical root area ratio over which root orientations do not have a significant effect in the practical displacement ranges (<16% strain).
- Contractive behaviour was shown to occur by rooted specimens. This observed phenomena could be due to two reasons, the additional confining stress exerted due to the tensile elongation of the vegetation roots during shear and the crevice formation due to root growth.
- The reinforcement effect of roots was seen to increase the frictional component of the shear strength. This differs from the conventional approach where the effect of roots are accounted as an increase in cohesion. Nonetheless, at low confining pressures and taking into account the root-soil interaction, through a straightforward analysis it was shown that an increase in frictional component of the shear strength is justified.
- Burger model was found to reasonably predict the viscous behaviour of rooted soils for the timescale under study. The elastic stiffness of rooted soils was found to be lesser than bare soil. This shows that rooted specimens would act as ductile material when loaded. However, the viscous stiffness of the rooted specimen was found to be slightly higher than that to bare soil. Thus, roots could not only increase the peak shear strength but could potentially improve the viscous behaviour of the composite.

#### *Root mechanical characteristics in tension*

- Tension strength of *Humulus lupulus* L. and *Salix fragilis* L. were determined in two different moisture conditions representing winter and summer conditions.

- Tension strength of *Salix fragilis* L. was observed to change with the variation in moisture content while the tension strength of *Humulus lupulus* L. did not show any significant difference in the tension strength when tested in either moisture content. The predominantly sandy soil used in this study did not possibly develop negative water potential high enough to drive water out of the roots on *Humulus lupulus* L. In addition to this the above ground biomass of *Humulus lupulus* L. was lesser in comparison to *Salix fragilis* L.
- Load controlled tests were conducted on roots of two diameters of *Humulus lupulus* L. Burger's model was able to qualitatively and quantitatively fit the time dependent strain behaviour of roots under constant load for the time period studied. The time to failure of roots was studied and it was shown that a power law model was able to describe the measurement outcomes. The roots may not fail under a constant load in creep at sufficiently low load levels. However significant deformations may occur that could affect the serviceability conditions when used as a replacement for a conventional sheet pile structure.

#### *Behavior of timber sheet pile-vegetation system*

- Physical model tests with model root analogues as inclusions showed an improvement in the stability of the system when compared to non-vegetated tests. For instance, when five root analogues were used the embankment did not fail even under full drawdown conditions (250 mm) and additional surcharge loading, whereas a non-reinforced system would fail at (120-140 mm).
- Analysis of the displacement of the sheet pile revealed that the roots only come into action after an initial higher displacement compared to bare soil. This observation combined with the results in direct shear results show that prior to failure large displacements could be expected in embankments reinforced by vegetation roots.
- The rooted soil develops a wider and deeper failure wedge compared to non-rooted embankment. This implies that a larger volume of soil is mobilized when rooted soil reaches failure.
- Finite element analysis (using PLAXIS) of the physical model tests with the rooted zone having additional cohesion due to the presence of roots was conducted. The model simulations were qualitatively able to predict the trend of displacements of the sheet pile.
- Parametric analysis with variation in cohesion distribution and rooted spatial area patterns revealed that the influence of the increase in cohesion had minimal effects on the acting bending moment and displacement of the sheet pile. Furthermore, the bending moment and displacement of the sheet pile decreased as the rooted spatial area increased, showing that the combined system could function in terms of reduced stresses in timber and increased system rigidity.

#### *Design approaches of timber sheet pile-vegetation system*

- Two design approaches were investigated, a system approach in which the vegetation and timber sheet pile are considered as a single system and the discrete approach in which timber sheet pile and vegetation are considered as discrete elements, each supporting the stream bank at different time periods.
- The system approach assumes that part of the load on the sheet pile will be supported by the vegetation over time, thereby reducing the required resistance of the timber sheet pile. This results in decrease in the mechanical damage accumulation of the wood of the sheet pile, thereby increasing the system's service life. An illustration of the approach on a stream bank with retaining height of 3 meters and using vegetation reinforcement values obtained in the shear tests and physical model tests, the service life of the sheet pile is prolonged by 3-6 years.
- In the discrete approach, the presence of vegetation in combination with the intact sheet pile is seen to increase the factor of safety of the stream bank. In addition, when the part of the sheet pile with air-water-soil interface suffers from biological decay, the vegetation was observed to be able to counteract the reduced load carrying capacity of the part where the sheet pile has undergone decay.

## 6.2. LIMITATIONS

Interdisciplinary research conducted in this thesis, involving three natural elements soil, vegetation and timber, all showing a high natural variability in their behavior, has theoretical and experimental limitations.

- Even though the results obtained from the shear tests could be analysed using sound engineering principles, the high variability in roots due to its biological nature warrants for increasing the number of repetitions of the tests. Due to large scale of the tests conducted, repetitions were limited.
- When the vegetation roots were tested in tension and comparisons were made, variations in the microscopic nature of wet and dry roots were not investigated. The comparisons were made solely on the macroscopic dimensions of the roots. A volume effect could be proven, but as this volume effect depends on both cross section and test length, more research is needed to clarify this further.
- Due to time, cost and effort involved in conducting physical model tests, only two different rooting patterns were investigated. Though, the effect of non-vegetated regions on the stability of the system were qualitatively estimated, quantitative understanding was limited and would require large scale field testing.
- Though the results of shear tests in low confining pressures and saturated conditions conducted in this study showed an increase of frictional angle of rooted specimens compared to non-rooted specimens, a precise theoretical framework or model could not be developed. Hence, in the design approaches, the rooted zones were both represented by an increased friction angle and cohesion and consequently compared to each other.

### 6.3. FUTURE RECOMMENDATIONS

**B**ased on the observations reported in this study and limitations identified recommendations for future research are given below:

- For practical application-based research, it is recommended to conduct a parametric analysis to see if the variation in root contribution has a significant influence on the stability or load carrying capacity of the system. If the influence is limited a fast field strength testing campaign can be adopted to obtain the range of shear strength enhancement.
- Since the vegetation roots are intended to stabilize the slopes for a long period of time, time dependent load carrying capacity of roots and time dependent root-soil interactions need to be investigated further. Such a study could give insight into potential large deformations that could become detrimental to stability of slopes.
- There is a lack of real field scale data. Hence, it is deemed necessary to scale the physical model developed in this study to an instrumented field scale study.

# CURRICULUM VITÆ

## Abhijith Chandrakaran KAMATH

08-07-1992      Born in Kerala, India.

### EDUCATION AND WORK EXPERIENCE

1996-2008      Spring valley school  
Kozhikode, Kerala, India

2008-2010      Prestige public school  
Calicut, Kerala, India

2010-2014      Bachelor of Technology, Civil Engineering  
Government Engineering College  
Thrissur, Kerala, India

2014-2016      Master of science, Civil engineering  
Texas A&M University  
College station, Texas, United states of America

2016-2021      Ph.D. student, Faculty of Civil engineering and Geosciences  
TU Delft

*Thesis:*      Bio-Engineered Earth Retaining Structure (BEERS)  
A Timber sheet pile-vegetation system for stream bank protection

2021-            Post-doc researcher  
Bio-Based Structures and Materials  
TU Delft, Netherlands



# LIST OF PUBLICATIONS

4. Kamath, A. C., Gard, W., & Van de Kuilen, J. W. (2021). Approaches in the design of softwood sheet pile vegetation system as an alternative to twin-wood sheet pile. *Paper presented at World Conference on Timber Engineering 2021, WCTE 2021*, Santiago, Chile.
3. Kamath, A., Gard, W., & Van de Kuilen, J. W. (2020). Biodynamic timber sheet pile walls: vegetation retaining structure. *European Journal of Wood and Wood Products*, 78(5), 1045-1055. <https://doi.org/10.1007/s00107-020-01598-7>
2. Tarantino, A., El Mountassir, G., Wheeler, S., Gallipoli, D., Augarde, C., Urciuoli, G., ... & Kamath, A. (2020). TERRE project: interplay between unsaturated soil mechanics and low-carbon geotechnical engineering. In *E3S Web of Conferences*, Vol. 195, pp. 01002-1. EDP Sciences. <https://doi.org/10.1051/e3sconf/202019501002>
1. Kamath, A., Gard, W., & Van de Kuilen, J. W. (2019). Timber sheet pile-vegetation model for stream bank retaining structure. In *E3S Web of Conferences*, Vol. 92, p. 12013. EDP Sciences. <https://doi.org/10.1051/e3sconf/20199212013>

## **Under preparation**

3. Kamath, A., Gard, W., & Van de Kuilen, J. W., Jommi, C. Physical and numerical modelling of timber sheet pile-vegetation system for stream bank protection. Under preparation.
2. Kamath, A., Gard, W., & Van de Kuilen, J. W., Jommi, C. Shear strength behavior of rooted soils. Under preparation.
1. Kamath, A., Gard, W., & Van de Kuilen, J. W., Jommi, C. Root tensile strength characteristics of *Humulus lupulus* L. & *Salix fragilis* L. under varying moisture and loading conditions. Under preparation